UNIVERSITY OF CALIFORNIA,
IRVINE

Exploring the Intricacies of Ancillary Ligand Effects on $4f^n5d^1$ Ln(II) Ions

DISSERTATION

submitted in partial satisfaction of the requirements
for the degree of

DOCTOR OF PHILOSOPHY

in Chemistry

by

Jessica Renee Kristianna White

Dissertation Committee:
Distinguished Professor William J Evans, Chair
Distinguished Professor A. S. Borovik
Chancellor's Professor Jenny Y. Yang

2022

DEDICATION

To

My life partner Gabriel, my father and hero Milford, my mother Kerrie, my brother Andre, and my angel, Candy

For I would not be here without them.

Words of wisdom

Those of us who stand outside the circle of this society's definition of acceptable women; those of us who have been forged in the crucibles of difference -- those of us who are poor, who are lesbians, who are Black, who are older -- know that survival is not an academic skill. It is learning how to take our differences and make them strengths. For the master's tools will never dismantle the master's house. They may allow us temporarily to beat him at his own game, but they will never enable us to bring about genuine change. And this fact is only threatening to those women who still define the master's house as their only source of support.

Audre Lorde
The Master's Tools Will Never Dismantle the Master's House

And words of revolution

Power anywhere where there's people. Power anywhere where there's people. Let me give you an example of teaching people. Basically, the way they learn is observation and participation. You know a lot of us go around and joke ourselves and believe that the masses have PhDs, but that's not true. And even if they did, it wouldn't make any difference. Because with some things, you have to learn by seeing it or either participating in it. ***And you know yourselves that there are people walking around your community today that have all types of degrees that should be at this meeting but are not here. Right?*** *Because you can have as many degrees as a thermometer. If you don't have any practice, they you can't walk across the street and chew gum at the same time.*

Fred Hampton
Power Anywhere Where There's People

TABLE OF CONTENTS

LIST OF FIGURES

LIST OF FIGURES

LIST OF FIGURES

LIST OF FIGURES

LIST OF TABLES

LIST OF TABLES

ACKNOWLEDGEMENTS

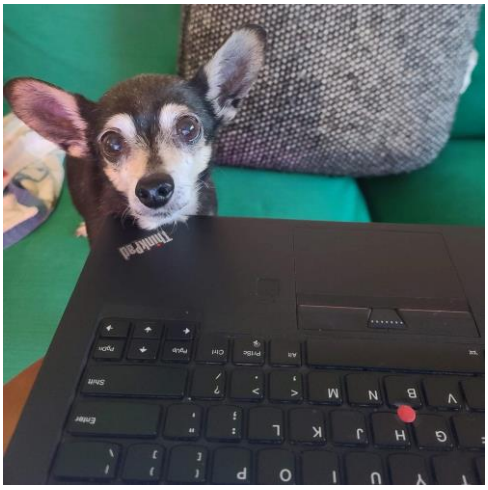

First, I would like to thank my late chihuahua, Candy, who passed on November 13th, 2022. Thank you so much for your hard work and support. You are my baby and will always be missed.

Thank you to the rest of my family, including my partner and better half, Gabriel, my father and hero, Milford, my mother Kerrie, my brother Andre, and my grandmother Juanita. I would not be here without any of you. To my late uncle, Orville, who passed November 12th, 2022, thank you for supporting my love for reading and learning from a young age.

I would like to acknowledge Makenna Lee Elrod, Layla Salazar, Maranda Mathis, Nevaeh Bravo, Jose Manuel Flores Jr., Xavier Lopez, Tess Marie Mata, Rojelio Torres, Eliahna "Ellie" Amyah Garcia, Eliahna A. Torres, Annabell Guadalupe Rodriguez, Jackie Cazares, Uziyah Garcia, Jayce Carmelo Luevanos, Maite Yuleana Rodriguez, Jailah Nicole Silguero, Amerie Jo Garza, Alexandria "Lexi" Aniyah Rubio, Alithia Ramirez, and the heroes that protected them, Irma Garcia and Eva Mireles. I see myself in each one of you. I am so sorry

school wasn't a haven for you as it was for me, and I am sorry your dreams were cut short. Truth and justice will prevail.

Thank you to my friends Erin Hanada, Jessica Maat, Joseph Solomon, Sam Gill, and Wilfred Russel. I will always cherish the time we shared, and I cannot thank you all enough for your support. Graduate school would not have been the same without you and thank you for the friendship that will last beyond our tenure here.

Thank you to my advisor, Professor William Evans. Your understanding and creativity helped me feel the magic of synthetic chemistry and for that I am grateful. Thank you to the Evans group, including Dr. Megan Dumas for training me when I first joined the group and for always being willing to support me and my research with a smile, Dr. Austin Ryan for the intellectual discussions and for challenging my thinking, Dr. Samuel Moehring for your friendship, for always lending a helping hand, and for being a kind leader of the lab, Sierra Ciccone for your friendship and teaching me that you shouldn't have to compromise who you are to belong in an academic setting, Dr. Amanda Chung for your friendship, warmth, kindness, and passion for creating a safe and welcoming community, Lauren Anderson-Sanchez for your drive, creative intellectualism, and refreshing authenticity, Will Moore for your contagious optimism and go-getter attitude, Joseph Nguyen for your frankness and quiet kindness, Kito Gilbert-Bass for keeping the magic of our chemistry alive, and Dr. Cary Stennet for your leadership and empathy. Thanks to Joe Ziller for crystallographic expertise.

Thank you to my committee members Professor Andy Borovik and Professor Jenny Yang. Andy, you always challenged me intellectually, which pushed me to be a better chemist. Jenny, you were the first professor I talked to at UCI and you always made me feel welcomed and wanted here.

VITA

Jessica Renee Kristianna White

2016	B.S. in Chemistry, University of Washington
2016-2017	National Institutes of Health Post-Baccalaureate Research Education Program Fellow, University of Washington
2017-2022	Teaching Assistant, Department of Chemistry, University of California, Irvine Courses taught include undergraduate general laboratory, undergraduate organic chemistry laboratory, and graduate organometallic chemistry
2022	Ph.D. in Chemsitry, University of California, Irvine

FIELD OF STUDY

Synthetic inorganic chemistry, particularly the isolation and reductive reactivity of rare-earth metal molecular complexes.

PUBLICATIONS

- "Reduction of Rare-Earth Metal Complexes Induced by γ Irradiation" William N. G. Moore, Jessica R. K. White, Justin C. Wedal, Filipp Furche, William J. Evans *Inorg. Chem.* **2022**, *61*, 17713-17718. DOI: 10.1021/acs.inorgchem.2c02857
- "A 9.2-GHz Clock Transition in a Lu(II) Molecular Spin Qubit Arising from a 3,467-MHz Hyperfine Interaction" Krishnendu Kundu, Jessica R. K. White, Samuel A. Moehring, Jason M. Yu, Joseph W. Ziller, Filipp Furche, William J. Evans, and Stephen Hill, *Nature Chemistry* **2022**, *14*, 392-397. DOI: 10.1038/s41557-022-00894-4
- "Crystallographic characterization of rare-earth cyanotriphenylborate complexes and the cyanoborates $[NCBPh_3]^{1-}$, $[NCBPh_2Me]^{1-}$, and $[NCBPh_2(\mu\text{-}O)BPh_2]^{1-}$" Megan T. Dumas, Jessica R. K. White, Joseph W. Ziller, and William J. Evans *Acta Crystallographica **2021**, E77*, 799-803. DOI: 10.1107/S2056989021006861
- "Mechanochemical C−H Bond Activation: Synthesis of the Tuckover Hydrides, $(C_5Me_5)_2Ln(\mu\text{-}H)(\mu\text{-}\eta^1\text{:}\eta^5\text{-}CH_2C_5Me_4)Ln(C_5Me_5)$ from Solvent-free Reactions of $(C_5Me_5)_2Ln(\mu\text{-}Ph)_2BPh_2$ with KC_5Me_5" David H. Woen, Jessica R. K. White, Joseph W. Ziller, William J. Evans. *Journal of Organometallic Chemistry* **2019**, *899*, 120885. DOI: 10.1016/j.jorganchem.2019.120885
- "An evolutionarily-conserved RNA structure in the functional core of the lincRNA Cyrano" Alisha N. Jones, Giuseppina Pisignano, Thomas Pavelitz, Jessica R. K. White, Martin Kinisu, Nicholas Forino, Dreycey Albin, Gabriele Varani. *RNA* **2020**, *26*, 1234-1246. DOI: 10.1261/rna.076117.120

ABSTRACT OF THE DISSERTATION

Exploring the Intricacies of Ancillary Ligand Effects on $4f^n5d^1$ Ln(II) Ions

by

Jessica Renee Kristianna White

Doctor of Philosophy in Chemistry

University of California, Irvine, 2022

Professor William J. Evans, Chair

This dissertation explores the effects of ancillary ligands on reductive lanthanide (Ln) chemistry and describes the isolation of Ln(II)-containing complexes with novel structural or magnetic properties. Chapter 1 demonstrates a molecular approach to developing qubits through the synthesis and reduction of the tris(aryloxide) Lu(III) complex, $Lu(OAr^*)_3$ (OAr^* = 2,6-Ad_2-4-^{t}Bu-$C_6H_2O^-$, where Ad is 1-adamantyl). Potassium reduction of $Lu(OAr^*)_3$ in the presence of 2.2.2-cryptand (crypt) generated the formally $4f^{14}5d^1$ Lu(II) complex, [K(crypt)][$Lu(OAr^*)_3$]. The OAr^* ligand greatly shielded the [Xe]$4f^{14}5d^1$ Lu^{2+} ion, which increased its thermal stability and enhanced the amount of *s* mixing into the $5d_{z^2}$ SOMO. The increase in *s* character led to a large hyperfine clock transition in its EPR spectrum and one of the largest hyperfine interactions ever observed for a molecular system.

In contrast to Chapter 1, which described the synthesis of the sterically saturated Lu(II) complex, Chapter 2 explores the limits of steric *unsaturation* of isolable Ln(II) ions by employing one of the smaller cyclopentadienyl ligands, $(C_5H_4Me)^{1-}$. The reduction of $Cp^{Me}_3Ln(THF)$ (Cp^{Me} = C_5H_4Me; Ln = Nd, Gd) with KC_8 in the presence of 18-crown-6 generated the [(18-crown-6)K(μ-(Cp^{Me}))K(18-crown-6)][$(Cp^{Me})_3Ln$] complexes, which were isolated and characterized by X-ray crystallography and EPR spectroscopy. The degree of

steric saturation was quantified and comparative analysis found that these complexes were the least sterically saturated Ln(II) complexes reported to date. These results corroborated the hypothesis that degree of shielding of the Ln(II) ion by its ancillary ligands has an influence on the thermal stability of the complex.

Chapter 3 describes the synthesis of unusual reduced arene complexes of the Ln(II) ions. These bimetallic lanthanide complexes containing reduced bridging ligands may be of value to the field of single-molecule magnet research because these compounds have shown remarkably enhanced magnetic exchange interactions. Previously, the only four crystallographically characterized examples of bimetallic lanthanide (II) complexes containing reduced arene bridging ligands contain cyclopentadienyl ancillary ligands. Reduction of the tris(amide) complexes, $Ln(NR_2)_3$ (Ln = La, Ce; R=$SiMe_3$), with potassium in the presence of toluene and crypt allows the isolation of the reduced arene bridged complexes, $[K(crypt)]_2[\{(R_2N)_2Ln^{II}\}_2(\mu\text{-}\eta^6\text{:}\eta^6\text{-}C_6H_5Me)]$, with amide ancillary ligands. The crystallographic and spectroscopic data, as well as computational analysis are consistent with the presence of two Ln(II) ions bridged by a toluene diradical dianion. Reduction of $[(THF)(R_2N)_2Tb]_2(\mu\text{-}Cl)_2$ with KC_8 in the presence of toluene and crypt allows the isolation of the first terbium reduced arene bridged complex, $[K(crypt)]_3[\{(R_2N)_2Tb^{II}\}_2(\mu\text{-}\eta^6\text{:}\eta^6\text{-}C_6H_5Me)][K(NR_2)_2(THF)_2]$.

INTRODUCTION

Lanthanide (Ln) complexes have little to no covalent character in their bonding due to the limited radial extension of their 4*f* orbitals, which do not extend past their inert [Xe] core.[1] This electronic structure leads to large, unquenched spin-orbit coupling and the highest magnetic moments of any elements on the periodic table. These properties make the lanthanides excellent candidates for technologies needing strong, dense magnetism such as MRI imaging, wind turbines, information storage, and quantum computing.

However, the ionic nature of lanthanide bonding and the relative inertness of the 4*f* orbitals led academics to believe that the chemistry of the lanthanides was limited, a textbook going as far to summarize their chemistry as follows: "Lanthanum has only one important oxidation state in aqueous solution, the +3 state. With few exceptions, this tells the whole boring story about the other lanthanides."[2] Though dismissive, the invariance of stable oxidation states across the lanthanides was the most widely told story for the first 90 years of lanthanide chemistry, Table 0.1. Other than the +3 oxidation state that is stable for all molecular lanthanide complexes, the only other isolable oxidation states at the time were Ce(IV), Sm(II), Eu(II), and Yb(II).[3]

Table 0.1: Valence electrons and accessible oxidation states of early lanthanide chemistry

	La	**Ce**	**Pr**	**Nd**	**Pm**	**Sm**	**Eu**	**Gd**	**Tb**	**Dy**	**Ho**	**Er**	**Tm**	**Yb**	**Lu**
Ln^{3+} $4f^n$ electron configuration	0	1	2	3	4	5	6	7	8	9	10	11	12	13	14
Valence electrons	3	4	5	6	7	8	9	10	11	12	13	14	15	16	17
Accessible Oxidation States	3	4 3	3	3	3	3 2	3 2	3	3	3	3	3	3	3 2	3

It wasn't until the 1990s that the molecular redox chemistry of the lanthanides proved to be not so boring when Cloke *et al.* isolated the first lanthanide complexes with an oxidation state of zero[4–6] and Bochkarev *et al.* demonstrated that molecular complexes of Nd,[7] Dy,[8] and Tm[9] could be isolated in the +2 oxidation state. Years later, Lappert *et al.* expanded the +2 oxidation state to lanthanum.[10] Following up on Lappert's discovery, the Evans group demonstrated that Ln(II) molecular complexes for all lanthanides (except Pm which has not been studied due to its radioactivity), could be isolated from LnA_3/M reduction reactions (A = anion, M = alkali metal) with silyl-substituted cyclopentadienyl ancillary ligands, eq 0.1.[11–13]

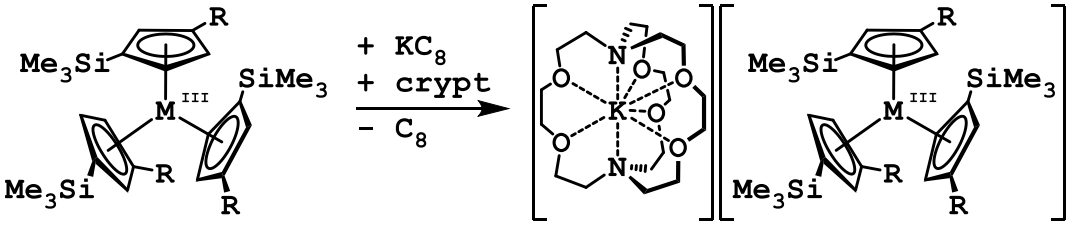

(0.1)

R = H, M = Y, La, Ce, Pr, Nd, Gd, Tb, Dy, Ho, Er, Lu
R = $SiMe_3$, M = La, Ce Pr, Nd

These compounds were a breakthrough result, as before it was believed that only Eu^{2+}, Yb^{2+}, Sm^{2+},[3] Tm^{2+},[9] Dy^{2+}, and Nd^{2+},[7] could form isolable, crystallographically characterizable Ln(II) complexes due to highly negative Ln^{3+}/Ln^{2+} reductive potentials calculated for a $4f^n \rightarrow 4f^{n+1}$ reduction for the other metals.[14–17] However, density functional theory (DFT) calculations supported crystallographic, magnetic, and spectroscopic data, which all suggested that these new Ln(II) ions adopted a $4f^n5d^1$ ground state configuration instead. In the trigonal coordination environment of these complexes, the $5d_{z^2}$ orbital is similar in energy to the $4f$ orbitals.[11–13,18] Following this result, it was established that these new Ln(II) ions can be isolated in molecular complexes of a variety of coordination

environments, such as with alkyl-substituted cyclopentadienyl ligands,[19–21] amide[22] and aryloxide[23] ligands, and as linear metallocenes.[24]

Table 0.2: Valence electrons and accessible oxidation states as of 2022

	La	Ce	Pr	Nd	Pm	Sm	Eu	Gd	Tb	Dy	Ho	Er	Tm	Yb	Lu
Ln^{3+} $4f^n$ electron configuration	0	1	2	3	4	5	6	7	8	9	10	11	12	13	14
Valence electrons	3	4	5	6	7	8	9	10	11	12	13	14	15	16	17
Accessible Oxidation States	3 2	4 3 2	4 3 2	3 2 0	3	3 2	3 2	3 2 0	4 3 2 0	3 2 0	3 2 0	3 2 0	3 2	3 2	3 2 0

Dissertation Outline

This dissertation explores the effects of ancillary ligands on reductive lanthanide (Ln) chemistry and describes the isolation of Ln(II)-containing complexes with novel structural or magnetic properties. Chapter 1 demonstrates a molecular approach to developing qubits through the synthesis and reduction of the bulky tris(aryloxide) Lu(III) complex, $Lu(OAr^*)_3$ (OAr^* = 2,6-Ad_2-4-^{t}Bu-$C_6H_2O^-$, where Ad is 1-adamantyl). Potassium reduction of $Lu(OAr^*)_3$ in the presence of 2.2.2-cryptand (crypt) generated the formally $4f^{14}5d^1$ Lu(II) complex, [K(crypt)][$Lu(OAr^*)_3$] which exhibits a large hyperfine clock transition frequency in its EPR spectrum. It has one of the largest hyperfine interactions ever observed for a molecular system. Chapter 2 explores the limits of steric unsaturation of isolable Ln(II) ions by employing one of the smaller cyclopentadienyl ligands, $(C_5H_4Me)^{1-}$. The reduction of $Cp^{Me}{}_3Ln(THF)$ (Cp^{Me} = C_5H_4Me; Ln = Nd, Gd) with KC_8 in the presence of 18-crown-6 generated [(18-crown-6)K(μ-(Cp^{Me}))K(18-crown-6)][(Cp^{Me})$_3$Ln] complexes, which were the least sterically saturated Ln(II) complexes isolated so far. Chapter 3 describes the discovery

that reduced arene complexes are readily formed in lanthanide reduction reactions that form Ln(II) ions. Reduction of the tris(amide) complexes, $Ln(NR_2)_3$ (Ln = La, Ce; R=$SiMe_3$), with potassium in the presence of toluene and crypt allows the isolation of the Ln(II) reduced arene bridged complexes, $[K(crypt)]_2[\{(R_2N)_2Ln^{II}\}_2(\mu\text{-}\eta^6\text{:}\eta^6\text{-}C_6H_5Me)]$. Reduction of $[(THF)(R_2N)_2Tb]_2(\mu\text{-}Cl)_2$ with KC_8 in the presence of toluene and crypt allows the isolation of the first terbium reduced arene bridged complex, $[K(crypt)]_3[\{(R_2N)_2Tb^{II}\}_2(\mu\text{-}\eta^6\text{:}\eta^6\text{-}C_6H_5Me)][K(NR_2)_2(THF)_2]$.

References

(1) Freeman, A. J.; Watson, R. E. *Phys. Rev.* **1962**, *127* (6), 2058–2075.

(2) Pimentel, G. C.; Spratley, R. D. *Understanding Chemistry*; Holden-Day: San Francisco, 1971.

(3) Meyer, G. *Chem. Rev.* **1988**, *88* (1), 93–107.

(4) Cloke, F. G. N. *Chem. Soc. Rev.* **1993**, *22* (1), 17–24.

(5) Arnold, P. L.; Cloke, F. G. N.; Hitchcock, P. B. *Chem. Commun.* **1997**, No. 5, 481–482.

(6) Anderson, D. M.; Cloke, F. G. N.; Cox, P. A.; Edelstein, N.; Green, J. C.; Pang, T.; Sameh, A. A.; Shalimoff, G. *J. Chem. Soc. Chem. Commun.* **1989**, *0* (1), 53–55.

(7) Bochkarev, M. N.; Fedushkin, I. L.; Dechert, S.; Fagin, A. A.; Schumann, H. *Angew. Chem. Int. Ed.* **2001**, *40* (17), 3176–3178.

(8) Bochkarev, M. N.; Fagin, A. A. *Chem. Eur. J.* **1999**, *5* (10), 2990–2992.

(9) Bochkarev, M. N.; Fedushkin, I. L.; Fagin, A. A.; Petrovskaya, T. V.; Ziller, J. W.; Broomhall-Dillard, R. N. R.; Evans, W. J. *Angew. Chem. Int. Ed.* **1997**, *36* (1–2), 133–135.

(10) Hitchcock, P. B.; Lappert, M. F.; Maron, L.; Protchenko, A. V. *Angew. Chem. Int. Ed.* **2008**, *47* (8), 1488–1491.

(11) MacDonald, M. R.; Bates, J. E.; Ziller, J. W.; Furche, F.; Evans, W. J. *J. Am. Chem. Soc.* **2013**, *135* (26), 9857–9868.

(12) MacDonald, M. R.; Bates, J. E.; Fieser, M. E.; Ziller, J. W.; Furche, F.; Evans, W. J. *J. Am. Chem. Soc.* **2012**, *134* (20), 8420–8423.

(13) MacDonald, M. R.; Ziller, J. W.; Evans, W. J. *J. Am. Chem. Soc.* **2011**, *133* (40), 15914–15917.

(14) Mikheev, N. B.; Auerman, L. N.; Rumer, I. A.; Kamenskaya, A. N.; Kazakevich, M. Z. *Russ.*

Chem. Rev. **1992**, *61*, 990.

(15) Nugent, L. J.; Baybarz, R. D.; Burnett, J. L.; Ryan, J. L. *J. Phys. Chem.* **1971**, *77* (12), 1528–1539.

(16) Morss, L. R. *Chem. Rev.* **1976**, *76* (6), 827–841.

(17) Johnson, D. A. *J. Chem. Soc. Dalt. Trans.* **1974**, 1671–1675.

(18) Fieser, M. E.; Macdonald, M. R.; Krull, B. T.; Bates, J. E.; Ziller, J. W.; Furche, F.; Evans, W. J. *J. Am. Chem. Soc.* **2015**, *137* (1), 369–382.

(19) Angadol, M. A.; Woen, D. H.; Windorff, C. J.; Ziller, J. W.; Evans, W. J. *Organometallics* **2019**, *38* (5), 1151–1158.

(20) Jenkins, T. F.; Woen, D. H.; Mohanam, L. N.; Ziller, J. W.; Furche, F.; Evans, W. J. *Organometallics* **2018**, *37* (21), 3863–3873.

(21) Huh, D. N.; Ziller, J. W.; Evans, W. J. *Dalt. Trans.* **2018**, *47*, 17285–17290.

(22) Ryan, A. J.; Darago, L. E.; Balasubramani, S. G.; Chen, G. P.; Ziller, J. W.; Furche, F.; Long, J. R.; Evans, W. J. *Chem. Eur. J.* **2018**, *24*, 7702–7709.

(23) Moehring, S. A.; Beltrán-Leiva, M. J.; Páez-Hernández, D.; Arratia-Pérez, R.; Ziller, J. W.; Evans, W. J. *Chem. Eur. J.* **2018**, *24*, 18059–18067.

(24) Gould, C. A.; McClain, K. R.; Yu, J. M.; Groshens, T. J.; Furche, F.; Harvey, B. G.; Long, J. R. *J. Am. Chem. Soc.* **2019**, *141* (33), 12967–12973.

CHAPTER 1

The Synthesis and Isolation of a Lu(II) Molecular Spin Qubit*

Introduction

Quantum computing is a rapidly emerging technology that aims to solve problems that are too complex for classical computers. The fundamental building block of a quantum computer is the physical quantum bit, or qubit. Unlike a classical computing bit, which could be in the state of "0" or "1", a qubit can be "0", "1", or a superposition of both "0" and "1" states simultaneously. A qubit can be any two-state quantum system. One of the simplest examples is the S = ½ spin of an unpaired electron with either a "spin up" or "spin down" state. One of the most heavily studied qubits is the $^{171}Yb^{+}$ ion (formally [Xe]$4f^{14}6s^{1}$), which can be trapped and organized into arrays with controllable interactions.[1] Aside from the trapped ion approach, other approaches to qubit design include superconducting circuits,[2] linear optic circuits,[3] solid-state topological systems,[4] and arrangements of individual spins on surfaces.[5–8] Challenges facing these strategies include scaling up and tunability of the qubit's quantum properties. Coordination chemistry can be utilized to address these challenges,[9,10] but the utilization of coordination complexes brings obstacles of their own. The designer environment of a molecular qubit is a double-edged sword; it can be tuned to enhance the qubit's properties, but it can also cause decoherence, or coupling of the spin with the environment, losing the quantum nature of the qubit.

* This work was in collaboration with Dr. Krishnendu Kundu of the Hill group at the Florida State University National High Magnetic Field Laboratory, who conducted the EPR experiments, and Dr. Jason Yu of the Furche group at UCI, who performed the electronic structure calculations. This work has been published elsewhere; Kundu, K., White, J.R.K., Moehring, S.A., Yu, J.M, Ziller, J.W., Furche, F., Evans, W.J., Hill, S. A 9.2-GHz clock transition in a Lu(II) molecular spin qubit arising from a 3,467-MHz hyperfine interaction. *Nat. Chem.* **14**, 392–397 (2022).

Decoherence can be minimized through the engineering of atomic clock transitions.[5,11–14] For an S = ½ spin system, the two spin states lose degeneracy upon the application of a magnetic field, B_0, due to the Zeeman effect. The transition frequency f between these two states depends linearly on B_0, Figure 1.1. The magnetic noise brought on by decoherence causes f to fluctuate and lowers the lifetime of the spin. A clock transition occurs at an avoided crossing of the two Zeeman levels, where f is insensitive to the magnetic field, or $df/dB_0 \rightarrow 0$. One can utilize this feature of clock transitions to shield a molecular qubit from magnetic noise and enhance the lifetime of the qubit if the clock transition is at an operational frequency.

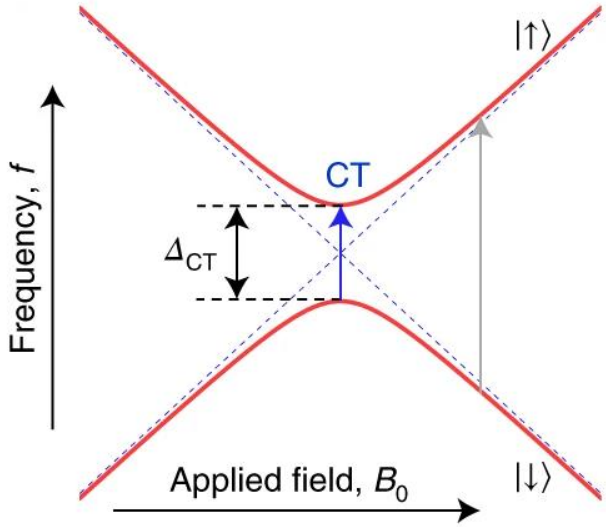

Figure 1.1. Schematic f versus B_0 energy diagram for a two-state quantum system (spin-up, |↑⟩ , spin-down, |↓⟩) illustrating the concept of a clock transition. The clock transition (blue arrow) occurs at the gap minimum, Δ_{CT}, whereas normal EPR transitions occur away from this region (grey arrow).

A new type of molecular qubit has been found through the discovery that $4f^n$ Ln(III) complexes of Ln = La, Ce, Pr, Gd, Tb, Ho, Er and Lu in the appropriate ligand environments

can be reduced to $4f^n5d^1$ Ln(II) complexes.[15–19] The new Ln(II) ions differ from the traditional $4f^{n+1}$ Ln(II) previously found for Eu, Yb, Sm and Tm.[17,20] This electronic structure has provided an alternative type of rare-earth electron configuration for development in quantum information science. In particular, the La(II) and Lu(II) congeners feature closed shell core configurations ([Xe] and [Xe]$4f^{14}$, respectively) and a single $S = ½$ unpaired electron residing in an orbital with mixed $5d/6s$ character. By varying the ligands in these Ln(II) complexes, synthetic control over the degree of *s*-orbital character that dominates the Fermi contact interaction with the associated nucleus provides a means of tuning the hyperfine interaction strength, therefore tuning the clock transition frequency and coherence time and thus reducing the sensitivity to magnetic noise.[21,22] As an added bonus, the dominant isotopes of both metals have large $I = {}^7/_2$ nuclear moments (99.9% and 97.4% natural abundance for ^{139}La and ^{175}Lu, respectively), which further enhances the corresponding clock transition frequency.[5,21] Moreover, increased *s*-orbital character minimizes spin-orbit coupling (SOC), resulting in reduced spin–lattice relaxation relative to most Ln species with spin–orbital moments $J > ½$.[23] These factors give rise to a molecular qubit platform similar to the $^{171}Yb^+$ ion (formally [Xe]$4f^{14}6s^1$, $I = ½$) that is heavily studied in quantum information science community,[1] but with the added benefit of chemical tunability.

Potassium reduction of the tris(cyclopentadienyl) Lu(III) complex, Cp'_3Lu ($Cp' = C_5H_4SiMe_3$) in the presence of 2.2.2-cryptand (crypt) generates a product, [K(crypt)][Cp'_3Lu] (**1**), containing a Lu(II) ion whose electron configuration is formally $4f^{14}5d^1$ based on density functional calculations.[16] The X-band (f = 9.7 GHz, $B_0 < 1$ T) EPR spectrum of complex **1** displays an eight-line pattern due to the lone unpaired electron ($S = ½$) and its hyperfine coupling with the $I = {}^7/_2$ ^{175}Lu isotope. The average hyperfine

coupling constant, A_{iso} = 428.5 G, was the largest observed for any Lu complex, suggesting significant *s*-orbital character in **1**.[24,25]

This chapter describes the synthesis of the tris(aryloxide) Lu(III) complex, $Lu(OAr^*)_3$ (OAr^* = 2,6-Ad_2-4-^{t}Bu-$C_6H_2O^-$, where Ad is 1-adamantyl). Similar to complex **1**, potassium reduction of $Lu(OAr^*)_3$ in the presence of crypt also generates the formally $4f^{14}5d^1$ Lu(II) complex, [K(crypt)][$Lu(OAr^*)_3$]. Interestingly, unlike complex **1**, the X-band EPR spectrum does not display the expected eight-line pattern. Because the hyperfine constants of the yttrium (II) tris(aryloxide) [K(crypt)][$Y(OAr^*)_3$] (A_{iso} = 156.5 G)[19] and tris(amide) [K(crypt)][$Y(NR_2)_3$] (A_{iso} = 110 G)[26] complexes are much larger than that of tris(cyclopentadienyl) complex [K(crypt)][YCp'_3][16] (A_{iso} = 36.6 G), it was predicted that the hyperfine constants of the corresponding Lu(II) complexes were much larger than the 428.5 G value of **1**. Thus, in collaboration with Dr. Krishnendu Kundu of the Hill group at the Florida State University National High Magnetic Field Laboratory, EPR investigations including higher-field (W band: f = 94 GHz and B_0 = 3–4 T) studies were conducted on a series of Ln(II) complexes: [K(crypt)][$La(OAr^*)_3$] (**2**), [K(crypt)][$Lu(NR_2)_3$] (**3**, R = $SiMe_3$), and [K(crypt)][$Lu(OAr^*)_3$] (**4**). It was found that **4** exhibits a very large hyperfine coupling constant and a large clock transition observable at X-band frequency. In collaboration with Dr. Jason Yu of the Furche group at UCI, electronic structure calculations were performed on the series of complexes and investigations were performed on the degree of *s*-mixing and any correlations it had with the hyperfine coupling interactions. Full details of the EPR studies and calculations are published elsewhere,[27] but are summarized in this chapter.

Results and Discussion

Lu(OAr*)$_3$. Similar to the synthesis of the yttrium analogue,[19] Lu(OAr*)$_3$ was synthesized via the protonolysis of 1.2 eq of Lu(NR$_2$)$_3$ with 3 eq HOAr* in toluene at 100 °C under an argon atmosphere, eq 1.1.

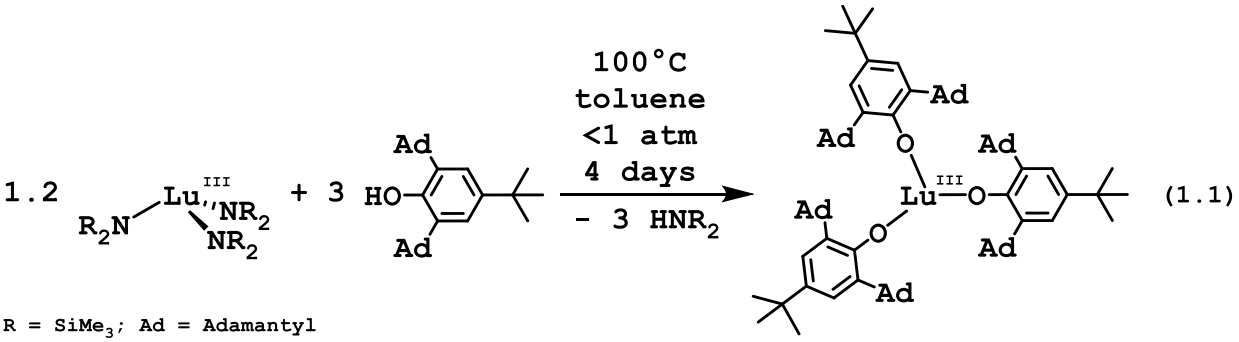

R = SiMe$_3$; Ad = Adamantyl

Unlike the yttrium analogue which took two days at ambient pressure, the reaction had to be heated under reduced pressure for 4 days to obtain higher yields of purer quality. The colorless Lu(OAr*)$_3$ precipitated from the toluene reaction solution at −35 °C. The precipitate was washed with cold (−35 °C) toluene, hexane and pentane, yielding a bright white powder which was identified as Lu(OAr*)$_3$ via ^{1}H NMR and IR spectroscopies, Figures S1.2 and S1.4, respectively. However, an O–H stretch at 3631 cm^{-1} observed in the IR spectrum and additional peaks in the associated region of the ^{1}H NMR spectrum indicated that residual HOAr* persisted. Lu(OAr*)$_3$ must be recrystallized, and the crystals must be washed multiple times to get rid of this impurity.

Single crystals suitable for X-ray diffraction were grown from boiling hexane. Lu(OAr*)$_3$ crystallizes in the $P2_1/n$ space group (Table A1) and has similar unit cell constants as the previously reported Y(OAr*)$_3$.[19] Like the Y analogue, Lu(OAr*)$_3$ is pseudo-C$_3$ symmetric, and the geometry about the Lu atom is slightly pyramidalized with the Lu atom displaced from O$_3$ plane by 0.500 Å, Figure 1.2.

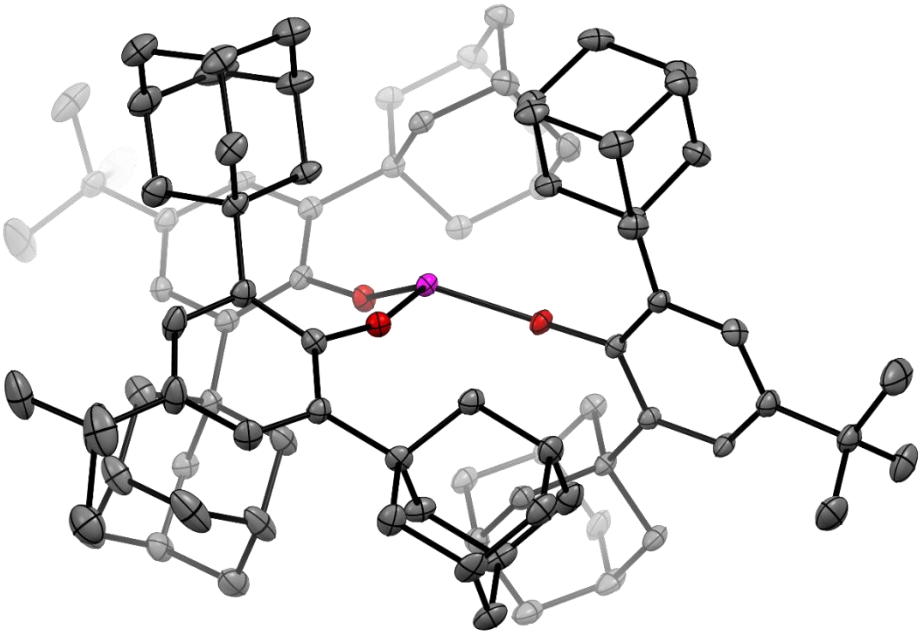

Figure 1.2. Thermal ellipsoid plot of $Lu(OAr^*)_3$ drawn at the 50% probability level. One hexane solvent molecule and H atoms are omitted for clarity. Color code: Grey = C, Red = O, Pink = Lu.

[K(crypt)][Lu(OAr*)$_3$] (**4**). A cloudy colorless Et_2O mixture of $Lu(OAr^*)_3$ and 1 equivalent of crypt was cooled to −35 °C and added to a vial containing KC_8, also chilled to −35 °C. The cloudy colorless mixture instantly turned dark blue. This mixture was left to react for 1 hour at −35 °C with occasional swirling before the KC_8 was filtered from the dark blue solution using a Kimwipe-packed glass pipette. The solvent was slowly removed *in vacuo* to yield dark blue X-ray quality single crystals of $[K(crypt)][Lu(OAr^*)_3]\cdot 3Et_2O$, eq 1.2, Figure 1.4.

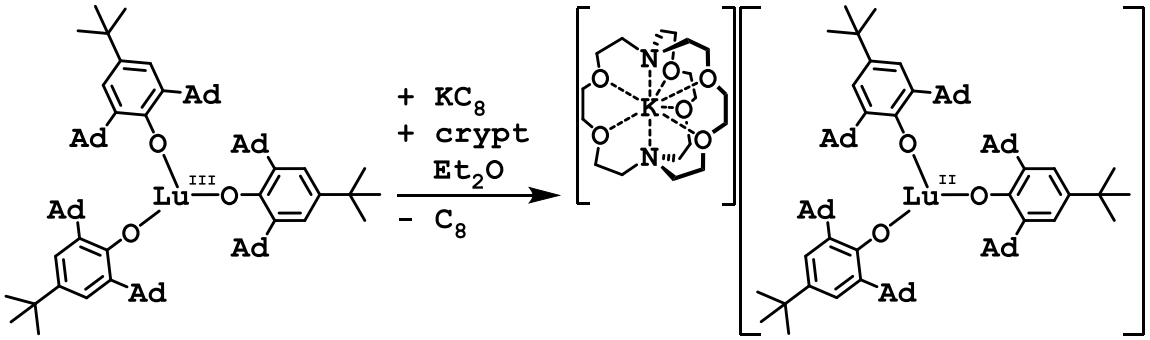

Like the yttrium analogue,[19] [K(crypt)][Lu(OAr*)$_3$] is stable at room temperature for several hours. The reduction of Lu(OAr*)$_3$ can also be performed at room temperature to successfully isolate [K(crypt)][Lu(OAr*)$_3$], but with lower yield than the cold reduction protocol. This contrasts to the only other reported Lu(II) compound, [K(crypt)][Cp′$_3$Lu], **1**, which decomposes within 2 hours at room temperature.[16] The room-temperature UV-visible spectrum of the dark blue [K(crypt)][Lu(OAr*)$_3$] is depicted in Figure 1.3. There is a broad absorption centered at 605 nm with an extinction coefficient of 3197 $M^{-1}cm^{-1}$. There is also a broad shoulder at 456 nm with an extinction coefficient of 1777 $M^{-1}cm^{-1}$. These peaks are slightly lower absorbing than and are red-shifted from peaks observed for the dark maroon-purple [K(crypt)][Cp′$_3$Lu].[16]

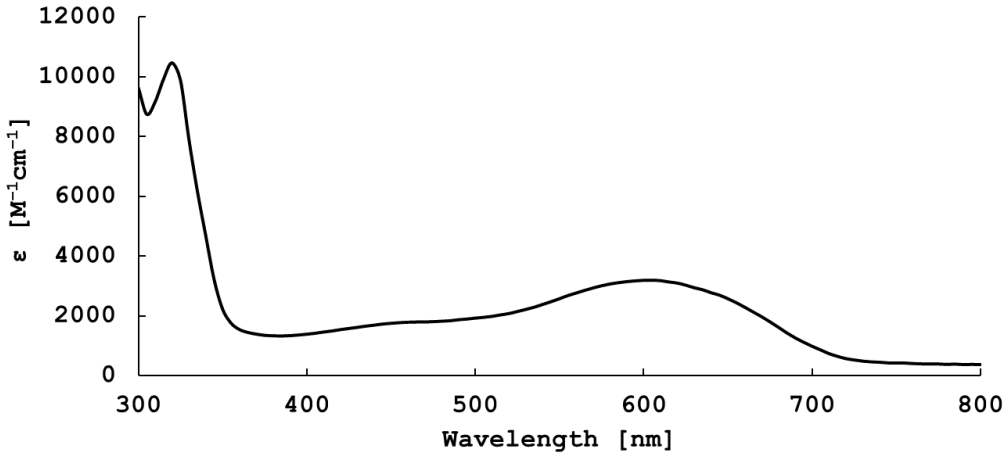

Figure 1.3. UV-visible spectrum of a 1 mM THF solution of [K(crypt)][Lu(OAr*)$_3$] collected at room temperature.

[K(crypt)][Lu(OAr*)$_3$] (**4**) crystallizes in the $P\bar{1}$ space group (Table A2) and is isomorphous with [K(crypt)][Y(OAr*)$_3$].[19] Interestingly, **4** is only the second crystallographically characterized Lu(II) complex, the other being [K(crypt)][Cp′$_3$Lu].[16] Like the Y analogue, **4** is more planar than the Lu(III) precursor: the Lu center is only 0.147 Å above the O$_3$ plane. The average of the 2.062(2), 2.069(2), and 2.074(2) Å Lu-O distances in **4** is 0.056 Å larger than the average of the 2.002(2), 2.014(2), and 2.020(2) Å Lu-O lengths in Lu(OAr*)$_3$. The analogous difference in the yttrium analogs is 0.06 Å.[19] Differences less than 0.1 Å are typical when comparing 4f^n Ln(III) and 4f^{n}5d^1 Ln(II) ions.[16]

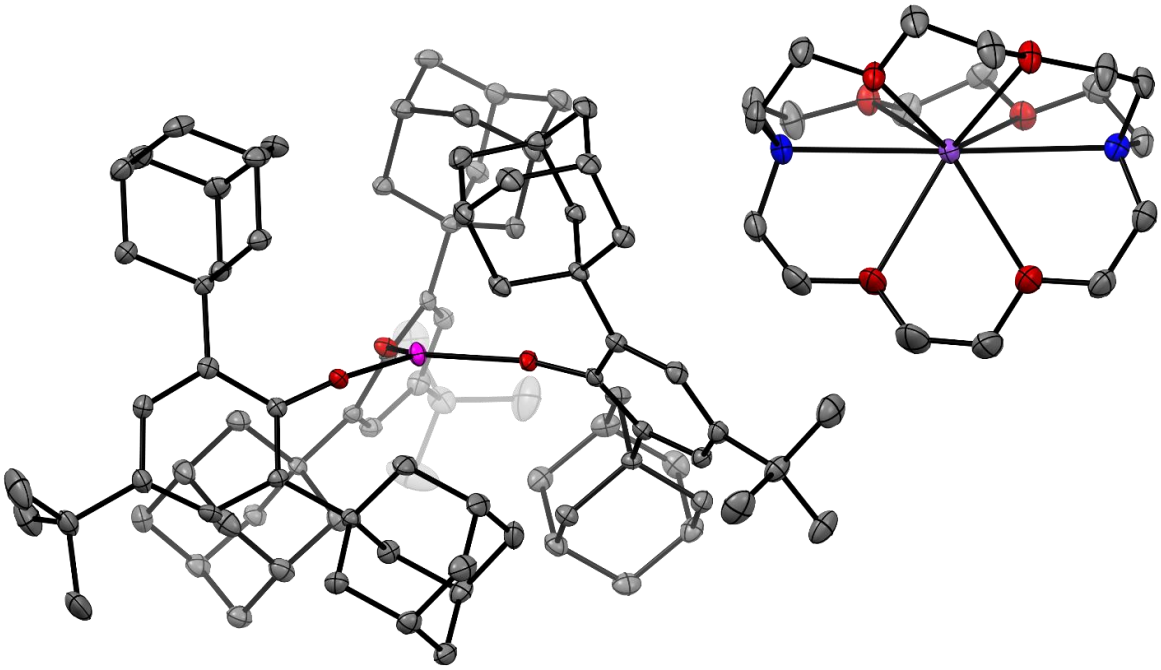

Figure 1.4. Thermal ellipsoid plot of [K(crypt)][Lu(OAr*)$_3$] (**4**) drawn at the 50% probability level. Three ether solvent molecules and H atoms are omitted for clarity. Color code: Grey = C, Red = O, Blue = N, Pink = Lu, Purple = K.

Guzei analysis. Steric saturation about the metal center in Ln(III) and Ln(II) complexes plays an important role in their stability and isolation. Solid-G analysis by Guzei[28] was employed to quantify the degree of steric saturation about the Lu(III) and Lu(II) ions in

$Lu(OAr^*)_3$ and $[K(crypt)][Lu(OAr^*)_3]$, respectively. The Solid-G program converts the calculated ligand solid angles into a percentage (the *G* parameter) to demonstrate how much of the coordination sphere of the metal center in a metal complex is shielded by its ligands. For instance, a percentage, or *G* value, of 100% indicates that the coordination sphere of the metal ion is fully saturated, and its ligands completely shield the metal from an outside molecule. Whereas a low *G* value indicates that the ligands only shield the metal ion by X%, leaving (100-X)% of the coordination sphere open for an outside molecule to reach the metal center. The *G* values of $Lu(OAr^*)_3$ and **4** were calculated to be 92% and 91%, respectively, Table 1.1. These *G* values are similar to those reported for $Y(OAr^*)_3$, 92%, and $[K(crypt)][Y(OAr^*)_3]$, 90%.[19]

Table 1.1: Selected structural parameters of $Lu(OAr^*)_3$ and $[K(crypt)][Lu(OAr^*)_3]$ and comparison of G values of rare-earth metal complexes. δ is the displacement of Lu from the O_3 plane in Å. R = $N(SiMe_3)_2$. Cp^{tet} = $C_5(CH_3)_4$. HOAr = 2,6-di-*t*-butyl-phenoxide.

Complex[Ref]	***G* [%]**	**δ**
$Lu(OAr^*)_3$	92	0.500
$[K(crypt)][Lu(OAr^*)_3]$	91	0.147
$Y(OAr^*)_3$[19]	92	0.431
$[K(crypt)][Y(OAr^*)_3]$[19]	90	0.125
Cp'_3Lu[29]	88	
$[K(crypt)][Cp'_3Lu]$[16]	88	
Cp^{tet}_3Lu[30]	87	
$Lu(NR_2)_3$[31]	86	
$Ln(OAr)_3$[32]	84	

The high *G* values of 92 and 91 % for $Lu(OAr^*)_3$ and $[K(crypt)][Lu(OAr^*)_3]$, **4**, respectively, indicate that the aryloxide ligands in **4** greatly shield the Lu ions. This may be a reason for the unusual thermal stability of **4**. Compared to other Ln(II) complexes which generally decompose rapidly at room temperature, **4** is stable at room temperature for several hours. Compared to other Lu(III) complexes, $Lu(OAr^*)_3$ is the most sterically

saturated. $Lu(DBP)_3$ (DBP = 2,6-di-t-butyl-phenoxide), another Lu aryloxide complex, is noticeably less sterically saturating with a *G* value of 84%, suggesting that the adamantyl substituents on the aryloxide of $Lu(OAr^*)_3$ are important in shielding the Lu center. It is important to note that the maximization of *G* is not necessarily the best strategy for isolating Ln(II) complexes, as Solid-G analysis does not take the countercation into effect, and the cation has shown to play an important role in the stability and isolation of Ln(II) complexes.[18] Also, different ligand sets seem to have their own optimum *G* value, so the most sterically saturated Ln(II) complex in a series is not necessarily the most stable.[33] However, even if steric saturation is not the most important factor in all ligand systems, the great amount of steric bulk that the adamantyl substituents provide in the OAr* ligand seems to be important for the stability of Ln(II) aryloxide complexes.

EPR Studies. Pulsed electron-spin echo (ESE) measurements were performed by Dr. Krishnendu Kundu of the Hill group at the Florida State University National High Magnetic Field Laboratory at W-band frequency, $f = 94$ GHz on frozen 10 mM THF solutions of a series of Ln(II) complexes: $[K(crypt)][La(OAr^*)_3]$ (**2**), $[K(crypt)][Lu(NR_2)_3]$ (**3**, $R = SiMe_3$), and $[K(crypt)][Lu(OAr^*)_3]$ (**4**), Figure S1.5. As seen in Table 1.2, the hyperfine interaction strength increases from $A_{iso}(\mathbf{2}) < A_{iso}(\mathbf{3}) < A_{iso}(\mathbf{4})$. Complex **4** was found to have a huge hyperfine interaction, $A_{iso} = 3{,}467 \pm 50$ MHz. The only larger molecular hyperfine interaction in the literature is the 3,799-MHz value reported for a Bi(II) radical,[34,35] although theoretical predictions of large hyperfine interactions have been suggested for Tb(II).[36] These large hyperfine interactions gives rise to observable hyperfine clock transitions in the X-band EPR spectra of **4**, Figure S1.6c**,** which ranges from 8.92 to 9.25 GHz. This frequency range is close to the frequency of the standard ^{133}Cs atomic clock (9.2 GHz) and can be compared to the

12.6-GHz hyperfine clock transition found for the $^{171}Yb^{+}$ ion qubit[1] that is also used as a frequency standard.[37] The clock transition of **4** exceeds all known solid-state and molecular hyperfine clock transition frequencies, for example, ^{209}Bi donors in Si.[21]

Table 1.2: Hyperfine Coupling Strengths

Complex	A_{iso} [MHz]	A_{iso} [Gauss]
2	1,840 ± 25	684±18
3	2,443 ± 50	906± 19
4	3,467 ± 50	1275± 18

Electronic Structure Calculations. To analyze the electronic structure responsible for the observed hyperfine interactions, scalar relativistic exact two-component (x2c) density functional theory (DFT) calculations[38] were performed by Dr. Jason Yu of the Furche group at UCI. The converged ground states for each compound are consistent with the electronic configurations of [Xe]$5d^1$ for **2** and [Xe]$4f^{14}5d^1$ for **3** and **4**. The spin density for the three compounds was found to arise almost exclusively from the singly occupied molecular orbital (SOMO) in every case, with predominant $5d_{z^2}$ character and varying degrees of 6*s*-orbital mixing. Isotropic hyperfine coupling constants for the Ln nuclei were obtained from the computed spin density using both point and finite nuclear charge models.[39] Although the calculations systematically overestimate the coupling strength, the experimental ordering, **2** < **3** < **4**, is reproduced from natural population analysis[40] of the SOMO. Two factors govern the magnitude of the hyperfine coupling in these compounds:[41] (1) the larger amplitude of the SOMO at the nucleus due to increasing nuclear charge and (2) an increased *s* character in the SOMO from La to Lu caused by greater energetic overlap between the 5*d* and 6*s* valence shell. The latter observation suggests that the *s*-orbital

character, $n(s)$, of the SOMO is a useful descriptor of electronic structure for designing similar compounds with large hyperfine coupling.

Conclusion

The bulky aryloxide ligand, 2,6-Ad_2-4-^{t}Bu-$C_6H_2O^-$ (OAr*) allowed the synthesis, isolation, and characterization of the Lu(II) complex, [K(crypt)][Lu(OAr*)$_3$]. The OAr* ligand greatly shielded the [Xe]$4f^{14}5d^1$ Lu^{2+} ion, which increased its thermal stability and the amount of *s* mixing into the $5d_{z^2}$ SOMO. The increase in *s* character led to a large hyperfine clock transition frequency and one of the largest hyperfine interactions for a molecular system. This work demonstrates a molecular approach to developing qubits comparable to current quantum computing technologies.[1]

Experimental Details

All manipulations and syntheses described below were conducted with the rigorous exclusion of air and water using standard Schlenk line and glovebox techniques under an argon atmosphere, unless stated otherwise. Solvents were sparged with UHP argon and dried by passage through columns containing Q-5 and molecular sieves prior to use. Potassium bis(trimethylsilyl)amide (KNR_2, R = $SiMe_3$) (Aldrich, 98%), was dissolved in toluene, centrifuged to remove tacky yellow insoluble material, and solvent was removed under reduced pressure before use. 2.2.2-Cryptand (crypt, Merck) was placed under vacuum (10^{-5} torr) for 12 h before use. Lu(NR_2)$_3$[42] and $HOAr^{Ad,Ad,t\text{-}Bu}$ (HOAr*)[43] were prepared according to the literature procedures. Deuterated NMR solvents were dried over NaK alloy, degassed by three freeze-pump-thaw cycles, and vacuum transferred before use. $^{13}C\{^1H\}$ NMR spectra were obtained on a Bruker AVANCE600 spectrometer with a BBO probe operating at 150 MHz for ^{13}C at 298 K and referenced internally to residual protio-solvent

resonances. ^{1}H NMR spectra were obtained on a Bruker CRYO500 MHz spectrometer with a TCI probe at 25 °C and referenced internally to residual protio-solvent resonances. UV/Vis spectra were collected in THF at 298 K using a Varian Cary 50 Scan UV/Vis spectrophotometer. Infrared (IR) transmittance measurements were taken as compressed solids on an Agilent Cary 630 FTIR spectrophotometer with a diamond ATR attachment. Complexes **2** and **3** were prepared in analogy to the preparation of **4**, which is detailed below.

Lu(OAr*)$_3$ was synthesized using modified procedures reported for Y(OAr*)$_3$.[19] In an argon glovebox, Lu(NR$_2$)$_3$ (625 mg, 0.953 mmol), HOAr* (998 mg, 2.38 mmol), and toluene (50 mL) were added to a 100 mL Schlenk flask fitted with a Teflon stopper. The flask was taken out of the glovebox and connected to a Schlenk line. The clear reaction solution was heated to 100 °C using an oil bath. After stirring for two days at 100 °C, the flask was briefly opened to vacuum to release vapor (presumably toluene and/or HNR$_2$). The reaction was stirred at 100 °C under reduced pressure for an additional 2 days. The reaction was then slowly concentrated to 15 mL and changed from colorless to pale-yellow. The reaction flask was brought back into an argon-filled glovebox and the pale-yellow solution was transferred to a 20 mL scintillation vial. After a few days in a −35 °C freezer, a colorless precipitate formed along the walls of the vial. The yellow toluene solution was decanted from the colorless precipitate and the precipitate was washed with pentane, yielding Lu(OAr*)$_3$ as a bright white powder. Single crystals suitable for X-ray diffraction were grown from boiling hexane. NMR, IR, and UV-visible spectra are shown in Figs. S3−S6. ^{1}H NMR (C$_6$D$_6$): δ 7.35 (s, 6H) 2.51 (d, J = 11.1 Hz, 18H), 2.39 (d, J = 11.0 Hz, 18H), 2.05 (s, 18H), 1.74 (d, J = 12.9 Hz, 18H), 1.65 (d, J = 12.0 Hz, 18H), 1.42 (s, 27H, *t-Bu*). ^{13}C{^{1}H} NMR (C$_6$D$_6$): δ 142.02, 139.34, 136.11, 135.65, 122.57, 44.41, 39.12, 37.35, 34.70, 32.11, 29.80. IR: 3631br, 2899str,

2846str, 2676w, 2654w, 1445m, 1428m, 1390w, 1359w, 1342w, 1312w, 1278m, 1241m, 1202w, 1170w, 1135w, 1100w, 1078w, 1034w, 978 w, 922 w, 900w, 872m, 845m, 817w, 766w, 710w cm^{-1}. Anal. Calcd for $(C_{90}H_{123}O_3Lu)\cdot(C_6H_{14})$: C, 76.15; H, 9.12. Found: C, 74.02; H, 8.88. The found values (74.02, 8.88), formulate to be $C_{96}H_{137}$, which matches the calculated formula $C_{96}H_{137}$ for crystalline $Lu(OAr^*)_3$ with one molecule of hexane present. The analytical data are not consistent with contamination of the sample with HOAr*. Incomplete combustion during elemental analysis is a well-reported issue within rare-earth metal chemistry,[15,44–47]and other reported rare-earth metal aryloxide complexes also have a low %C value.[19,48,49]

[K(crypt)][Lu(OAr*)$_3$] (**4**): A mixture of $Lu(OAr^*)_3$ (80 mg, 0.056 mmol) and crypt (21 mg, 0.056 mmol) in 5 mL Et_2O was chilled to −35 °C and then added to a vial containing chilled (−35 °C) KC_8 (10 mg, 0.067 mmol). The cloudy colorless mixture instantly turned dark blue. After 1 hour at −35 °C with occasional swirling, the KC_8 was filtered from the dark blue solution using a Kimwipe-packed glass pipette. The solvent was slowly removed *in vacuo* to yield dark blue X-ray quality single crystals of $[K(crypt)][Lu(OAr^*)_3]\cdot 3Et_2O$. THF and a potassium smear were used instead of Et_2O and KC_8 when preparing samples of $[K(crypt)][Lu(OAr^*)_3]$ *in situ* for EPR measurements. UV/Vis λ_{max} (ε, THF, RT): 456 nm (shoulder, 1777 $M^{-1}\,cm^{-1}$), 605 nm (3197 $M^{-1}\,cm^{-1}$).

General protocol for preparation of samples for EPR measurements.

With a soldering iron, holes were made through a 1.5 mL Eppendorf tube and a 50 mL Falcon tube and cap so that they easily submerge under liquid nitrogen, Figure S1.1.

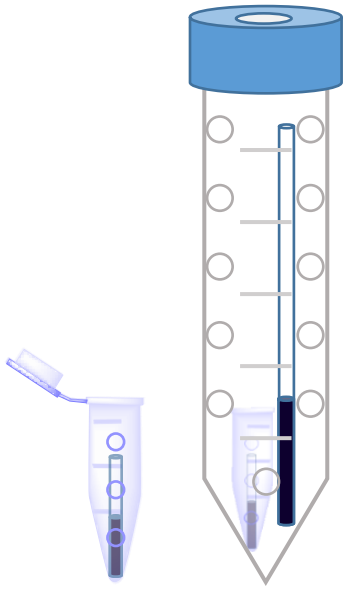

Figure S1.1. A depiction of (left) the Eppendorf tube holding the W-band EPR sample and (right) the 50 mL Falcon tube holding both W-band and X-band EPR samples.

LnA_3 (Ln = La, Lu; A = $N(SiMe_3)_2$, OAr*) and crypt were dissolved in the appropriate amount of THF to result in final Ln(II) concentrations of approximately 1 mM, 5 mM, 10 mM and 20 mM. In an argon-filled glovebox, a Wilmad quartz 100 mm tube for X-band EPR, a custom-made plastic W-band EPR tube contained in the Eppendorf tube, a vial containing the THF solution of LnA_3 and crypt, a vial containing an excess (>10 eq) of potassium smear, and several glass pipettes, one of which had a Kimwipe packed into it, were placed in a cold well and were allowed to cool to −78 °C. The THF solution of LnA_3 and crypt was added to the vial containing the potassium smear. Upon swirling the vial, a gradual change in color from colorless to dark blue was observed. After 1 hour at −78 °C, the dark blue THF solution containing [K(crypt)][LuA_3] was filtered. An aliquot was placed in the W-band tube (still in

the Eppendorf) so that the tube was approximately half filled, and then the Eppendorf tube was capped. An aliquot was placed in the X-band tube so that the sample height was 1.5 cm, and then the tube was capped. Both tubes were quickly placed in a chilled beaker containing chilled Lab Armor metal beads so that both tubes were upright and stable. This beaker was immediately taken out of the glovebox, the Eppendorf and X-band tubes were uncapped, and the samples were immediately frozen in liquid nitrogen. Both tubes were then placed in a prechilled 50 mL Falcon tube, Figure S1.1. The Falcon tube was then capped and submerged in liquid nitrogen inside of a shipping Dewar and sent to FSU for measurements by Dr. Kundu.

X-ray Data Collection, Structure Solution and Refinement for Lu(OAr*)$_3$.

A colorless crystal of approximate dimensions 0.295 × 0.386 × 0.569 mm was mounted in a cryoloop and transferred to a Bruker SMART APEX II diffractometer. The APEX2[50] program package was used to determine the unit-cell parameters and for data collection (120 sec/frame scan time). The raw frame data was processed using SAINT[51] and SADABS[52] to yield the reflection data file. Subsequent calculations were carried out using the SHELXTL[53] program package. The diffraction symmetry was 2/*m* and the systematic absences were consistent with the monoclinic space group $P2_1/n$ that was later determined to be correct.

The structure was solved by direct methods and refined on F^2 by full-matrix least-squares techniques. The analytical scattering factors[54] for neutral atoms were used throughout the analysis. Hydrogen atoms were included using a riding model. There was one molecule of *n*-hexane solvent present. Disordered atoms were included using multiple components with partial site-occupancy-factors. Least-squares analysis yielded wR2 = 0.1086 and Goof = 1.186 for 912 variables refined against 22343 data (0.75 Å), R1 = 0.0468 for those 19679 data with I > 2.0σ(I). There were several high residuals present in the final difference-Fourier map. It was not possible to determine the nature of the residuals although it was probable that additional *n*-hexane solvent was present. The SQUEEZE[55] routine in the PLATON[55] program package was used to account for the electrons in the solvent accessible voids.

X-ray Data Collection, Structure Solution and Refinement for [K(crypt)][Lu(OAr*)$_3$]·3Et$_2$O.

A purple crystal of approximate dimensions 0.198 × 0.267 × 0.274 mm was mounted in a cryoloop and transferred to a Bruker SMART APEX II diffractometer. The APEX2[Error! Bookmark not defined.] program package was used to determine the unit-cell parameters and for data collection (120 sec/frame scan time). The raw frame data was processed using SAINT[Error! Bookmark not defined.] and SADABS[Error! Bookmark not defined.] to yield the reflection data file. Subsequent calculations were carried out using the SHELXTL[Error! Bookmark not defined.] program package. There were no systematic absences nor any diffraction symmetry other than the Friedel condition. The centrosymmetric triclinic space group $P\bar{1}$ was assigned and later determined to be correct.

The structure was solved by direct methods and refined on F^2 by full-matrix least-squares techniques. The analytical scattering factors[Error! Bookmark not defined.] for neutral atoms were used throughout the analysis. Hydrogen atoms were included using a riding model. There were three molecules of diethylether solvent present. Least-squares analysis yielded wR2 = 0.1183 and Goof = 1.055 for 1240 variables refined against 27368 data (0.75 Å), R1 = 0.0465 for those 22821 data with I > 2.0σ(I).

Spectra

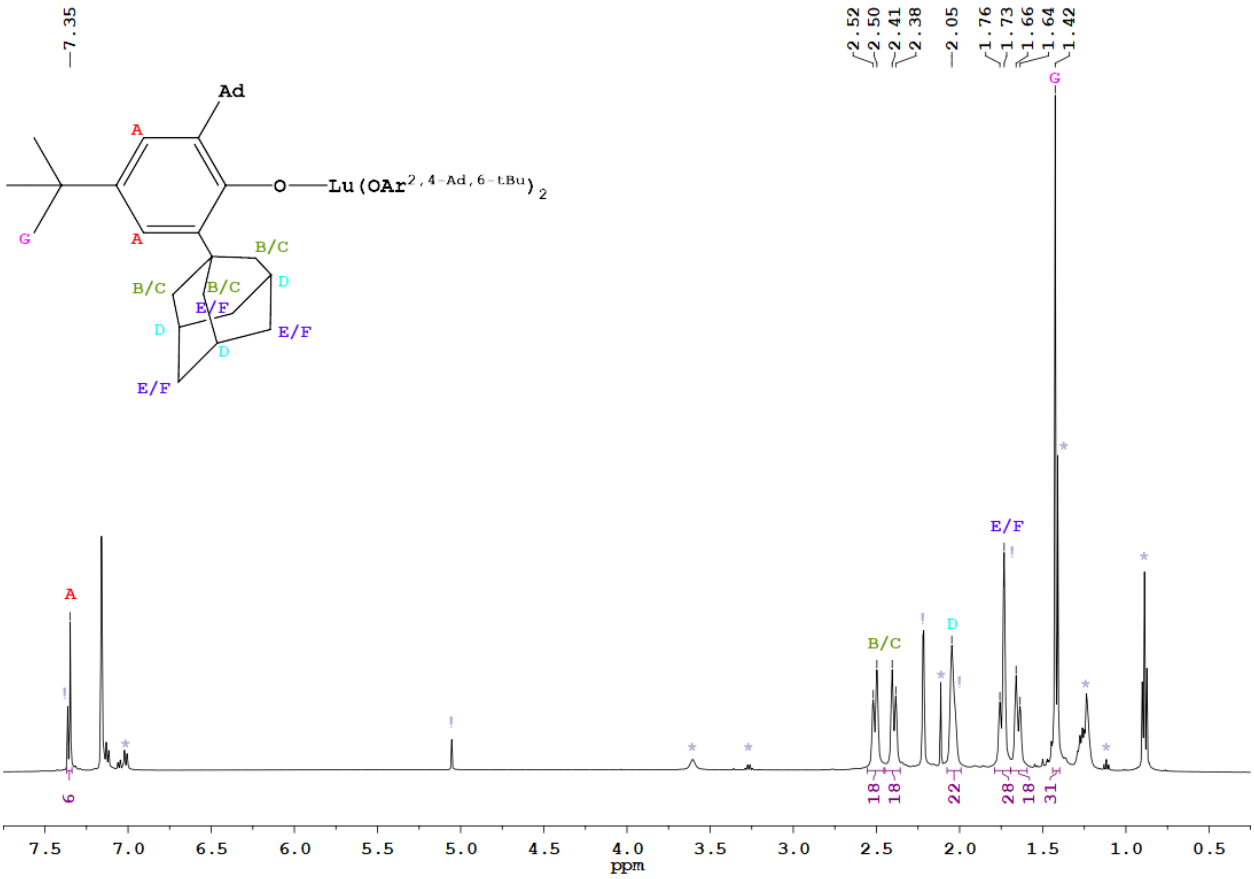

Figure S1.2. ^{1}H NMR spectrum of Lu(OAr*)$_3$. Peaks marked with '!' indicate peaks originating from residual HOAr* and peaks marked with '*' indicate peaks originating from residual solvent.

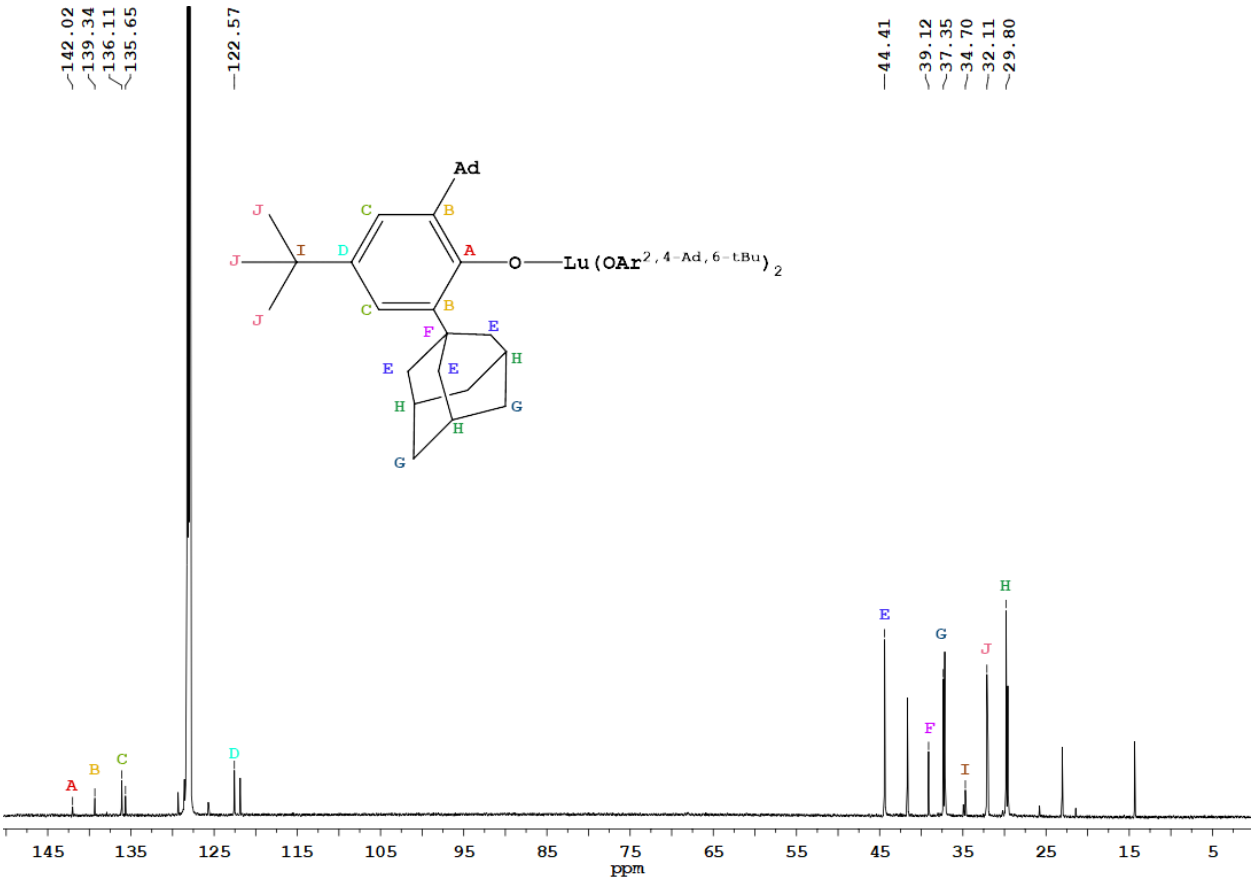

Figure S1.3. $^{13}C\{^{1}H\}$ NMR spectrum of Lu(OAr*)$_3$. Unmarked peaks originate from residual solvent.

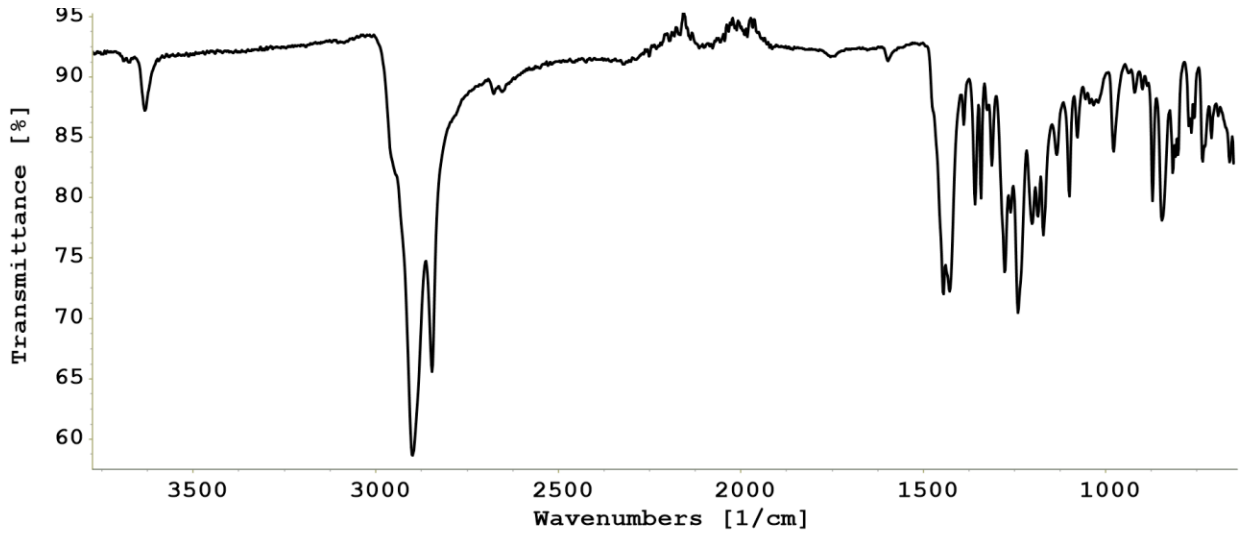

Figure S1.4. IR spectrum of $Lu(OAr^*)_3$ solids with residual HOAr* present. Recrystallization is necessary to remove all traces of HOAr* as it persists through multiple washings of $Lu(OAr^*)_3$ solids with hexane and pentane.

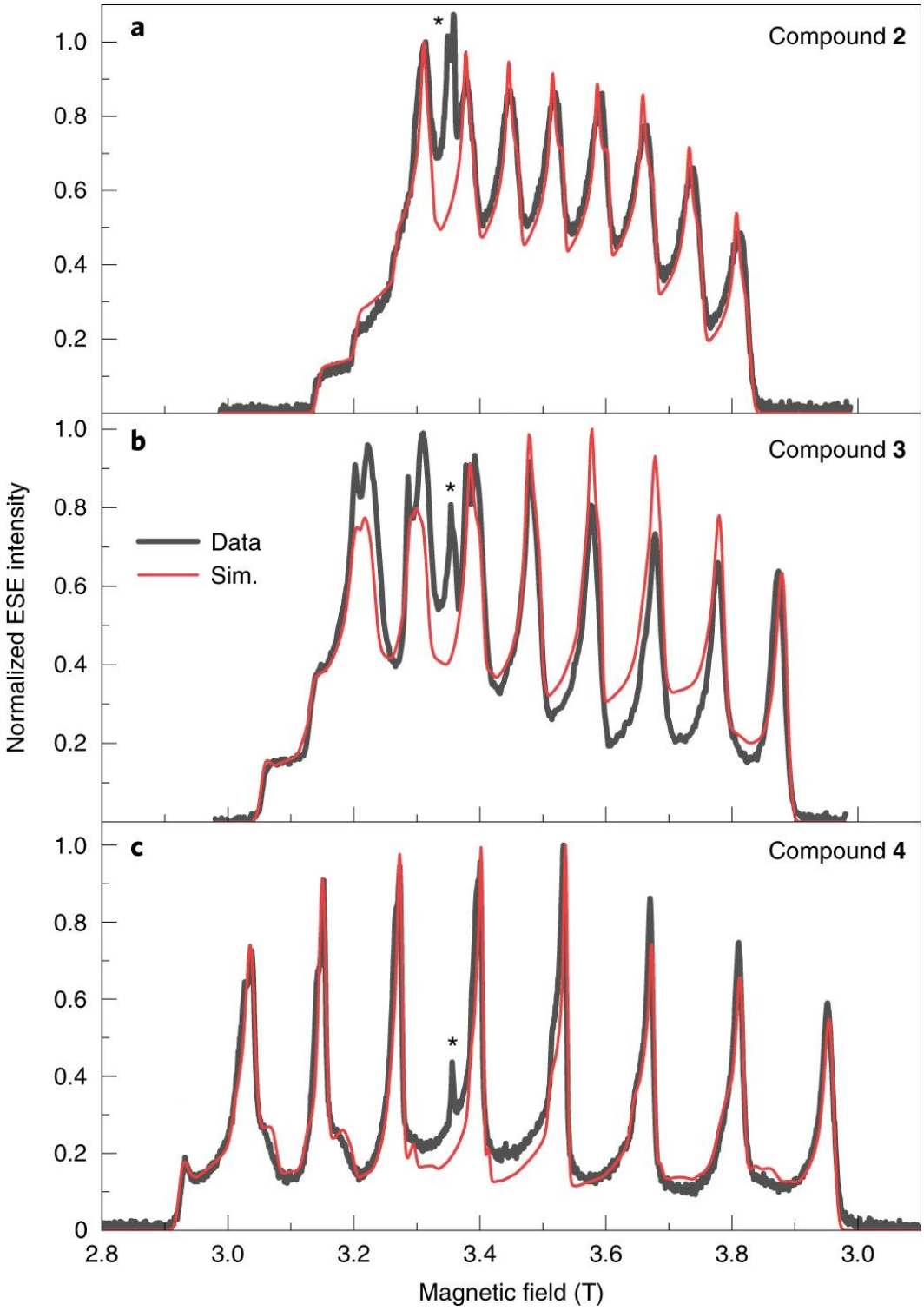

Figure S1.5. Experimental ESE spectra (black) and simulations (red) recorded at the W-band frequency of 94.0 GHz and $T = 5.0$ K for frozen solution samples of compounds **2** (a), **3** (b) and **4** (c). Asterisks denote a $g = 2.00$ electride in the solution.

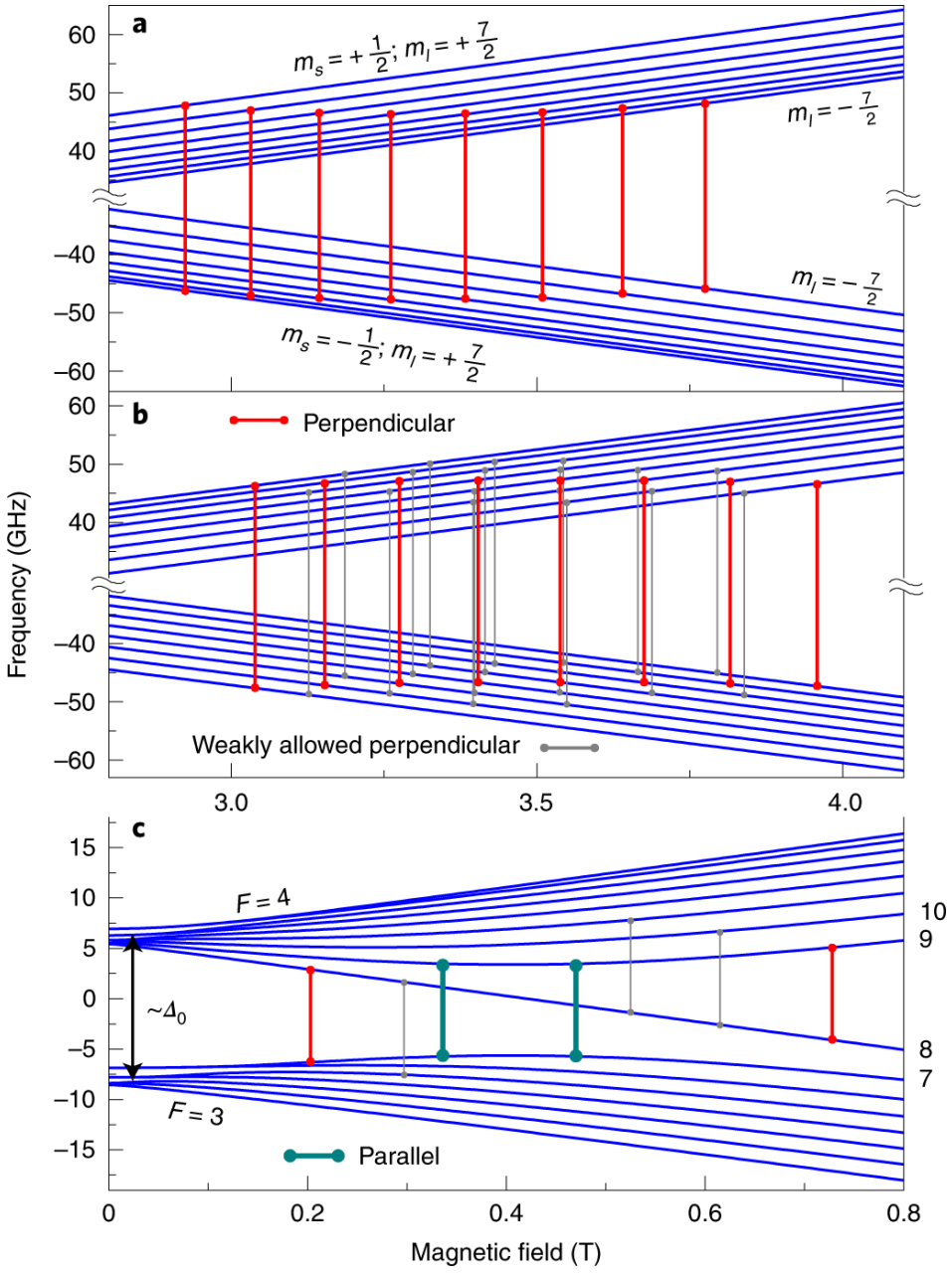

Figure S1.6. a–c, Simulated energy diagrams for the $\mathbf{B}_0||z$ (**a**) and $\mathbf{B}_0||xy$ (**b**,**c**) orientations of the applied magnetic field, corresponding to regions of interest in the W-band (**a**,**b**) and X-band (**c**) EPR spectra of complex **4**. Allowed and weakly allowed transitions are indicated by vertical lines (corresponding to 94 GHz in **a**,**b** and 9.2 GHz in **c**) both for conventional perpendicular (π) and parallel (σ) mode excitation. The zero-field gap, Δ_0, between electron–nuclear hyperfine multiplets is indicated in **c**.

References

(1) Wright, K.; Beck, K. M.; Debnath, S.; Amini, J. M.; Nam, Y.; Grzesiak, N.; Chen, J. S.; Pisenti, N. C.; Chmielewski, M.; Collins, C.; et al. *Nat. Commun.* **2019**.

(2) Devoret, M. H.; Schoelkopf, R. J. *Science (80-.).* **2013**, *339* (6124), 1169–1174.

(3) Carolan, J.; Harrold, C.; Sparrow, C.; Martín-López, E.; Russell, N. J.; Silverstone, J. W.; Shadbolt, P. J.; Matsuda, N.; Oguma, M.; Itoh, M.; et al. *Science (80-.).* **2015**, *349* (6249), 711–716.

(4) Sarma, S. Das; Freedman, M.; Nayak, C. *npj Quantum Inf. 2015 11* **2015**, *1* (1), 1–13.

(5) Shiddiq, M.; Komijani, D.; Duan, Y.; Gaita-Ariño, A.; Coronado, E.; Hill, S. *Nature* **2016**.

(6) Kane, B. E. *Nat. 1998 3936681* **1998**, *393* (6681), 133–137.

(7) Yang, K.; Paul, W.; Phark, S. H.; Willke, P.; Bae, Y.; Choi, T.; Esat, T.; Ardavan, A.; Heinrich, A. J.; Lutz, C. P. *Science (80-.).* **2019**, *366* (6464), 509–512.

(8) Thiele, S.; Balestro, F.; Ballou, R.; Klyatskaya, S.; Ruben, M.; Wernsdorfer, W. *Science (80-.).* **2014**, *344* (6188), 1135–1138.

(9) Nguyen, T. N.; Wernsdorfer, W.; Shiddiq, M.; Abboud, K. A.; Hill, S.; Christou, G. *Chem. Sci.* **2016**.

(10) Zadrozny, J. M.; Niklas, J.; Poluektov, O. G.; Freedman, D. E. *ACS Cent. Sci.* **2015**, *1* (9), 488–492.

(11) Gaita-Ariño, A.; Luis, F.; Hill, S.; Coronado, E. Molecular Spins for Quantum Computation. *Nature Chemistry*. 2019.

(12) Zadrozny, J. M.; Gallagher, A. T.; Harris, T. D.; Freedman, D. E. *J. Am. Chem. Soc.* **2017**.

(13) Collett, C. A.; Santini, P.; Carretta, S.; Friedman, J. R. *Phys. Rev. Res.* **2020**.

(14) Giménez-Santamarina, S.; Cardona-Serra, S.; Clemente-Juan, J. M.; Gaita-Ariño, A.;

Coronado, E. *Chem. Sci.* **2020**.

(15) Hitchcock, P. B.; Lappert, M. F.; Maron, L.; Protchenko, A. V. *Angew. Chem. Int. Ed.* **2008**, *47* (8), 1488–1491.

(16) MacDonald, M. R.; Bates, J. E.; Ziller, J. W.; Furche, F.; Evans, W. J. *J. Am. Chem. Soc.* **2013**, *135* (26), 9857–9868.

(17) Evans, W. J. Tutorial on the Role of Cyclopentadienyl Ligands in the Discovery of Molecular Complexes of the Rare-Earth and Actinide Metals in New Oxidation States. *Organometallics*. 2016.

(18) Ryan, A. J.; Ziller, J. W.; Evans, W. J. *Chem. Sci.* **2020**, *11*, 2006–2014.

(19) Moehring, S. A.; Miehlich, M.; Hoerger, C. J.; Meyer, K.; Ziller, J. W.; Evans, W. J. *Inorg. Chem* **2020**, *59*, 3207–3214.

(20) Woen, D. H.; Evans, W. J. Expanding the + 2 Oxidation State of the Rare-Earth Metals, Uranium, and Thorium in Molecular Complexes. In *Handbook on the Physics and Chemistry of Rare Earths*; 2016.

(21) Wolfowicz, G.; Tyryshkin, A. M.; George, R. E.; Riemann, H.; Abrosimov, N. V.; Becker, P.; Pohl, H. J.; Thewalt, M. L. W.; Lyon, S. A.; Morton, J. J. L. *Nat. Nanotechnol.* **2013**.

(22) Zhang, G.; Liu, H.; He, Z.; Chen, B. *J. Phys. Chem. C* **2022**, *126* (23), 9926–9936.

(23) Ariciu, A. M.; Woen, D. H.; Huh, D. N.; Nodaraki, L. E.; Kostopoulos, A. K.; Goodwin, C. A. P.; Chilton, N. F.; McInnes, E. J. L.; Winpenny, R. E. P.; Evans, W. J.; et al. *Nat. Commun.* **2019**.

(24) Anderson, D. M.; Cloke, F. G. N.; Cox, P. A.; Edelstein, N.; Green, J. C.; Pang, T.; Sameh, A. A.; Shalimoff, G. *J. Chem. Soc. Chem. Commun.* **1989**, *0* (1), 53–55.

(25) Knapp, C.; Weiden, N.; Dinse, K. P. *Appl. Phys. A 1998 663* **1998**, *66* (3), 249–255.

(26) Ryan, A. J.; Ziller, J. W.; Evans, W. J. *Chem. Sci.* **2020**, *11*, 2006–2014.

(27) Kundu, K.; White, J. R. K.; Moehring, S. A.; Yu, J. M.; Ziller, J. W.; Furche, F.; Evans, W. J.; Hill, S. *Nat. Chem.* **2022**, *14*, 392–397.

(28) Guzei, I. A.; Wendt, M. *J. Chem. Soc. Dalt. Trans.* **2006**.

(29) Peterson, Jeffrey K.; MacDonald, Matthew R.; Ziller, J. W. .; Evans, W. J. . *Organometallics* **2013**, *32* (9), 2625–2631.

(30) Evans, W. J.; Lee, D. S.; Johnston, M. A.; Ziller, J. W. *Organometallics* **2005**, *24* (26), 6393–6397.

(31) Scarel, G.; Wiemer, C.; Fanciulli, M.; Fedushkin, I. L.; Fukin, G. K.; Domrachev, G. A.; Lebedinskii, Y.; Zenkevich, A.; Pavia, G. *Zeitschrift fur Anorg. und Allg. Chemie* **2007**, *663* (11–12), 2097–2103.

(32) Steele, L. A. M.; Boyle, T. J.; Kemp, R. A.; Moore, C. *Polyhedron* **2012**, *42* (1), 258–264.

(33) Moehring, S. A.; Beltrán-Leiva, M. J.; Páez-Hernández, D.; Arratia-Pérez, R.; Ziller, J. W.; Evans, W. J. *Chem. – A Eur. J.* **2018**, *24* (68), 18059–18067.

(34) Schwamm, R. J.; Harmer, J. R.; Lein, M.; Fitchett, C. M.; Granville, S.; Coles, M. P. *Angew. Chem. Int. Ed.* **2015**, *54* (36), 10630–10633.

(35) Cutsail, G. E. *Dalt. Trans.* **2020**, *49* (35), 12128–12135.

(36) Smith, R. L.; Wysocki, A. L.; Park, K. *Phys. Chem. Chem. Phys.* **2020**, *22* (38), 21793–21800.

(37) Schwindt, P. D. D.; Jau, Y. Y.; Partner, H. L.; Serkland, D. K.; Ison, A.; McCants, A.; Winrow, E.; Prestage, J.; Kellogg, J.; Yu, N.; et al. *2015 Jt. Conf. IEEE Int. Freq. Control Symp. Eur. Freq. Time Forum, FCS 2015 - Proc.* **2015**, 752–757.

(38) Peng, D.; Middendorf, N.; Weigend, F.; Reiher, M. *J. Chem. Phys.* **2013**, *138* (18), 184105.

(39) Visscher, L.; Dyall, K. G. *At. Data Nucl. Data Tables* **1997**, *67* (2), 207–224.

(40) Reed, A. E.; Weinstock, R. B.; Weinhold, F. *J. Chem. Phys.* **1998**, *83* (2), 735.

(41) Pyykkö, P.; Pyykkö, P. *https://doi.org/10.1146/annurev-physchem-032511-143755* **2012**, *63*, 45–64.

(42) Edelmann, F. T. *Synthetic Methods of Organometallic and Inorganic Chemistry, Volume 6: Lanthanides and Actinides*; Herrmann, W. A., Ed.; 1996.

(43) Watanabe, T.; Ishida, Y.; Matsuo, T.; Kawaguchi, H. *Dalt. Trans.* **2010**, *39* (2), 484–491.

(44) Jenkins, T. F.; Woen, D. H.; Mohanam, L. N.; Ziller, J. W.; Furche, F.; Evans, W. J. *Organometallics* **2018**, *37* (21), 3863–3873.

(45) Goodwin, C. A. P.; Chilton, N. F.; Vettese, G. F.; Pineda, E. M.; Crowe, I. F.; Ziller, J. W.; Winpenny, R. E. P.; Evans, W. J.; Mills, D. P. *Inorg. Chem.* **2016**, *55* (20), 10057–10067.

(46) Goodwin, C. A. P.; Reta, D.; Ortu, F.; Chilton, N. F.; Mills, D. P. *J. Am. Chem. Soc.* **2017**, *139* (51), 18714–18724.

(47) Goodwin, C. A. P.; Joslin, K. C.; Lockyer, S. J.; Formanuik, A.; Morris, G. A.; Ortu, F.; Vitorica-Yrezabal, I. J.; Mills, D. P. *Organometallics* **2015**, *34* (11), 2314–2325.

(48) Huh, D. N.; Roy, S.; Ziller, J. W.; Furche, F.; Evans, W. J. *J. Am. Chem. Soc.* **2019**, *141* (32), 12458–12463.

(49) Moehring, S. A.; Beltrán-Leiva, M. J.; Páez-Hernández, D.; Arratia-Pérez, R.; Ziller, J. W.; Evans, W. J. *Chem. Eur. J.* **2018**, *24*, 18059–18067.

(50) *APEX2*; Version 2014.11-0; Bruker AXS, Inc.: Madison, WI, 2014.

(51) *SAINT*; Version 8.34a; Bruker AXS, Inc.: Madison, WI, 2013.

(52) Sheldrick, G. M. *SADABS*; Version 2014/5; Bruker AXS, Inc.: Madison, WI, 2014.

(53) Sheldrick, G. M. *SHELXTL*; Version 2014/7; Bruker AXS, Inc.: Madison, WI, 2014.

(54) *International Tables for Crystallography*, Vol. C.; Prince, E., Ed.; Dordrecht: Kluwer Academic Publishers., 2006.

(55) Spek, A. L. *Acta Crystallogr. Sect. C Struct. Chem.* **2015**, *c71*, 9–19.

CHAPTER 2

Isolation of Sterically Unsaturated Complexes of Ln(II) ions in a Tris(methylcyclopentadienyl) Ligand Environment

Introduction

The stability and reactivity of complexes of lanthanide (Ln) metals in the +3 oxidation state are largely influenced by steric factors.[1] Ln(III) complexes have little to no covalent character in their bonding due to the limited radial extension of their 4*f* orbitals.[2] Because of their highly electropositive nature,[3] the synthesis and isolation of stable Ln(III) complexes typically requires the optimization of electrostatic interactions between the Ln(III) ion and its ligands in order to balance the electrostatic charge. As described in Chapter 1, there also needs to be a balance between the steric bulk of the ligand and size of the metal to appropriately saturate the coordination sphere. Sterically unsaturated lanthanide complexes react readily to fill their open coordination sites to form stable sterically saturated compounds.[4] Therefore, examples of isolated and characterized sterically unsaturated rare-earth metal complexes are rare.[5,6]

Recent research in rare-earth metal reductive chemistry demonstrated that Ln(II) molecular complexes for all lanthanides (except Pm which has not been studied due to its radioactivity), can be isolated from LnA_3/M reduction reactions (A = anion, M = alkali metal) with silyl-substituted cyclopentadienyl ancillary ligands, eq 2.1.[7–9]

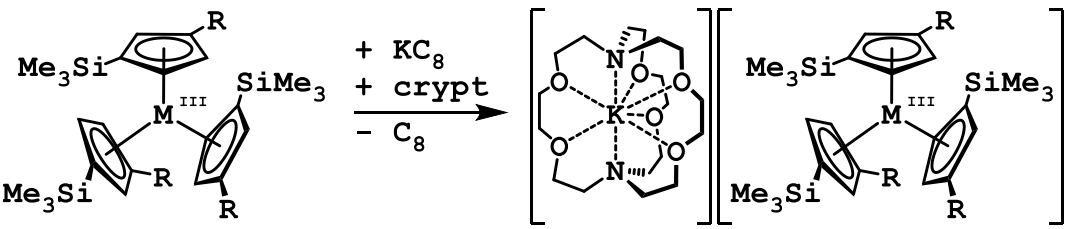

(2.1)

R = H, M = Y, La, Ce, Pr, Nd, Gd, Tb, Dy, Ho, Er, Lu
R = $SiMe_3$, M = La Ce, Nd, Pr

The synthesis of these complexes was a breakthrough result, as before it was believed that only Eu^{2+}, Yb^{2+}, Sm^{2+},[10] Tm^{2+},[11] Dy^{2+}, and Nd^{2+},[12] could form isolable, crystallographically characterizable Ln(II) complexes due to highly negative Ln^{3+}/Ln^{2+} reductive potentials calculated for a $4f^n \rightarrow 4f^{n+1}$ reduction.[13–16] However, density functional theory (DFT) calculations supported crystallographic, magnetic, and spectroscopic data, which all suggested that these new Ln(II) ions adopted a $4f^n5d^1$ ground state configuration instead. In the trigonal coordination environment of these complexes, the $5d_{z^2}$ orbital is similar in energy to the $4f$ orbitals.[7–9,17] Following this result, it was established that these new Ln(II) ions can be isolated in molecular complexes of a variety of coordination environments, such as with alkyl-substituted cyclopentadienyl ligands,[18–20] amide[21] and aryloxide[22] ligands, and as linear metallocenes.[23] These results suggested that synthetic studies of the new Ln(II) ions should be expanded to a wider variety of ligands to explore the limits of +2 oxidation state lanthanide chemistry.

This chapter describes the synthesis of complexes of the new Ln(II) ions with one of the smaller cyclopentadienyl ligands, $(C_5H_4Me)^{1-}$ (Cp^{Me}), to probe the limits of steric unsaturation with this lower oxidation state. Previously, $[Cp^{Me}{}_3Ln^{II}]^-$ complexes were isolated for the smaller Ln(II) ions (Ln = Tb, Ho) and crystallized with an inverse sandwich countercation, forming [(18-crown-6)K(μ-Cp^{Me})K(18-crown-6)][$Cp^{Me}{}_3Ln$].[20] In addition, electron paramagnetic resonance (EPR) spectrum of the reduction product of $Cp^{Me}{}_3Y$ suggested the formation of an Y(II),[24] and for the reduction of $Cp^{Me}{}_3Dy$ in the presence of 2.2.2-cryptand (crypt), the crystallographically characterized Dy(II) complex, [K(crypt)][$Cp^{Me}{}_3Dy$], was isolated.[20] Reported attempts to reduce $Cp^{Me}{}_3Ln$ complexes with larger rare-earth metals (Ln = La, Pr, and Gd) gave spectroscopic evidence for the formation

of Ln(II) complexes, but these products rapidly decomposed and could not be isolated.[25] Characterization of the decomposition products for La and Pr by X-ray crystallography showed why these sterically unsaturated Ln(II) complexes could not be isolated; the decomposition products were the alkoxyalkyl bridged Ln(III) compounds, $[K(crypt)]_2[(Cp^{Me_3}Ln)_2(\mu\text{-}OCH_2CH_2CH_2CH_2)]$, derived from the ring-opening of the THF solvent, eq 2.2.[25]

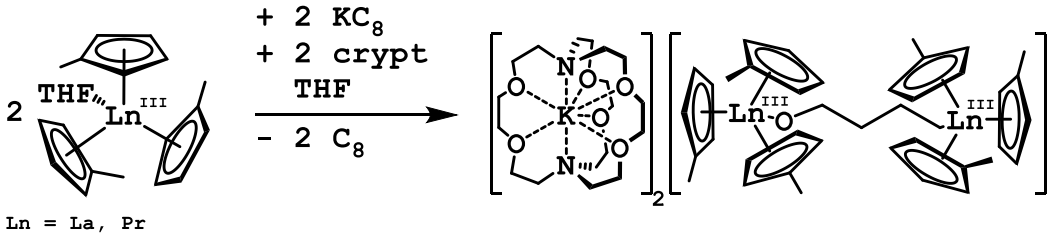

(2.2)

This chapter details the isolation of crystallographically-characterizable $[Cp^{Me_3}Ln^{II}]^-$ (Ln = Nd, Gd) complexes with the inverse-sandwich countercation, $[(18\text{-crown-6})K(\mu\text{-}Cp^{Me})K(18\text{-crown-6})]^+$. To my knowledge, these $[(18\text{-crown-6})K(\mu\text{-}Cp^{Me})K(18\text{-crown-6})][Cp^{Me_3}Ln]$ complexes are the least sterically saturated $[A_3Ln^{II}]^-$ (A = anionic ligand) complexes known.

Results and Discussion

$[(18\text{-crown-6})K(\mu\text{-}Cp^{Me})K(18\text{-crown-6})][Cp^{Me_3}Gd]$, 2.1-Gd. $Cp^{Me_3}Gd(THF)$ and 2 equivalents of 18-crown-6 were dissolved in 1 mL THF and placed in a −35 °C freezer. The next day, the THF solution was reacted with KC_8 at −35 °C for an hour and then filtered, leaving a black solution. This solution was layered with hexanes and placed at −35 °C. Overnight, dark purple needlelike crystals of $[(18\text{-crown-6})K(\mu\text{-}Cp^{Me})K(18\text{-crown-6})][Cp^{Me_3}Gd]$, **2.1-Gd**, were isolated, eq 2.3, and was identified by X-ray crystallography, Figure 2.1.

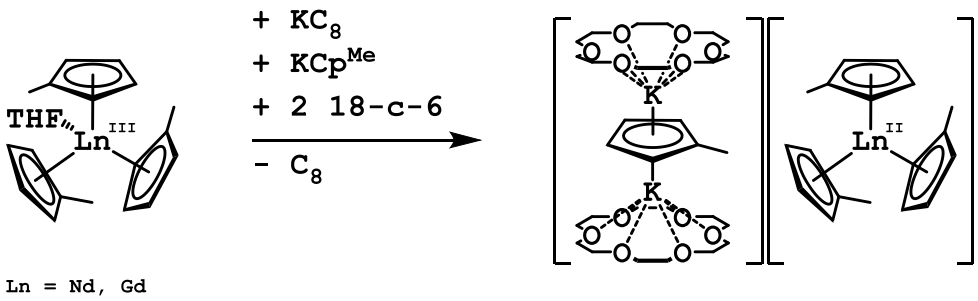

(2.3)

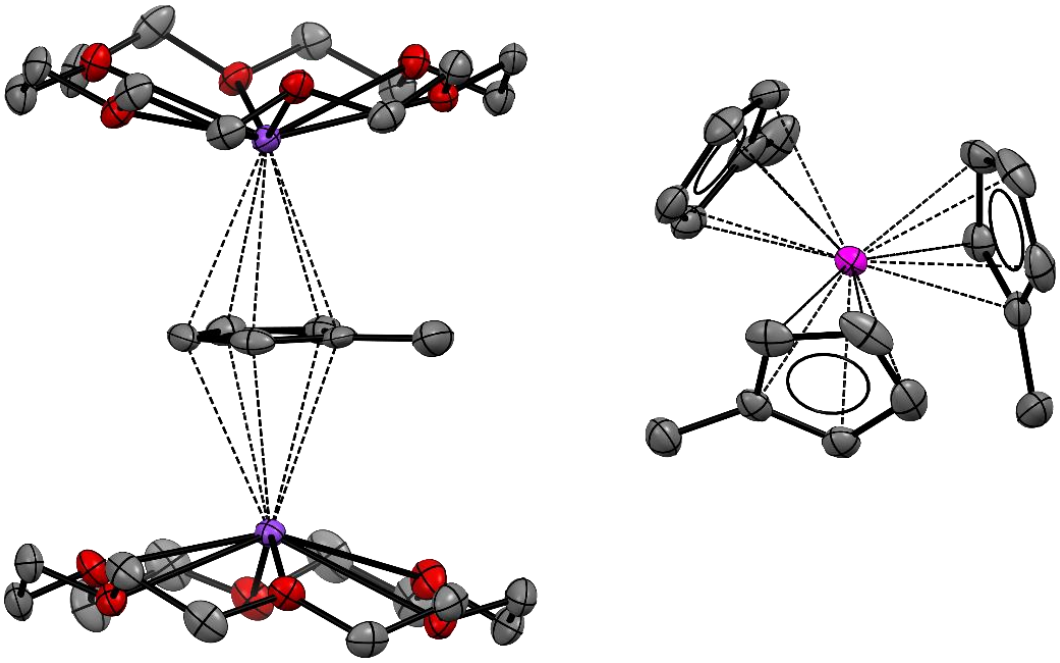

Figure 2.1. Thermal ellipsoid plot of **2.1-Gd** drawn at the 50% probability level. Hydrogen atoms and 4 co-crystallized THF molecules were omitted for clarity. Color code: Grey = C, Red = O, Blue = N, Pink = Gd, Purple = K.

The structural data for **2.1-Gd** are summarized in Table 2.1. **2.1-Gd** is isomorphous with the **2.1-Ln** complexes of the smaller metals Tb and Ho.[20] Both contain the inverse sandwich countercation, [(18-crown-6)K(μ-Cp^{Me})K(18-crown-6)]$^{+}$. Like the Tb and Ho analogues, the countercation in **2.1-Ln** is essentially linear, having a K–Cp$^{Me}_{centroid}$–K angle of approximately 178°. Comparisons of the Gd^{II}–Cp$_{centroid}$ distances of **2.1-Gd** cannot be made with Cp$^{Me}_3$Gd since there are no crystallographic data for the Gd(III) complex without a

coordinated THF molecule, which raises the coordination number and would not make a suitable comparison.

Table 2.1: Selected bond lengths [Å] and angles [°] of **2.1-Gd**.

[a]Cnt1 = centroid of C1–C5. [b]Cnt2 = centroid of C7–C11.[c]Cnt3 = centroid of C13–C17. [d]Cnt4 = centroid of C19–C23.

Gd–Cnt1[a]	2.475
Gd–Cnt2[b]	2.473
Gd–Cnt3[c]	2.468
K(1)–Cnt4[d]	2.843
K(2)–Cnt4	2.859
Cnt1–Gd–Cnt2	119.8
Cnt1–Gd–Cnt3	119.6
Cnt2–Gd–Cnt3	120.4
K(1)–Cnt4–K(2)	177.5

Table 2.2: Comparison of Ln-Cnt_{Cp} distances [Å] in $[Cp^{x}_{3}Gd^{II}]^{-}$ complexes.

[a]This value is the difference in Gd–Cnt distances between $Cp^{x}_{3}Gd^{III}$ and $[Cp^{x}_{3}Gd^{II}]^{-}$.

Complex	**Gd–Cnt avg**	**$Cnt_{Gd(III)}$–$Cnt_{Gd(II)}$**[a]	**Ref**
2.1-Gd	2.472	-	This work
$[K(18\text{-crown-6})(THF)_2][Cp^{t}_{3}Gd]$	2.482	-	18
$[K(crypt)][Cp'_{3}Gd]$	2.468	0.031	7
$[K(crypt)][Cp^{tet}_{3}Gd]$	2.516	0.047	19

While comparisons cannot be made between **2.1-Gd** and its $Cp^{Me}_{3}Gd^{III}$ precursor, **2.1-Gd** can be compared with other $[Cp^{x}_{3}Gd^{II}]^{-}$ complexes (Cp^{x} = $C_5H_4CMe_3$ (Cp^{t}), $C_5H_4SiMe_3$ (Cp′), C_5Me_4H (Cp^{tet})). The average Gd–$Cp_{centroid}$ distances for **2.1-Gd** are similar to the distances reported for other $[Cp^{x}_{3}Gd^{II}]^{-}$ complexes, Table 2.2.[7,18,19] Two of the $[Cp^{x}_{3}Gd^{II}]^{-}$ complexes had Ln–Cnt_{Cp} distances that were 0.03–0.05 Å longer than the corresponding $Cp^{x}_{3}Ln^{III}$ complexes. The slight increase is in contrast to the $4f^{n+1}$ complexes of the traditional Ln(II) ions, which had Ln-Cnt_{Cp} distances 0.1–0.2 Å longer than their trivalent precursors.[26–28] The differences in Ln-Cnt_{Cp} distances is presumably due to the large difference in the ionic

radii of $4f^n$ Ln^{3+} and $4f^{n+1}$ Ln^{2+} ions[29] and the little-to-no metal-ligand interaction. The similar average Ln–Cnt_{Cp} distances for **2.1-Gd** to other Gd(II) complexes suggests that **2.1-Gd** also adopts a $4f^7 5d^1$ electronic configuration.

The steric parameters of **2.1-Gd** were evaluated with Solid-G, a program developed by Guzei *et. al.* that calculates the percentage of the coordination sphere of a metal shielded by its ligands, using the atomic coordinates of the complex obtained from X-ray crystallographic data.[30] Using Solid-G, the extent of steric saturation of **2.1-Gd** was quantified and compared with other crystallographically-characterized $[A_3Ln^{II}]^-$ complexes. Table 2.3 summarizes the quantified value of steric saturation around the Gd center ($G_{complex}$), the percentage of the coordination sphere shielded by the ligands (G_L), and the Tolman cone angle of the ligand. **2.1-Gd** is much less sterically saturated than the other reported Gd(II) complexes with a *G* value of 74% versus the typical 83-85% range. This could explain why previously only Ln(II) ions of the smaller metals Dy, Tb, and Ho could be isolated with Cp^{Me} ancillary ligands and why **2.1-Gd** is fleeting at room temperature.

Table 2.3: Comparison of G-parameters [%] of $[A_3Gd^{II}]^-$ complexes.

[a] $Cp^t = C_5H_4CMe_3$. [b] $Cp' = C_5H_4SiMe_3$. [c] $Cp^{tet} = C_5Me_4H$.

Complex	$G_{complex}$	G_L (avg)	Ref
2.1-Gd	74	25	This work
$[K(18\text{-crown-6})(THF)_2][Cp^t{}_3Gd]$[a]	83	28	18
$[K(crypt)][Cp'_3Gd]$[b]	85	29	7
$[K(crypt)][Cp^{tet}{}_3Gd]$[c]	83	28	19
$[K(crypt)][(N(SiMe_3)_2)_3Gd]$	85	29	21

Spectroscopic analysis.

EPR spectroscopy was performed on **2.1-Gd** at room temperature (RT) and at 77 K, Figure 2.2. The RT spectrum consists of an isotropic signal centered at g_{iso} = 1.982. This

value is similar to the g_{iso} = 1.9786[19] and 1.987[7] values for other isolated Gd(II) complexes. The spectrum taken at 77 K has an approximate g value of 1.95, which is slightly lower than that of [K(crypt)][Cp′$_3$Gd].[7] A comparison of EPR parameters of **2.1-Gd** with other isolated [Cp$^x_3$Gd^{II}]$^-$ complexes is summarized in Table 2.4.

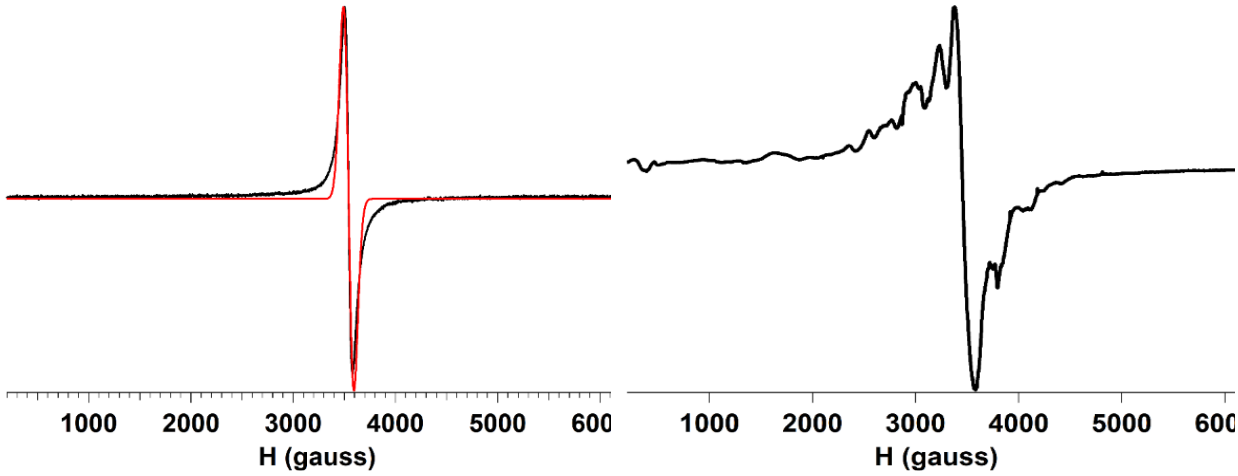

Figure 2.2. Experimental (black) and simulated (red) X-band EPR spectra of **2.1-Gd** taken at RT (left) and 77 K (right).

Table 2.4: Comparison of EPR parameters of [Cp$^x_3$Gd^{II}]$^-$ complexes.

[a] Cp^t = $C_5H_4CMe_3$. [b] Cp′ = $C_5H_4SiMe_3$. [c] Cp^{tet} = C_5Me_4H.

Complex	T	g	Ref
2.1-Gd	RT	1.982	This work
	77 K	1.95	
[K(18-crown-6)(THF)$_2$][Cp$^t_3$Gd][a]	RT	1.88	18
[K(crypt)][Cp′$_3$Gd][b]	RT	1.987	7
	77 K	1.984	
[K(crypt)][Cp$^{tet}_3$Gd][c]	RT	1.9786	19

[(18-crown-6)K(μ-Cp^{Me})K(18-crown-6)][Cp$^{Me}_3$Nd], 2.1-Nd. Cp$^{Me}_3$Nd(THF), 1 equivalent of KCp^{Me}, and 2 equivalents of 18-crown-6 were dissolved in 2 mL THF and placed in a −35 °C freezer. The next day, the THF solution was reacted with 2 equivalents of chilled

(−35 °C) KC_8 for an hour and filtered, leaving a black solution. This solution was layered with hexanes and placed at −35 °C. Overnight, dark purple needle-like crystals were isolated and identified by X-ray diffraction as [(18-crown-6)K(μ-Cp^{Me})K(18-crown-6)][Cp^{Me}_3Nd], **2.1-Nd**, eq 2.3.

2.1-Nd crystallizes in the same unit cell as **2.1-Gd**, Figure 2.1. However, the X-ray data obtained on these crystals was not high enough quality to obtain metrical parameters. Crystals of **2.1-Nd** are stable at −35 °C for at least four months but decompose almost instantly at room temperature. This instability made it difficult to obtain quality X-ray data. However, Guzei analysis was still performed the on the crystal data of **2.1-Nd** as most of the disorder was contained on the countercation and co-crystallized THF molecules, not the [Cp^{Me}_3Nd]$^-$ anion. Though the calculated Guzei parameters may not be entirely accurate due to the quality of the crystal data, they are still helpful for comparison of other [A_3Nd^{II}]$^-$ complexes.

Table 2.5: Comparison of G-parameters [%] of [A_3Nd^{II}]$^-$ complexes.

[a] Cp^t = $C_5H_4CMe_3$. [b] Cp′ = $C_5H_4SiMe_3$. [c] Cp^{tet} = C_5Me_4H.

Complex	$G_{complex}$	G_L (avg)	Ref
2.1-Nd	72	24	This work
[K(crypt)][Cp′′$_3$Nd][a]	89	30	31
[K(crypt)][Cp′$_3$Nd][b]	83	28	17
[K(crypt)][Cp^{tet}_3Nd][c]	82	27	19
[Rb(crypt)][(N($SiMe_3$)$_2$)$_3$Nd]	83	28	21

Like **2.1-Gd**, **2.1-Nd** is much less sterically saturated than other isolated [A_3Nd^{II}]$^-$ complexes, with a *G* value of 72% compared to the 82-89% range of the reported [A_3Nd^{II}]$^-$ complexes. The unsaturation of the coordination sphere of **2.1-Nd** could be an explanation for its extreme thermal instability. Figure 2.3 provides a visualization of the degree of

unsaturation of the coordination sphere of **2.1-Nd** with a comparison to the more sterically saturated $[Cp''_3Nd]^-$. The shaded regions indicate the shielding of the coordination sphere by the Cp ligands. Much of the Nd(II) ion is left unshielded in **2.1-Nd**, as depicted by the large percentage of unshaded areas in Figure 2.3, particularly on the axis perpendicular to the trigonal plane of the three Cp ligands. The trimethylsilyl substituents on the Cp rings in more saturated Nd(II) complex, $[Cp''_3Nd]^-$ (G = 89%) do a much better job in shielding the Nd(II) ion than the methyl substituent in Cp^{Me}, as this complex does not have such a large opening perpendicular to the trigonal plane as seen in **2.1-Nd**. In fact, a percentage of the coordination sphere of $[Cp''_3Nd]^-$ is shielded by two of the Cp'' ligands simultaneously, as demonstrated by the overlapping shaded areas. No such overlap is seen for **2.1-Nd**.

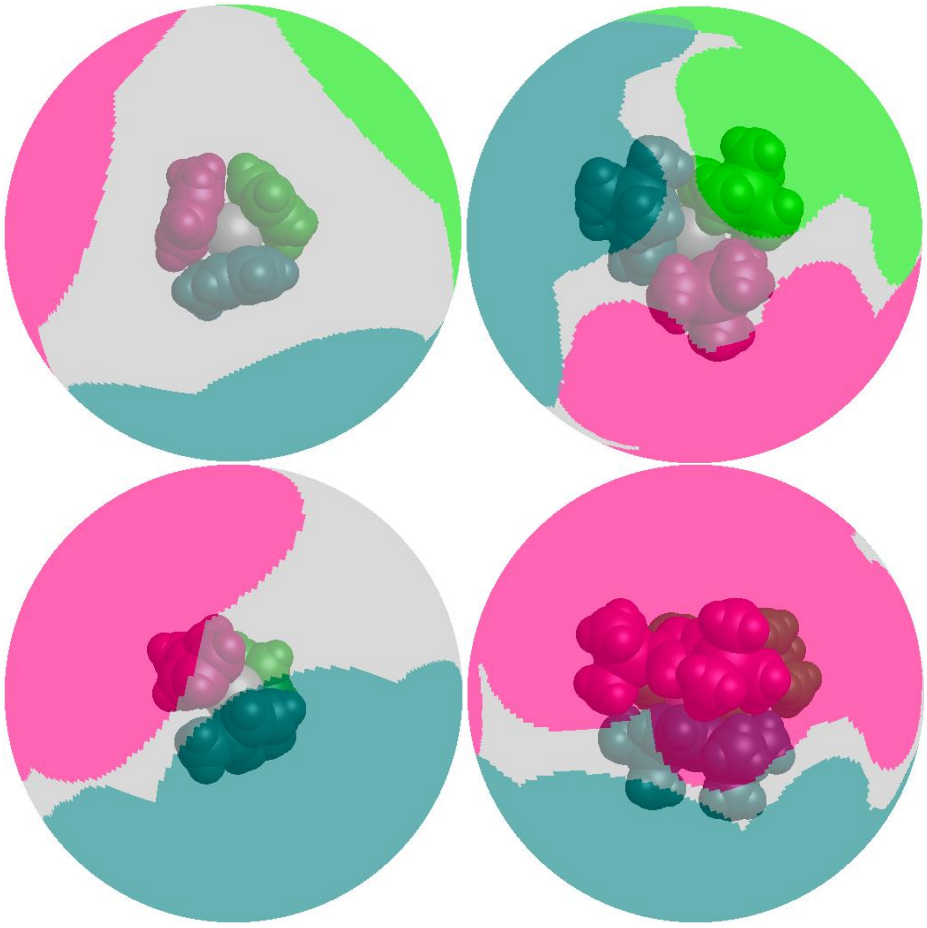

Figure 2.3. Comparative visualization of how the ligands in **2.1-Nd** (left) versus the ligands in $[Cp''_3Nd]^-$ (right) saturate the Nd coordination sphere.

Table 2.6: Comparison of G-parameters [%] of $[Cp^{Me}_3Ln^{II}]^-$ complexes.

Ln	$G_{complex}$	Ref
Nd	72	This work
Gd	74	This work
Tb	74	[20]
Ho	75	[20]

Conclusion

The **2.1-Ln** complexes are the least sterically saturated crystallographically characterized Ln(II) complexes isolated. The low *G* values of 74% and 72% for **2.1-Gd** and **2.1-Nd**, respectively, compared to the typical 82-86 % range of more stable Ln(II) complexes show that the Cp^{Me} ligand does not shield the Ln ions as sufficiently as the bulkier Cp analogues. The series of isolable $[Cp^{Me}_3Ln^{II}]^-$ complexes have *G* values which range from 72-75%, which is lower than more stable isolated Ln(II) complexes, which range 80–92% (Table 2.6).[21,32–34] However, as stated in Chapter 1, a higher *G* value does not always mean a more stable Ln(II) complex. For example, $[Cp''_3Nd]^-$ has the most saturated coordination sphere of the reported $[A_3Nd^{II}]^-$ compounds with *G* value of 89%, but it is less thermally stable than $[Cp'_3Nd]^-$ (*G* = 83%). Therefore, factors other than ligand bulk should be considered when designing thermally stable and isolable Ln(II) complexes.

The choice of countercation has shown to be important in isolating these unstable $[Cp^{Me}_3Ln^{II}]^-$ complexes. Countercations containing a cyclopentadienyl anion sandwiched between two K(crown) cations have been reported before,[7,35–40] but $[(18\text{-crown-6})K(\mu\text{-}Cp^{Me})K(18\text{-crown-6})]^+$ is just the third example of a countercation of this type containing a substituted cyclopentadienyl ring.[20] The $[K(crypt)]^+$ cation was only suitable to crystallize

$[Cp^{Me}_3Dy^{II}]^-$.[20] However, the $[(18\text{-crown-6})K(\mu\text{-}Cp^{Me})K(18\text{-crown-6})]^+$ countercation was able to facilitate crystallization of $[Cp^{Me}_3Ln^{II}]^-$ complexes for Tb, Ho, and now, the larger metals Nd and Gd. Along with the choice of countercation, solvent choice is also important when isolating Ln(II) complexes and will be described in the following chapter.

Experimental

All manipulations and syntheses described below were conducted with the rigorous exclusion of air and water using standard Schlenk line and glovebox techniques under an argon atmosphere, unless stated otherwise. Solvents were sparged with UHP argon and dried by passage through columns containing Q-5 and molecular sieves prior to use. 18-crown-6 (Alfa Aesar) was sublimed under high vacuum (10^{-5} torr) for 12 h at 50 °C. Anhydrous $LnCl_3$[41] (Ln = Nd, Gd) and KC_8[42] were prepared according to literature procedures. KCp^{Me} [43] was prepared according to modified literature procedures by cracking the $(Cp^{Me})_2$ dimer to HCp^{Me} and distilling it onto a toluene solution of $KN(SiMe_3)_2$. The resulting colorless precipitate, KCp^{Me}, was washed with cold toluene and hexane and dried. $(C_5H_4Me)_3Ln(THF)$ (Ln = Nd, Gd) were synthesized according to modified literature procedures.[24] $LnCl_3$ was stirred with either KCp^{Me} or $NaCp^{Me}$ in THF overnight. The slurry was centrifuged to remove insoluble and THF was removed *in vacuo*. The resulting tacky solids were dissolved in toluene to remove more insoluble material. Crystals of $(C_5H_4Me)_3Ln(THF)$ were grown from concentrated toluene solutions at −35 °C.

$[(18\text{-crown-6})K(\mu\text{-}Cp^{Me})K(18\text{-crown-6})][Cp^{Me}_3Gd]$, 2.1-Gd. $Cp^{Me}_3Gd(THF)$ (60 mg, 0.13 mmol) and 18-crown-6 (68 mg, 0.26 mmol) were dissolved in 1 mL of THF and placed in a −35 °C freezer. The next day, the colorless THF solution was reacted with KC_8 (19 mg,

0.14 mmol) for an hour and filtered. Dark purple needlelike crystals of **2.1-Gd**, suitable for X-ray diffraction, were grown overnight from THF/hexane at −35 °C.

[(18-crown-6)K(μ-Cp^{Me})K(18-crown-6)] [Cp$^{Me}_3$Nd], 2.1-Nd. Cp$^{Me}_3$Nd(THF) (50 mg, 0.11 mmol), KCp^{Me} (13 mg, 0.11 mmol), and 18-crown-6 (58 mg, 0.22 mmol) were dissolved in 2 mL of THF and placed in a −35 °C freezer. The next day, the pale blue THF solution was reacted with KC_8 (33 mg, 0.24mmol) for an hour at −35 °C and filtered, yielding a black solution. Dark purple needlelike crystals of **2.1-Nd**, suitable for X-ray diffraction, were grown overnight from THF/hexane at −35 °C.

X-ray Data Collection, Structure Solution and Refinement for [(18-crown-6)K(μ-Cp^{Me})K(18-crown-6)][Cp^{Me}_3Gd], 2.1-Gd.

A purple crystal of approximate dimensions 0.042 x 0.243 x 0.484 mm was mounted in a cryoloop and transferred to a Bruker SMART APEX II diffractometer. The APEX2[44] program package was used to determine the unit-cell parameters and for data collection (30 sec/frame scan time for a sphere of diffraction data). The raw frame data was processed using SAINT[45] and SADABS[46] to yield the reflection data file. Subsequent calculations were carried out using the SHELXTL[47] program. The diffraction symmetry was $2/m$ and the systematic absences were consistent with the monoclinic space group $P2_1/c$ that was later determined to be correct.

The structure was solved using the coordinates of the isomorphous terbium complex (structure code: HIPLOK) and refined on F^2 by full-matrix least-squares techniques. Based on the isomorphous terbium complex and from residual peaks observed in the difference-Fourier map, it appeared that one solvent molecule was disordered and included using multiple components, partial site-occupancy factors, and equivalent anisotropic thermal parameters. The analytical scattering factors[48] for neutral atoms were used throughout the analysis. Hydrogen atoms were included using a riding model.

Least-squares analysis yielded wR2 = 0.1070 and Goof = 1.027 for 680 variables refined against 15384 data (0.75 Å), R1 = 0.0421 for those 11511 data with $I > 2.0\sigma(I)$.

References

(1) Evans, W. J. *Inorg. Chem.* **2007**, *46*, 3435–3449.

(2) Freeman, A. J.; Watson, R. E. *Phys. Rev.* **1962**, *127* (6), 2058–2075.

(3) Anwander, R.; Herrmann, W. A. Features of Organolanthanide Complexes. In *Organolanthoid Chemistry: Synthesis, Structure, Catalysis*; Springer Berlin Heidelberg: Berlin, Heidelberg, 1996; pp 1–32.

(4) Evans, W. J. *Polyhedron* **1987**, *6* (5), 803–835.

(5) Evans, W. J.; Peterson, T. T.; Rausch, M. D.; Hunter, W. E.; Zhang, H.; Atwood, J. L. *Organometallics* **1985**, *4*, 554–559.

(6) Evans, W. J.; Kozimor, S. A.; Ziller, J. W. *Polyhedron* **2006**, *25*, 484–492.

(7) MacDonald, M. R.; Bates, J. E.; Ziller, J. W.; Furche, F.; Evans, W. J. *J. Am. Chem. Soc.* **2013**, *135* (26), 9857–9868.

(8) MacDonald, M. R.; Bates, J. E.; Fieser, M. E.; Ziller, J. W.; Furche, F.; Evans, W. J. *J. Am. Chem. Soc.* **2012**, *134* (20), 8420–8423.

(9) MacDonald, M. R.; Ziller, J. W.; Evans, W. J. *J. Am. Chem. Soc.* **2011**, *133* (40), 15914–15917.

(10) Meyer, G. *Chem. Rev.* **1988**, *88* (1), 93–107.

(11) Bochkarev, M. N.; Fedushkin, I. L.; Fagin, A. A.; Petrovskaya, T. V.; Ziller, J. W.; Broomhall-Dillard, R. N. R.; Evans, W. J. *Angew. Chem. Int. Ed.* **1997**, *36* (1–2), 133–135.

(12) Bochkarev, M. N.; Fedushkin, I. L.; Dechert, S.; Fagin, A. A.; Schumann, H. *Angew. Chem. Int. Ed.* **2001**, *40* (17), 3176–3178.

(13) Mikheev, N. B.; Auerman, L. N.; Rumer, I. A.; Kamenskaya, A. N.; Kazakevich, M. Z. *Russ. Chem. Rev.* **1992**, *61*, 990.

(14) Nugent, L. J.; Baybarz, R. D.; Burnett, J. L.; Ryan, J. L. *J. Phys. Chem.* **1971**, *77* (12), 1528–1539.

(15) Morss, L. R. *Chem. Rev.* **1976**, *76* (6), 827–841.

(16) Johnson, D. A. *J. Chem. Soc. Dalt. Trans.* **1974**, 1671–1675.

(17) Fieser, M. E.; Macdonald, M. R.; Krull, B. T.; Bates, J. E.; Ziller, J. W.; Furche, F.; Evans, W. J. *J. Am. Chem. Soc.* **2015**, *137* (1), 369–382.

(18) Angadol, M. A.; Woen, D. H.; Windorff, C. J.; Ziller, J. W.; Evans, W. J. *Organometallics* **2019**, *38* (5), 1151–1158.

(19) Jenkins, T. F.; Woen, D. H.; Mohanam, L. N.; Ziller, J. W.; Furche, F.; Evans, W. J. *Organometallics* **2018**, *37* (21), 3863–3873.

(20) Huh, D. N.; Ziller, J. W.; Evans, W. J. *Dalt. Trans.* **2018**, *47*, 17285–17290.

(21) Ryan, A. J.; Darago, L. E.; Balasubramani, S. G.; Chen, G. P.; Ziller, J. W.; Furche, F.; Long, J. R.; Evans, W. J. *Chem. Eur. J.* **2018**, *24*, 7702–7709.

(22) Moehring, S. A.; Beltrán-Leiva, M. J.; Páez-Hernández, D.; Arratia-Pérez, R.; Ziller, J. W.; Evans, W. J. *Chem. Eur. J.* **2018**, *24*, 18059–18067.

(23) Gould, C. A.; McClain, K. R.; Yu, J. M.; Groshens, T. J.; Furche, F.; Harvey, B. G.; Long, J. R. *J. Am. Chem. Soc.* **2019**, *141* (33), 12967–12973.

(24) Corbey, J. F.; Woen, D. H.; Palumbo, C. T.; Fieser, M. E.; Ziller, J. W.; Furche, F.; Evans, W. J. *Organometallics* **2015**, *34*, 3909–3921.

(25) Woen, D. H.; Huh, D. N.; Ziller, J. W.; Evans, W. J. *Organometallics* **2018**, *37*, 3055–3063.

(26) Gun'ko, Y. K.; Hitchcock, P. B.; Lappert, M. F. *Chem. Commun.* **1998**, 1843–1844.

(27) Evans, W. J.; Hunter, W. E.; Grate, J. W.; Choi, H. W.; Bloom, I.; Atwood, J. L. *J. Am. Chem. Soc.* **1985**, *107* (4), 941–946.

(28) Evans, W. J.; Foster, S. E. *J. Organomet. Chem.* **1992**.

(29) Shannon, R. D. *Acta Crystallogr. Sect. A* **1976**, *A32*, 751–767.

(30) Guzei, I. A.; Wendt, M. *J. Chem. Soc. Dalt. Trans.* **2006**.

(31) Palumbo, C. T.; Darago, L. E.; Windorff, C. J.; Ziller, J. W.; Evans, W. J. *Organometallics* **2018**, *37* (6), 900–905.

(32) Fieser, M. E.; Macdonald, M. R.; Krull, B. T.; Bates, J. E.; Ziller, J. W.; Furche, F.; Evans, W. J. *J. Am. Chem. Soc.* **2015**, *137* (1), 369–382.

(33) Moehring, S. A.; Miehlich, M.; Hoerger, C. J.; Meyer, K.; Ziller, J. W.; Evans, W. J. *Inorg. Chem* **2020**, *59*, 3207–3214.

(34) Kundu, K.; White, J. R. K.; Moehring, S. A.; Yu, J. M.; Ziller, J. W.; Furche, F.; Evans, W. J.; Hill, S. *Nat. Chem.* **2022**, *14*, 392–397.

(35) Berthet, J. C.; Villiers, C.; Le Maréchal, J. F.; Delavaux-Nicot, B.; Lance, M.; Nierlich, M.; Vigner, J.; Ephritikhine, M. *J. Organomet. Chem.* **1992**, *440* (1–2), 53–65.

(36) Arp, H.; Zirngast, M.; Marschner, C.; Baumgartner, J.; Rasmussen, K.; Zark, P.; Müller, T. *Organometallics* **2012**, *31* (11), 4309–4319.

(37) Zirngast, M.; Flörke, U.; Baumgartner, J.; Marschner, C. *Chem. Commun.* **2009**, 5538–5540.

(38) Benda, C. B.; Waibel, M.; Fässler, T. F. *Angew. Chem. Int. Ed.* **2015**, *54* (2), 522–526.

(39) Zitz, R.; Arp, H.; Hlina, J.; Walewska, M.; Marschner, C.; Szilvási, T.; Blom, B.; Baumgartner, J. *Inorg. Chem.* **2015**, *54* (7), 3306–3315.

(40) Sänger, I.; Kückmann, T. I.; Dornhaus, F.; Bolte, M.; Wagner, M.; Lerner, H. W. *Dalt. Trans.* **2012**, *41*, 6671–6676.

(41) Meyer, G.; Ax, P. *Mater. Res. Bull.* **1982**, *17* (11), 1447–1455.

(42) Bergbreiter, D. E.; Killough, J. M. *J. Am. Chem. Soc.* **1978**.

(43) Reynolds, L. T.; Wilkinson, G. *J. Inorg. Nucl. Chem.* **1959**, *9* (1), 86–92.

(44) *APEX2*; Version 2014.11-0; Bruker AXS, Inc.: Madison, WI, 2014.

(45) *SAINT*; Version 8.34a; Bruker AXS, Inc.: Madison, WI, 2013.

(46) Sheldrick, G. M. *SADABS*; Version 2014/5; Bruker AXS, Inc.: Madison, WI, 2014.

(47) Sheldrick, G. M. *SHELXTL*; Version 2014/7; Bruker AXS, Inc.: Madison, WI, 2014.

(48) *International Tables for Crystallography*, Vol. C.; Prince, E., Ed.; Dordrecht: Kluwer Academic Publishers., 2006.

CHAPTER 3

Isolation of Ln^{2+} Complexes Bridged by a Toluene Dianion

Introduction

As discussed in previous chapters, there are many factors that can influence the stability of the nontraditional $4f^n5d^1$ Ln^{2+} ions. The steric properties of the ancillary ligand of a Ln^{2+}-containing complex can be tuned to increase its thermal stability.[1–3] The choice of the $[M(chelate]^+$ countercation can affect the thermal stability of the Ln^{2+} complex[4] as well as its rate of crystallization.[5] The solvent used during the reduction of the Ln^{3+} precursor also plays an important role. Due to their highly reducing nature, Ln^{2+} ions have been reported to activate solvents such as THF[6] and dimethoxyethane (DME).[7] In 1997, Lappert *et al.* reported the first EPR evidence of a La^{2+} intermediate via the potassium reduction of Cp''_3La ($Cp'' = C_5H_3(SiMe_3)_2$-1,3).[8] However, it rapidly decomposed in the DME solvent by facilitating the C–O bond cleavage of a DME molecule.[7] A year later, Lappert *et al.* isolated the first crystallographically characterized example of a La^{2+} compound via the potassium reduction of Cp^{tt}_3La ($Cp^{tt} = C_5H_3(CMe_3)_2$-1,3) in benzene, where a benzene molecule was also reduced to form the complex, $[K(18\text{-crown-}6)(\eta^2\text{-}C_6H_6)][(Cp^{tt}_2La)_2(\mu\text{-}\eta^6\text{:}\eta^6\text{-}C_6H_6)]$.[9] The solvent in this case stabilized the Ln^{2+} ion via co-reduction to form a monoanionic bridging ligand instead of facilitating its decomposition as observed during the earlier reductions in DME.

Subsequently, other reduced arene complexes were identified with the rare-earths and actinides with siloxide and cyclopentadienyl ancillary ligands, as well as amide ligands with the actinides, but no reduced arene rare-earth complexes were known with amide ligands.[10–29] There are only four examples of bimetallic reduced arene rare-earth complexes

containing Ln^{2+} ions, and all contain cyclopentadienyl ligands: $[K(crypt)]_2[(Cp'_2La)_2(\mu\text{-}\eta^6\text{:}\eta^6\text{-}C_6H_6)]$[11] ($Cp'$ = $C_5H_4SiMe_3$, crypt = 2.2.2-cryptand), $[K(18\text{-crown-6})(\eta^2\text{-}C_6H_5Me)_2][(Cp''_2Ce)_2(\mu\text{-}\eta^6\text{:}\eta^6\text{-}C_6H_5Me)]$,[10] $[K(18\text{-crown-6})][(Cp''_2La)_2(\mu\text{-}\eta^6\text{:}\eta^6\text{-}C_6H_6)]$,[9,30] and $[K(18\text{-crown-6})(\eta^2\text{-}C_6H_6)][(Cp^{tt}_2La)_2(\mu\text{-}\eta^6\text{:}\eta^6\text{-}C_6H_6)]$.[9] Out of these four examples, only $[K(crypt)]_2[(Cp'_2La)_2(\mu\text{-}\eta^6\text{:}\eta^6\text{-}C_6H_6)]$ contains an arene dianion while the rest are arene monoanions.

The tris(amido)lanthanide complexes with the formula $[K(crypt)][Ln(NR_2)_3]$ ($R = SiMe_3$) have been identified for Ln = Sc,[31] Nd, Gd, Tb, Dy, Ho, Er, and Tm.[32] However, these complexes were not isolated for the largest members of the series, La, Ce, and Pr. I attempted to expand the $[K(crypt)][Ln(NR_2)_3]$ series to La, Ce, and Pr to probe the limits of steric unsaturation of these Ln^{2+} complexes. During these attempts, the formation of bimetallic complexes bridged by a reduced toluene occurred unexpectedly, $[K(crypt)]_2[\{(R_2N)_2Ln\}_2(\mu\text{-}\eta^6\text{:}\eta^6\text{-}C_6H_5Me)]$, **1-Ln** (Ln = La, Ce). Part of this chapter will describe the synthesis and characterization of the **1-Ln** complexes.

Reduced arene complexes of the lanthanide and actinides have shown to have remarkable magnetic properties. Single-molecule magnet (SMM) behavior has been observed for a reduced toluene-bridged diuranium complex[33] and a reduced biphenyl-bridged didysprosium complex,[23] meaning they retain their magnetization in the absence of an applied magnetic field. The SMM behavior of the Dy complex was influenced by the high magnetic exchange interactions that the reduced biphenyl facilitated between the Dy ions. Maximizing magnetic exchange is an important factor for designing SMMs. Previously, our group made a breakthrough in the field of SMMs by synthesizing the $(N_2)^{3-}$ -bridged compounds, $[K(18\text{-crown-6})(THF)_2]\{[(R_2N)_2Ln(THF)]_2(\mu\text{-}\eta^2\text{:}\eta^2\text{-}N_2)\}$ (Ln = Tb, Dy, Gd, Er,

Ho), which had increased the maximum SMM blocking temperatures from 4K to 8 K for Dy and to 14 K for Tb.[34,35] The magnetic studies performed by the group of Professor Jeffrey Long at UC Berkeley suggested that the diffuse orbital of the $(N_2)^{3-}$ radical enhanced the magnetic exchange coupling of the lanthanide centers it bridged. The magnetic exchange between the metal centers facilitated by the $(N_2)^{3-}$ radical in the Gd(III) complex, [K(18-crown-6)(THF)$_2$]{[(R$_2$N)$_2$Gd(THF)]$_2$(μ-η^2:η^2-N$_2$)}, led to a coupling constant of J = −27 cm^{-1}, the strongest rare-earth magnetic coupling ever observed.[34]

Arene-bridged lanthanide complexes have particularly strong magnetic exchange coupling between the lanthanide and reduced arene bridging ligand. The monoanionic benzene-bridged-La^{2+} complex, [K(18-crown-6)][(Cp″$_2$La)$_2$(μ-η^6:η^6-C$_6$H$_6$)], showed strong antiferromagnetic exchange coupling, J > −400 cm^{-1}, which was one of the highest exchange values observed for a lanthanide ion.[30] Therefore, it was of interest to see if the **1-Ln** series could be extended to other metals beyond the La and Ce examples mentioned earlier. Described in this chapter are the reduction reactions of Ln(NR$_2$)$_3$ (Ln = Y, Gd, Tb, Dy) in toluene, which showed evidence of the formation of [{(R$_2$N)$_2$Ln}$_2$(μ-η^6:η^6-C$_6$H$_5$Me)]$^{2-}$. Also described is the reduction of [(THF)(R$_2$N)$_2$Tb]$_2$(μ-Cl)$_2$ in toluene which afforded the first crystallographically characterized terbium complex featuring a reduced arene, [K(crypt)]$_3$[{(R$_2$N)$_2$Tb}$_2$(μ-η^6:η^6-C$_6$H$_5$Me)][K(NR$_2$)$_2$(THF)$_2$], **2-Tb**.

Results and Discussion

Synthesis of [K(crypt)]$_2$[{(R$_2$N)$_2$Ln}$_2$(μ-η^6:η^6-C$_6$H$_5$Me)], 1-Ln (Ln = La, Ce). The reduction of Ln(NR$_2$)$_3$ (Ln = La, Ce) with excess potassium metal in the presence of crypt in THF at −35 °C yielded dark purple single crystals which were identified by X-ray crystallography as not the expected [K(crypt)][Ln(NR$_2$)$_3$] complex, but as

[K(crypt)]$_2$[{(R$_2$N)$_2$Ln}$_2$(μ-η^6:η^6-C$_6$H$_5$Me)], **1-Ln**, eq 3.1, figure 3.1. Residual toluene in the glovebox atmosphere or toluene contamination in the THF solvent was evidently the source of the arene. The deliberate addition of stoichiometric toluene to a THF solution of Ln(NR$_2$)$_3$ and crypt followed by reduction with potassium metal reproduced **1-Ln** in 80% yield for Ce and 78% yield for La.

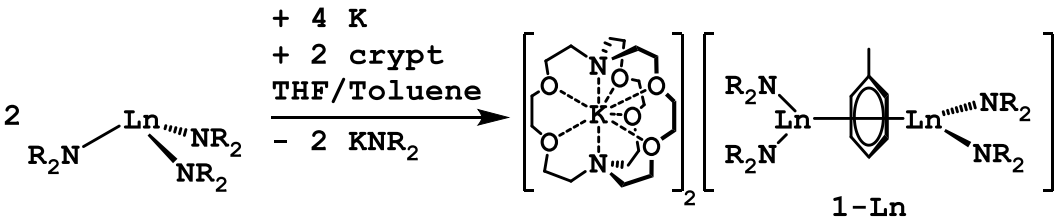

(3.1)

Ln = La and Ce; R = SiMe$_3$;
crypt = 2.2.2-cryptand

The formal reaction involves the reduction of two equivalents of Ln(NR$_2$)$_3$ and one toluene molecule with four equivalents of potassium. Each Ln ion in **1-Ln** has lost an anionic NR$_2$ ligand from the starting Ln(NR$_2$)$_3$ complex with a formal loss of two equivalents of K(NR$_2$) from the reaction. The [{(R$_2$N)$_2$Ln}$_2$(μ-η^6:η^6-C$_6$H$_5$Me)]$^{2-}$ complex could be described two ways: a pair of Ln^{2+} ions bridged by a toluene dianion (Ln^{2+}/(toluene)$^{2-}$/Ln^{2+}) or a pair of Ln^{3+} ions bridged by a toluene tetraanion (Ln^{3+}/(toluene)$^{4-}$/Ln^{3+}). Though a mixed-valent Ln^{2+}/(toluene)$^{3-}$/Ln^{3+} configuration is theoretically possible, it is highly improbable and will not be considered.

1-La displayed diamagnetic behavior: its EPR spectrum was featureless and it had a well-resolved, non-broadened ^{1}H spectrum. The ^{1}H NMR spectrum displayed the expected 2.2.2-cryptand resonances and peaks from 0.0 to 0.2 ppm attributed to the trimethylsilyl protons of the amide ancillary ligands. Interestingly, there is a singlet that is shifted relatively upfield, at −0.59 ppm, but it could not be confidently assigned to any protons in **1-La**. Reduction of La(NR$_2$)$_3$ using toluene-d$_8$ was explored to assign the protons from the bridging

toluene ligand. Three multiplet peaks at 6.69, 6.64, and 6.14 ppm were assigned to the protons of the reduced toluene ring in **1-La** due to their absence from the toluene-d_8 reaction. The methyl group of the toluene ring could not be confidently assigned, though there is a singlet at −0.22 ppm that is absent from the toluene-d_8 reaction. The UV-visible spectrum was taken for **1-Ce** and features an absorption peak at 360 nm (ε = 2030 $M^{-1}cm^{-1}$) as well as broad shoulder peaks at 434, 496, and 672 nm (ε = 843, 569, and 435 $M^{-1}cm^{-1}$, respectively). The peaks for **1-Ce** are not nearly as intense as other reported Ce(II) complexes (ε = 3000 – 5000 $M^{-1}cm^{-1}$)[36] and reduced arene-bridged Ce(II) complexes (ε = 6000 – 8000 $M^{-1}cm^{-1}$).[37]

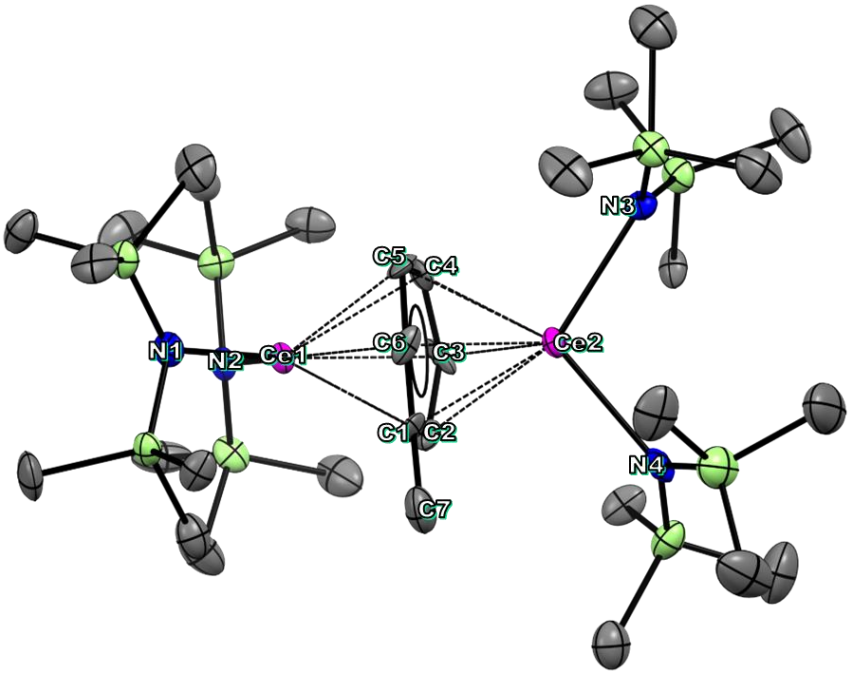

Figure 3.1. Thermal ellipsoid plot of **1-Ce** drawn at the 50% probability level. Hydrogen atoms, a co-crystallized THF molecule, and two $[K(crypt)]^+$ cations were omitted for clarity. Color code: Grey = C, Red = O, Blue = N, Green = Si, Pink = Ce.

The structural data of **1-Ce** are summarized in Table 3.1. The four NR_2 ligands in **1-Ce**, which feature Ce–N lengths ranging from 2.532(7)–2.559(8) Å, are staggered around the

$Ce_2(\mu\text{-}C_6H_5Me)$ core, producing a tetrahedral rather than a square planar geometry. The tetrahedral arrangement of the amide ligands differs from other bimetallic bis(amido)cerium complexes, such as $[\{Ce(NR_2)_2(\mu\text{-}O)\}_2]$[38], $[\{Ce(TMP)_2(\mu\text{-}OEt)\}_2]$[39] (TMP = tetramethylpiperidinate) and $[\{Ce(TMP)_2(\mu\text{-}OCH{=}CH_2)\}_2]$,[40] where the NR_2 ligands eclipse each other in a square planar arrangement.

Table 3.1: Selected bond lengths [Å] and angles [°] of **1-Ce**.

[a] Cnt is the centroid of the toluene. [b]Pln1 and Pln2 are the planes defined by C1, C2, C3, C6 and C3–C6, respectively. Θ = the dihedral angle between Pln1 and Pln2

Ce(1)–C(1)	2.675(8)	**Ce(2)–C(1)**	2.630(10)	**C(1)–C(2)**	1.452(11)	**Ce(1)–N(1)**	2.532(7)
Ce(1)–C(2)	2.594(10)	**Ce(2)–C(2)**	2.662(11)	**C(2)–C(3)**	1.471(14)	**Ce(1)–N(2)**	2.557(7)
Ce(1)–C(3)	2.683(9)	**Ce(2)–C(3)**	2.534(10)	**C(3)–C(4)**	1.442(15)	**Ce(2)–N(3)**	2.559(8)
Ce(1)–C(4)	2.580(10)	**Ce(2)–C(4)**	2.632(11)	**C(4)–C(5)**	1.446(12)	**Ce(2)–N(4)**	2.536(9)
Ce(1)–C(5)	2.569(11)	**Ce(2)–C(5)**	2.686(10)	**C(5)–C(6)**	1.482(14)	**Ce(1)–Cnt[a]**	2.183
Ce(1)–C(6)	2.675(8)	**Ce(2)–C(6)**	2.549(9)	**C(6)–C(1)**	1.432(15)	**Ce(2)–Cnt[a]**	2.176
						$\Theta_{Pln1-Pln2}$[b]	8.24

The bridging toluene unit is not planar. **1-Ce** has a dihedral angle of 8.24° between the planes defined by C1, C2, C3, C6 and C3–C6. However, the toluene in **1-Ce** is more planar than the benzene dianion in the previously reported $[K(crypt)]_2[(Cp'_2La)_2(\mu\text{-}\eta^6\text{:}\eta^6\text{-}C_6H_6)]$,[11] as this complex has a dihedral angle of 11°. Because of the increased planarity of the toluene ring in **1-Ce**, the ring does not have the same bent, boat configuration with two out of plane carbons being closer to the lanthanide ions to the same extent as in the previously reported benzene 1,4-dianions.[11,41] Yet, the shortest Ce–C_{arene} distances for Ce(1), Ce(1)–C(2), Ce(1)–C(4) and Ce(1)–C(5), are the longest Ce–C_{arene} distances for Ce(2). The longest Ce–C_{arene} distances for Ce(1), (*i.e.,* Ce(1)–C(1), Ce(1)–C(3), and Ce(1)–C(6)), are the shortest Ce–C_{arene} distances for Ce(2). This correlation is similar to the correlation in La–C_{arene} distances in $[K(crypt)]_2[(Cp'_2La)_2(\mu\text{-}\eta^6\text{:}\eta^6\text{-}C_6H_6)]$ containing the 1,4-cyclohexa-2,5-dienyl bridge.[11] The

C–C_{arene} bond lengths of the toluene ring in **1-Ce** have an average length of 1.454(14) Å compared to 1.385(3) Å in free toluene.[42] Within the error limits, the C–C_{arene} distances in **1-Ce** are indistinguishable from one another and are similar to singly and doubly reduced arene complexes, Table 3.2.

Table 3.2: A comparison of C–C_{arene} bond lengths in reduced arene compounds [Å].
[a] X = $^{-}OSi(OtBu)_3$

Compound	Avg C–C_{arene}	Ref
$\{[(R_2N)_2Ce]_2(\mu\text{-}\eta^6\text{:}\eta^6\text{-}C_6H_5Me)\}^{2-}$	1.454(14)	this work
$[(Cp'_2La)_2(\mu\text{-}\eta^6\text{:}\eta^6\text{-}C_6H_6)]^{2-}$	1.453(5)	[11]
$[(Cp^{tt}_2La)_2(\mu\text{-}\eta^6\text{:}\eta^6\text{-}C_6H_6)]^{-}$	1.44(1)	[9]
$[\{KX_3Ce\}((\mu\text{-}\eta^6\text{:}\eta^6\text{-}C_6H_5Me)_2Ce]^{2-}$ [a]	1.441(18)	[15]
$[(Cp''_2La)(C_6H_6)]^{1-}$	1.425(56)	[41]
$[\{(R_2N)_2U\}_2(\mu\text{-}\eta^6\text{:}\eta^6\text{-}C_6H_5Me)]$	1.451	[20]
$[\{U(BIPM^{TMS}H)(I)\}_2(\mu\text{-}\eta^6\text{:}\eta^6\text{-}C_6H_5Me)]$	1.436(16)	[33]
Toluene	1.385(3)	[42]

DFT calculations were performed by Dr. Luke Mohanam from the group of Professor Filipp Furche at UCI on the **1-Ln** complexes. It was found that **1-La** has closed shell singlet electronic ground state and **1-Ce** has an open shell singlet electronic ground state with contributions from the two $4f^1$ electrons of opposite spins between the two Ce atoms. The singlet electronic ground state for **1-Ln** could be explained by either the complex consisting of two Ln^{3+} ions and a toluene tetraanion, or antiferromagnetic coupling between two Ln^{2+} ions and a toluene dianion. The crystallographic data of **1-Ln** suggest that this complex contains two Ln^{2+} ions bridged by a toluene dianion. The 1.460(17) Å average C–C_{arene} bond length in the toluene bridge of **1-Ln** is similar to other arene dianions. Furthermore, the average C–C_{arene} bond length in **1-Ln** is larger than the C–C_{arene} bond lengths in free toluene.[15,20,33] However, the increased planarity of the toluene ring in **1-Ln** compared to

previously reported arene dianions and the lack of a highly absorbing peak, characteristic for $4f^n5d^1$ Ln^{2+} ions, in the U-visible spectrum of **1-Ce**, could suggest that **1-Ln** consists of two Ln^{3+} ions and a toluene tetraanion and thus adds ambiguity to the charge of the toluene and the oxidation states of the metals in **1-Ln**.

Reductions of $Ln(NR_2)_3$ (Gd, Tb, Dy, Y). Though bimetallic Ln^{3+} complexes featuring reduced arene bridging ligands have been reported before for metals other than La or Ce, the only other Ln^{2+} examples are those of the traditional $4f^n$ ions Sm and Yb.[43] Therefore, it was of interest to see if **1-Ln** could extend to other nontraditional ions.

$Gd(NR_2)_3$ and crypt were dissolved in a mixture of toluene and THF and cooled to −35 °C. This colorless solution was added to excess KC_8 and immediately turned dark blue. The reaction mixture was placed in a −35 °C freezer and it turned dark green overnight. Over the course of a week the color became a dark red brown. The red brown reaction mixture was filtered, layered with hexane, and placed at −35 °C, where a dark red oil precipitated overnight from a yellow supernatant. The hexane was removed *in vacuo* to isolate the dark red oil. The oil was washed with hexane, dissolved in minimum THF, and placed at −35 °C. Dark single crystals formed over the course of a week. The quality of the crystals isolated from the Gd reaction was not high enough to obtain a resolved structure via X-ray crystallography. However, three $[K(crypt)]^+$ cations and a $[\{(R_2N)_2Gd\}_2(\mu\text{-}\eta^6\text{:}\eta^6\text{-}C_6H_5Me)]^{2-}$ dianion were observed in the crystal lattice among the disorder.

The same reaction was repeated for $Tb(NR_2)_3$ and $Dy(NR_2)_3$. As observed for the reduction of $Gd(NR_2)_3$ in the presence of toluene, the reaction mixtures for both Tb and Dy immediately turned dark blue before turning dark red brown over the course of a week. Also like the Gd reaction, only intractable red-brown oils were produced. From these

observations it was hypothesized that $Ln(NR_2)_3$ was reduced to $[Ln(NR_2)_3]^-$ first before reacting with toluene to form the red-brown products. Reductions of $Ln(NR_2)_3$ were then performed in neat toluene to investigate if that would destabilize any formation of $[Ln(NR_2)_3]^-$ and facilitate a cleaner reaction than performing the reduction in THF. The toluene solution remained colorless as red-brown oils precipitated from the reaction, no dark blue color indicative of $[Ln(NR_2)_3]^-$ was observed. UV-visible spectra were taken of the red brown oils from the reduction of $Dy(NR_2)_3$ and $Tb(NR_2)_3$ and compared to **1-Ce**, figure 3.2. As the composition of these oils could not be confirmed, molar extinction coefficients were not calculated. The reduction products of Tb and Dy feature similar broad shoulder peaks centered at approximately λ_{max} = 435, 496, and 680 nm and do not contain the characteristic peaks seen in the UV-visible spectra of $[Ln(NR_2)_3]^-$.[32]

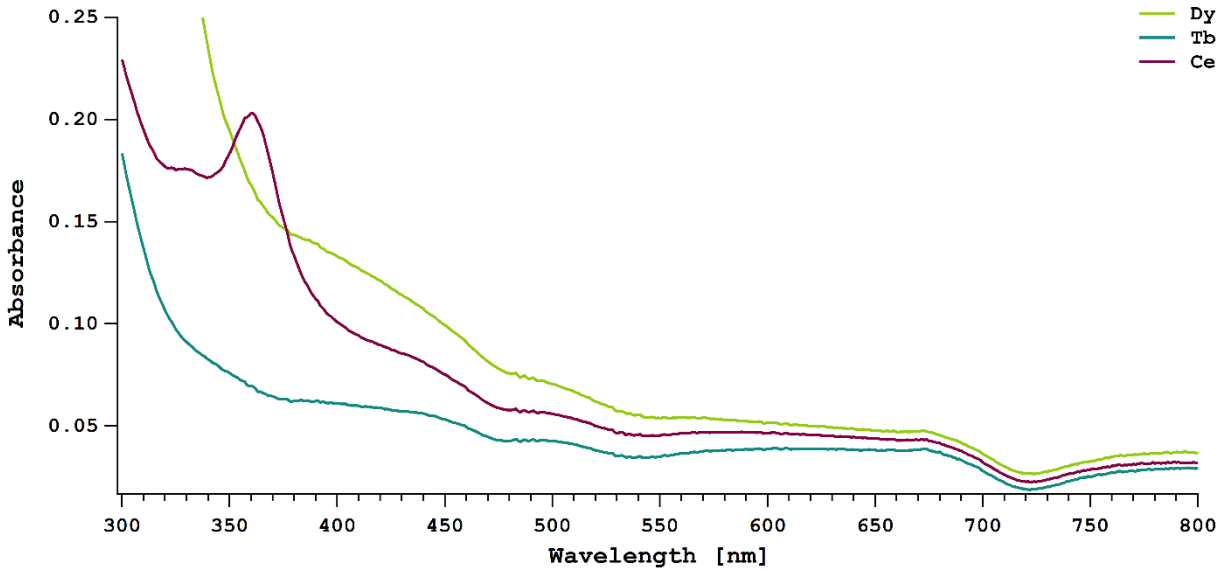

Figure 3.2. Room temperature UV-visible spectra of the reduction products of $Dy(NR_2)_3$ (green trace) and $Tb(NR_2)_3$ (blue trace), compared to a ~1 mM solution of **1-Ce** (purple trace).

Since $[Y(NR_2)_3]^-$ is much less stable than the Gd, Tb, and Dy analogues and could not be isolated with a $[K(crypt)]^+$ countercation,[5] it was hypothesized that the potassium reduction of $Y(NR_2)_3$ in the presence of crypt and toluene may behave similarly to $La(NR_2)_3$ and $Ce(NR_2)_3$ and form a reduced arene compound similar to **1-Ln**. As described previously, $Y(NR_2)_3$ and crypt were dissolved in toluene and THF and cooled to −35 °C. Upon addition to a cooled vial of excess potassium metal, the colorless solution turned to a clear dark yellow. After one day, it became greener. The solution was filtered and after another day at −35 °C, colorless needle crystals precipitated from the now clear orange-yellow solution. The solution was filtered from the crystals and the solvent was removed *in vacuo* to yield tacky orange solids, which were then washed with toluene and pentane to remove the tackiness. These solids were dissolved in THF, layered with hexane, and placed in a −35 °C freezer. After several days, colorless needles as well as deep brownish-red rectangular plate crystals precipitated. The red crystals did not produce X-ray data of sufficient quality, so metrical parameters and a non-disordered structure could not be obtained. However, like described above for the reduction of $Gd(NR_2)_3$, three $[K(crypt)]^+$ cations and a $[\{(R_2N)_2Y\}_2(\mu\text{-}\eta^6\text{:}\eta^6\text{-}C_6H_5Me)]^{2-}$ dianion were identified in the crystal lattice among the disorder.

Synthesis and reduction of $[(THF)(R_2N)_2Tb]_2(\mu\text{-}Cl)_2$. Since reducing $Ln(NR_2)_3$ (Ln = Tb, Gd, Dy, Y) in the presence of toluene did not produce any isolable or structurally characterizable products, a different strategy was employed. $[(THF)(R_2N)_2Ln]_2(\mu\text{-}Cl)_2$ was chosen as a potential precursor to **1-Ln** as the loss of the bridging chloride ligands during chemical reduction with potassium to form KCl may be more favorable than the loss of a NR_2 ligand to form KNR_2 during the reduction of $Ln(NR_2)_3$. Since $[(THF)(R_2N)_2Tb]_2(\mu\text{-}Cl)_2$ had not yet been reported in the literature, it was synthesized for the first time to attempt chemical

reduction in the presence of toluene. Reaction of $TbCl_3$ with 2 equivalents of $Li(NR_2)(Et_2O)$ in THF followed by extraction with hexane and crystallization in pentane at −35 °C yields colorless plate crystals of $[(THF)(R_2N)_2Tb]_2(\mu\text{-}Cl)_2$, eq 3.2. The crystal structure of $[(THF)(R_2N)_2Tb]_2(\mu\text{-}Cl)_2$ is isomorphous with the reported Gd compound, figure 3.3.[44]

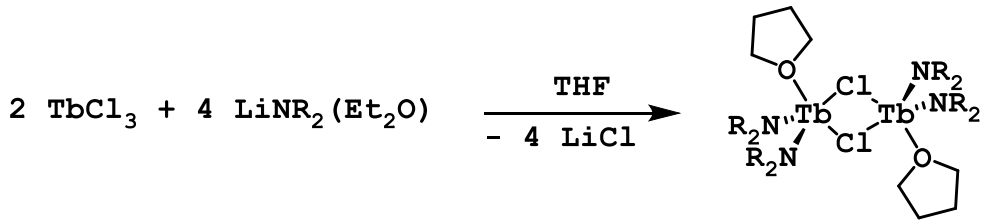

(3.2)

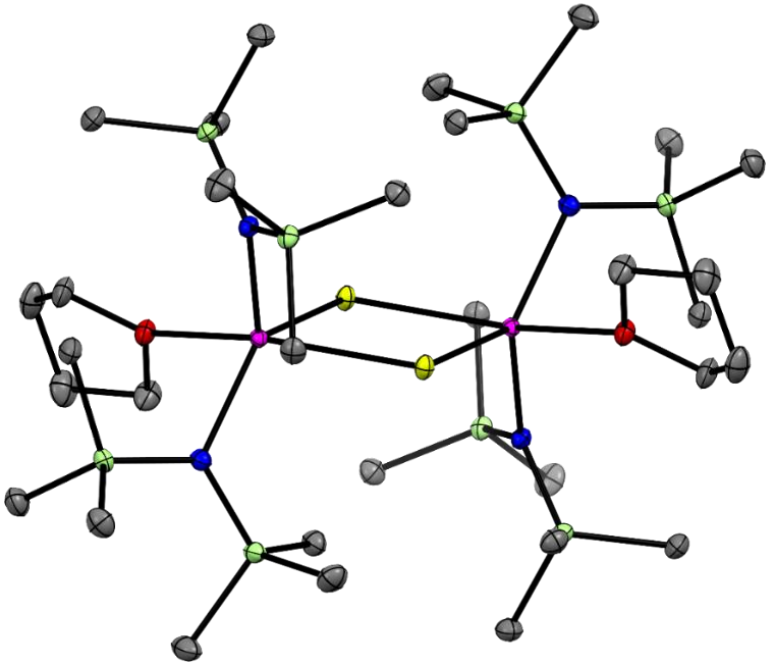

Fig. 3.3. Thermal ellipsoid plot of $[(THF)(R_2N)_2Tb]_2(\mu\text{-}Cl)_2$ drawn at the 50% probability level. H atoms are omitted for clarity. Color code: Grey = C, Red = O, Blue = N, Green = Si, Yellow = Cl, Pink = Tb.

$[(THF)(R_2N)_2Tb]_2(\mu\text{-}Cl)_2$ and crypt were dissolved in a mixture of toluene and THF and cooled to −35 °C. This colorless solution was then added to excess KC_8. The reaction instantly darkened to a brownish black. After one day at −35 °C, the reaction mixture was filtered and layered with cold hexane. A deep red-violet oil precipitated from the now clear

yellow solution after one day. The oil was isolated, washed with cold hexane, and dissolved in minimum THF. Dark purple single crystals of $[K(crypt)]_3[\{(R_2N)_2Tb\}_2(\mu\text{-}\eta^6\text{:}\eta^6\text{-}C_6H_5Me)][K(NR_2)_2(THF)_2]$, **2-Tb**, suitable for X-ray diffraction, were grown over 5 days from the concentrated THF solution at −35 °C, figure 3.4, eq 3.3.

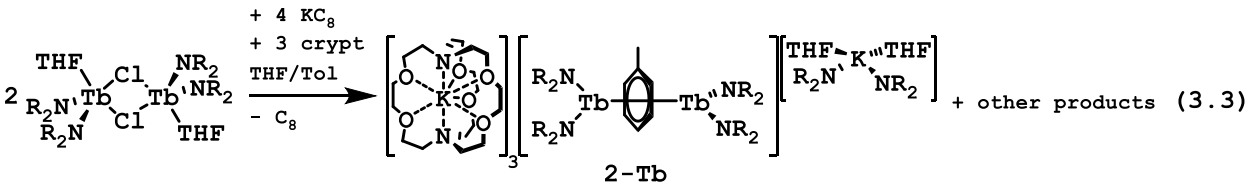

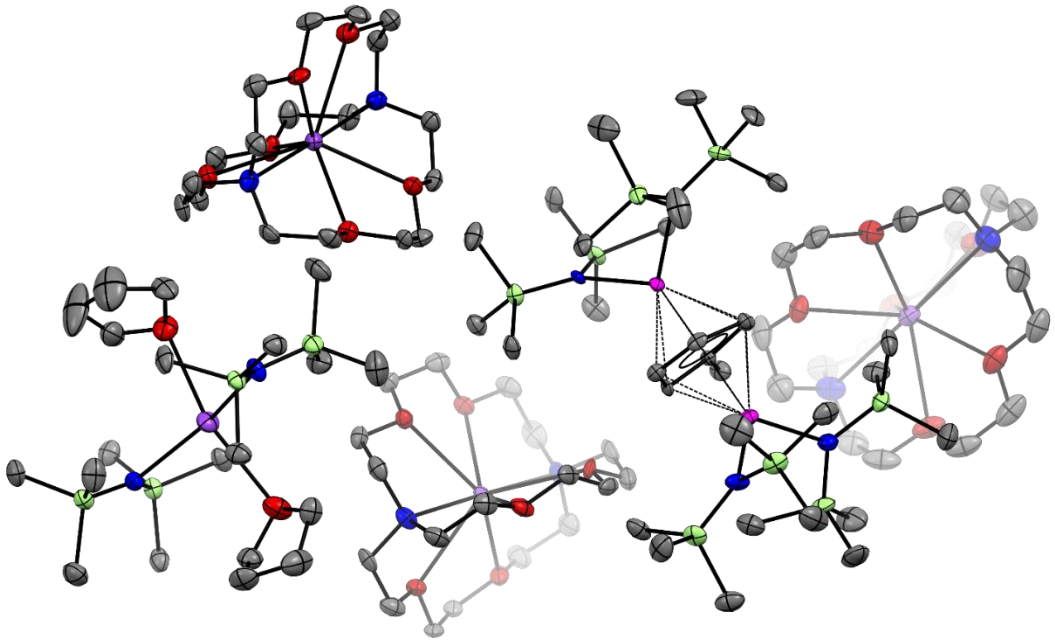

Figure 3.4. Thermal ellipsoid plot of **2-Tb** drawn at the 50% probability level. Depth cueing of the background $[K(crypt)]^+$ molecules is enabled for clarity. Color code: Grey = C, Red = O, Blue = N, Green = Si, Pink = Tb.

2-Tb is the first crystallographically characterized terbium reduced arene complex. The structural data of **2-Tb** are summarized in Table 3.3. **2-Tb** crystallizes with the unique anion, $[K(NR_2)_2(THF)_2]^-$. This anion has not been reported in the literature and no similar four-coordinate monopotassium compounds have been identified. The four-coordinate

geometry index, τ_4,[45] was calculated to be 0.33, meaning the geometry of $[K(NR_2)_2(THF)_2]^-$ anion is best described as seesaw and closer to square planar (τ_4 = 0.00) than tetrahedral (τ_4 = 1.00).

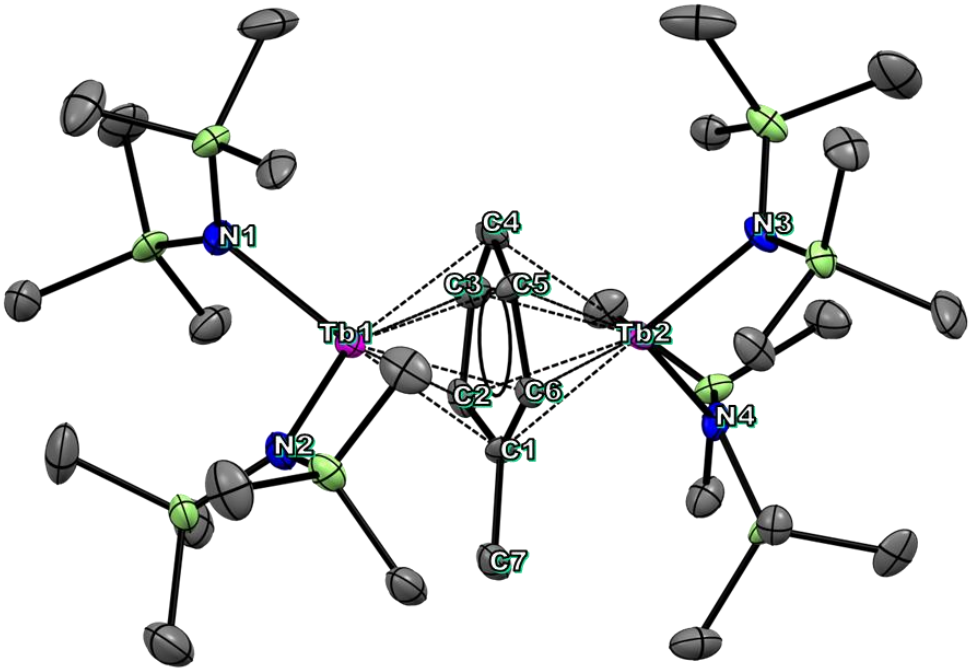

Figure 3.5. Thermal ellipsoid plot of **2-Tb** drawn at the 50% probability level. Hydrogen atoms, a $[K(NR_2)_2(THF)_2]^-$ anion, and three $[K(crypt)]^+$ cations were omitted for clarity. Color code: Grey = C, Red = O, Blue = N, Green = Si, Pink = Tb.

Like **1-Ln**, the four NR_2 ligands are staggered around the $Tb_2(\mu\text{-}C_6H_5Me)$ core, producing a tetrahedral rather than a square planar geometry. This differs from the $[(THF)(R_2N)_2Tb]_2(\mu\text{-}Cl)_2$ precursor to **2-Tb**, where the NR_2 ligands are in a distorted square planar arrangement. The Tb–N lengths range from 2.383(8)–2.426(7) Å and are shorter than the Ln–N lengths in the other **1-Ln** complexes because Tb is smaller than La and Ce. The Tb–N distances in **2-Tb** are elongated from the $[(THF)(R_2N)_2Tb]_2(\mu\text{-}Cl)_2$ precursor, whose Tb–N lengths range from 2.2268(11)–2.2470(12) Å. The toluene ring is noticeably less planar than in **1-Ln**, with a dihedral angle of 12.17° compared to 8.24°. This angle is closer to that of the

benzene 1,4-dianion bridge in $[K(crypt)]_2[(Cp'_2La)_2(\mu\text{-}\eta^6\text{:}\eta^6\text{-}C_6H_6)]$,[11] which had an analogous dihedral angle of 11°. Within the error limits, the $C–C_{arene}$ distances in **2-Tb** are indistinguishable from one another, but average to 1.466(11) Å. This value is similar to the average $C–C_{arene}$ distance for singly and doubly reduced arene complexes, Table 3.2.

Table 3.3: Selected bond lengths [Å] and angles [°] of **2-Tb**.
[a] Cnt is the centroid of the toluene. Θ = the dihedral angle between Pln1 and Pln2.
[b] Pln1 and Pln2 are the planes defined by C1, C2, C3, C6 and C3–C6, respectively.
[c] τ_4 is the four-coordinate geometry index of the $[K(NR_2)_2(THF)_2]^-$ anion.

Tb(1)–C(1)	2.570(9)	**Tb(2)–C(1)**	2.513(9)	**C(1)–C(2)**	1.471(12)	**Tb(1)–N(1)**	2.405(8)
Tb(1)–C(2)	2.427(9)	**Tb(2)–C(2)**	2.617(9)	**C(2)–C(3)**	1.451(13)	**Tb(1)–N(2)**	2.383(8)
Tb(1)–C(3)	2.580(10)	**Tb(2)–C(3)**	2.430(10)	**C(3)–C(4)**	1.462(14)	**Tb(2)–N(3)**	2.404(7)
Tb(1)–C(4)	2.506(9)	**Tb(2)–C(4)**	2.476(10)	**C(4)–C(5)**	1.483(12)	**Tb(2)–N(4)**	2.426(7)
Tb(1)–C(5)	2.416(9)	**Tb(2)–C(5)**	2.603(9)	**C(5)–C(6)**	1.456(12)	$\Theta_{Pln1–Pln2}$[b]	12.17
Tb(1)–C(6)	2.596(9)	**Tb(2)–C(6)**	2.460(9)	**C(6)–C(1)**	1.470(13)	τ_4[c]	0.33
Tb(1)–Cnt[a]		**Tb(2)–Cnt**[a]		**C–C$_{arene, avg}$**	1.466(11)		

Conclusion

The crystallographic data of **1-Ln** suggest that this complex contains two Ln^{2+} ions bridged by a toluene dianion. However, ambiguity in the spectroscopic data make it difficult to assign the charge of the toluene and the oxidation states of the metals with certainty. Magnetic studies should be performed on **1-Ln** to clear the ambiguity and to measure the exchange interactions between the metals and bridging toluene. Though reductions of $Ln(NR_2)_3$ (Ln = Dy, Gd, Tb, Y) produced red-brown oils with similar UV-visible spectra to **1-Ln**, and $[\{(R_2N)_2Ln\}_2(\mu\text{-}\eta^6\text{:}\eta^6\text{-}C_6H_5Me)]^{2-}$ dianions were observed in the crystal data for Y and Gd, these reactions were not clean and did not produce any pure compounds of appreciable quality and quantity. Changing the reduction precursor to $[(THF)(R_2N)_2Ln]_2(\mu\text{-}Cl)_2$ proved

successful for Tb as it resulted in the isolation of the first crystallographically characterized Tb reduced arene compound, **2-Tb**, which features the novel $[K(NR_2)_2(THF)_2]^-$ anion. Reduction of $[(THF)(R_2N)_2Ln]_2(\mu\text{-}Cl)_2$ for other metals such as Y or Gd should be performed to investigate if a series of $[\{(R_2N)_2Ln\}_2(\mu\text{-}\eta^6\text{:}\eta^6\text{-}C_6H_5Me)]^{2-}$ complexes could be isolated. Magnetic studies should be performed on **2-Tb**. If the reduced toluene bridge in **2-Tb** leads to high magnetic exchange interactions, this complex could be of interest to the SMM community.

Overall, these results show that reduced arene complexes can be formed in reductions of the Ln^{3+} amide complexes, $Ln(NR_2)_3$ and $[(THF)(R_2N)_2Ln]_2(\mu\text{-}Cl)_2$. Hence, any reductions of such complexes in a glovebox that contains arene vapor could be susceptible to reaction pathways involving arene reduction even if the solvent is not an arene.

Experimental

All manipulations and syntheses described below were conducted with the rigorous exclusion of air and water using standard Schlenk line and glovebox techniques under an argon atmosphere, unless stated otherwise. Solvents were sparged with UHP argon and dried by passage through columns containing Q-5 and molecular sieves prior to use. Potassium bis(trimethylsilyl)amide (KNR_2, R=$SiMe_3$) (Aldrich, 98%), was dissolved in toluene, centrifuged to remove tacky yellow insoluble material, and solvent was removed under reduced pressure before use. 2.2.2-cryptand (crypt, Merck) was placed under vacuum (10^{-5} torr) for 12 h before use. Grease was removed from the potassium metal (Aldrich) before use. $Ln(NR_2)_3$ (Ln= Y, La, Ce, Gd, Tb, Dy),[46] and $Li(NR_2)(Et_2O)$[47] were prepared according to modified literature procedures. Deuterated NMR solvents were dried over NaK alloy, degassed by three freeze-pump-thaw cycles, and vacuum transferred before use.

$^{13}C\{^{1}H\}$ NMR spectra were obtained on a Bruker AVANCE600 spectrometer with a BBO probe operating at 150 MHz for ^{13}C at 298 K and referenced internally to residual protio-solvent resonances. ^{1}H NMR spectra were obtained either on a Bruker AVANCE600 spectrometer with a BBO probe or a Bruker CRYO500 MHz spectrometer with a TCI probe at 298 K and referenced internally to residual protio-solvent resonances. UV-visible spectra were collected in THF at 298 K using a Varian Cary 50 Scan UV/Vis spectrophotometer. Infrared (IR) transmittance measurements were taken as compressed solids on an Agilent Cary 630 FTIR spectrophotometer with a diamond ATR attachment.

$[K(crypt)]_2\{[(R_2N)_2Ce]_2(\mu\text{-}\eta^6\text{:}\eta^6\text{-}C_6H_5Me)\}$, 1-Ce. 1 mL of THF was added to a vial containing $Ce(NR_2)_3$ (62 mg, 0.10 mmol), 2.2.2-cryptand (38 mg, 0.10 mmol) and 0.5 mL toluene and then cooled to −35 °C. The yellow-green THF solution was then added to a vial containing a smear of potassium (21 mg, 54 mmol).The resulting greenish black mixture was filtered after 1 hour at −35 °C. Dark purple single crystals of **1-Ce** (74 mg, 0.040 mmol, 80 % yield), suitable for X-ray diffraction, were grown overnight from THF/hexane at −35 °C. UV-visible (THF) λ_{max} [nm] (ε = $M^{-1}cm^{-1}$): 360 (2030), 434 (843, broad shoulder), 496 (569, broad shoulder), 672 (435, shoulder). IR [cm^{-1}]: 2938w, 2883w, 2814w, 1477w, 1444w, 1355m, 1296w, 1235m, 1103str, 1013m, 949str, 864m, 813str.

$[K(crypt)]_2\{[(R_2N)_2La]_2(\mu\text{-}\eta^6\text{:}\eta^6\text{-}C_6H_5Me)\}$, 1-La. As described for **1-Ce**, $La(NR_2)_3$ (572 mg, 0.923 mmol) and 2.2.2-cryptand (347 mg, 0.923 mmol) were dissolved in 5 mL THF and 5 mL toluene and then cooled to −35 °C. The colorless solution was then added to a vial containing cold KC_8 (274 mg, 2.03 mmol). The resulting dark red-brown mixture was filtered after one day at −35 °C. The solvent was removed *in vacuo*, which yielded tacky dark red-brown oily solids. These solids were washed with toluene, hexane, and pentane to remove

the tackiness. Dark purple single crystals of **1-La** (662 mg, 0.461 mmol, 78 %), suitable for X-ray diffraction, were grown overnight from THF/hexane at −35 °C. IR [cm^{-1}]: 2937w, 2884w, 2815w, 1476w, 1444w, 1356m, 1296w, 1235m, 1104str, 1024m, 951str, 864m, 815str.

$[(THF)(R_2N)_2Tb]_2(\mu\text{-}Cl)_2$. $TbCl_3$ (260 mg, 0.97 mmol) and KNR_2 (370 mg, 1.84 mmol) were added to 10 mL of THF and was left to stir overnight. The THF was removed *in vacuo* and 20 mL hexane was added to the gray solids. After 30 minutes of stirring, the gray slurry was centrifuged and the clear, colorless solution was isolated. Hexane was removed *in vacuo* to yield colorless solids. Colorless single crystals of $[(THF)(R_2N)_2Tb]_2(\mu\text{-}Cl)_2$, suitable for X-ray diffraction, were grown from a concentrated hexane solution at −35 °C.

$[K(crypt)]_3[\{(R_2N)_2Tb\}_2(\mu\text{-}\eta^6\text{:}\eta^6\text{-}C_6H_5Me)][K(NR_2)_2(THF)_2]$, 2-Tb. $[(THF)(R_2N)_2Tb]_2(\mu\text{-}Cl)_2$ (60 mg, 0.58 mmol) and 2.2.2-cryptand (440 mg, 0.12 mmol) were dissolved in 2 mL toluene and placed in a −35 °C freezer. The next day, 1 mL of cold THF was added to the reaction vial, and this colorless solution was then added to KC_8 (35 mg, 0.26 mmol). The reaction instantly turned dark brown. After one day at −35 °C, the reaction mixture was filtered and layered with cold hexane. The next day, the solvent in crystallization vial was a clear yellow, and a deep red-violet oil appeared at the bottom of the vial. The oil was isolated and dissolved in minimum THF. Dark purple single crystals of **2-Tb**, suitable for X-ray diffraction, were grown over 5 days from the concentrated THF solution at −35 °C.

X-ray Data Collection, Structure Solution and Refinement for [K(crypt)]$_2${[(R$_2$N)$_2$Ce]$_2$(μ-η^6:η^6-C$_6$H$_5$Me)}•C$_4$H$_8$O, 1-Ce. A purple crystal of approximate dimensions 0.251 x 0.325 x 0.348 mm was mounted in a cryoloop and transferred to a Bruker SMART APEX II diffractometer. The APEX2[48] program package was used to determine the unit-cell parameters and for data collection (20 sec/frame scan time for a sphere of diffraction data). The raw frame data was processed using SAINT[49] and SADABS[50] to yield the reflection data file. Subsequent calculations were carried out using the SHELXTL[51] program. The diffraction symmetry was *mmm* and the systematic absences were consistent with the orthorhombic space group $P2_12_12_1$ that was later determined to be correct.

The structure was solved by direct methods and refined on F^2 by full-matrix least-squares techniques. The analytical scattering factors[52] for neutral atoms were used throughout the analysis. Hydrogen atoms were included using a riding model. There was one molecule of tetrahydrofuran solvent present. Disordered atoms were included using multiple components with partial site-occupancy-factors.

Least squares analysis yielded wR2 = 0.0835 and Goof = 1.062 for 941 variables refined against 22067 data (0.78 Å), R1 = 0.0402 for those 19517 data with I > 2.0σ(I). The structure was refined as a two component twin. The absolute structure was assigned by refinement of the Flack parameter.[53]

X-ray Data Collection, Structure Solution and Refinement for $[(THF)(R_2N)_2Tb]_2(\mu\text{-}Cl)_2$. A colorless crystal of approximate dimensions 0.333 x 0.304 x 0.208 mm was mounted in a cryoloop and transferred to a Bruker SMART APEX II diffractometer. The APEX2[48] program package was used to determine the unit-cell parameters and for data collection (20 sec/frame scan time for a sphere of diffraction data). The raw frame data was processed using SAINT[49] and SADABS[50] to yield the reflection data file. Subsequent calculations were carried out using the SHELXTL[51] program. The diffraction symmetry was $2/m$ and the systematic absences were consistent with the monoclinic space group $P2_1/n$ that was later determined to be correct.

The structure was solved by dual space methods and refined on F^2 by full-matrix least-squares techniques. The analytical scattering factors[52] for neutral atoms were used throughout the analysis. Hydrogen atoms were included using a riding model. The structure was a dimmer located about an inversion center.

Least-squares analysis yielded wR2 = 0.0336 and Goof = 1.087 for 238 variables refined against 7657 data (0.72 Å), R1 = 0.0156 for those 7156 data with $I > 2.0\sigma(I)$.

X-ray Data Collection, Structure Solution and Refinement for [K(crypt)]$_3$[{(R$_2$N)$_2$Tb}$_2$(μ-η^6:η^6-C$_6$H$_5$Me)][K(NR$_2$)$_2$(THF)$_2$], 2-Tb. A purple crystal of approximate dimensions 0.273 x 0.274 x 0.397 mm was mounted in a cryoloop and transferred to a Bruker SMART APEX II diffractometer system. The APEX2[48] program package was used to determine the unit-cell parameters and for data collection (20 sec/frame scan time). The raw frame data was processed using SAINT[49] and SADABS[50] to yield the reflection data file. Subsequent calculations were carried out using the SHELXTL[51] program package. The diffraction symmetry was 2/*m* and the systematic absences were consistent with the monoclinic space group $P2_1/c$ that was later determined to be correct.

The structure was solved by direct methods and refined on F^2 by full-matrix least-squares techniques. The analytical scattering factors[52] for neutral atoms were used throughout the analysis. Hydrogen atoms were included using a riding model.

Least-squares analysis yielded wR2 = 0.1924 and Goof = 1.211 for 1434 variables refined against 28309 data (0.82 Å), R1 = 0.0831 for those 24123 data with I > 2.0σ(I). The structure was refined as a two-component twin.

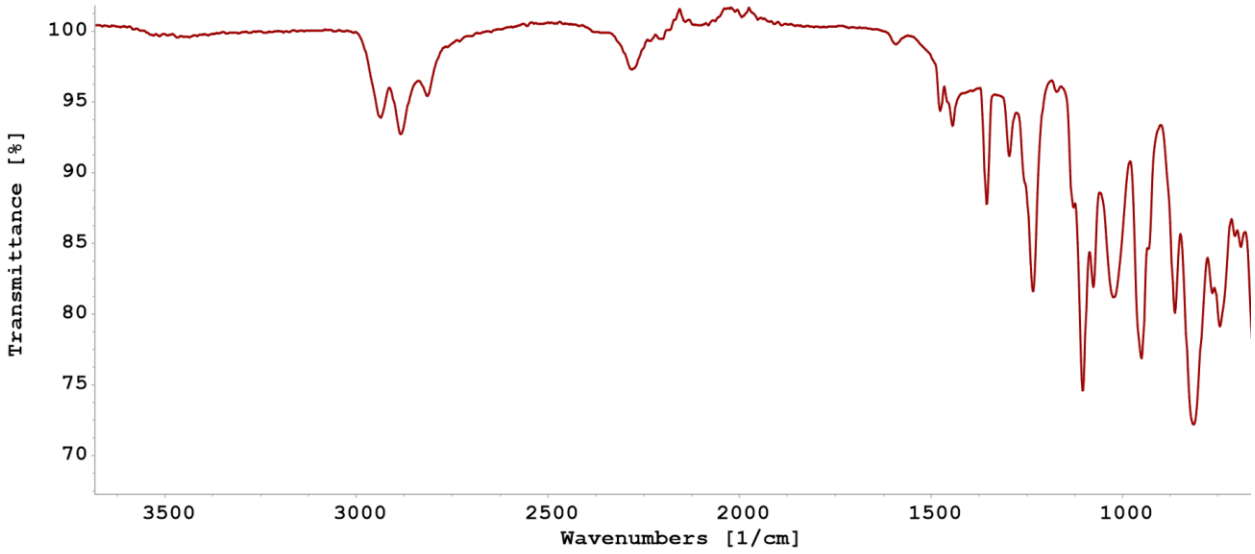

Figure S3.1. IR spectrum of [K(crypt)]$_2${[(R$_2$N)$_2$La]$_2$(μ-η^6:η^6-C$_6$H$_5$Me)}, **1-La**.

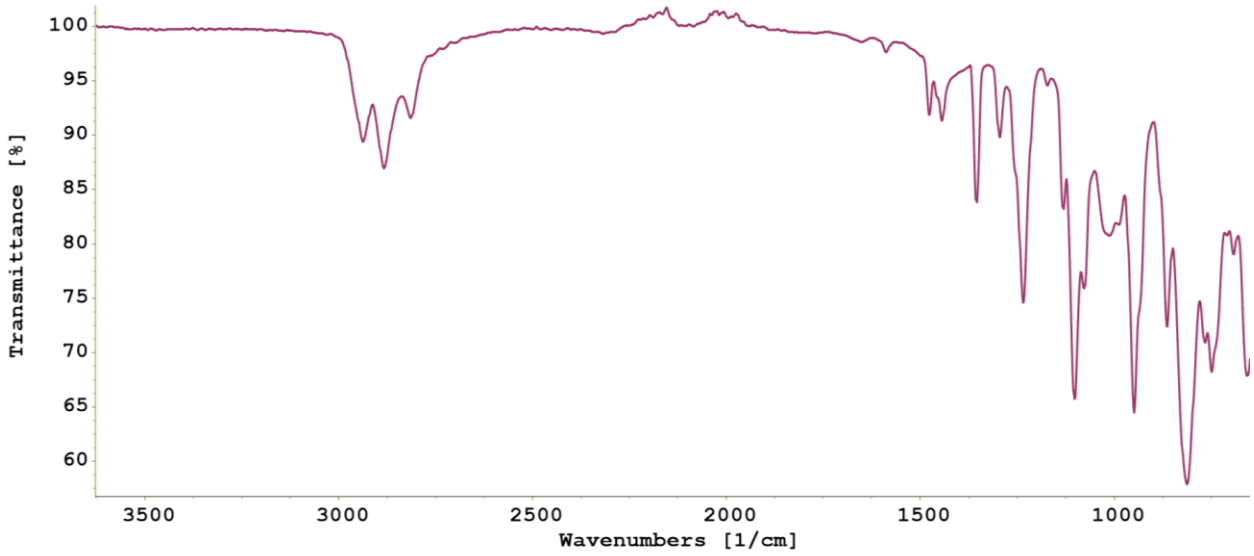

Figure S3.2. IR spectrum of $[K(crypt)]_2\{[(R_2N)_2Ce]_2(\mu\text{-}\eta^6\text{:}\eta^6\text{-}C_6H_5Me)\}$, **1-Ce**.

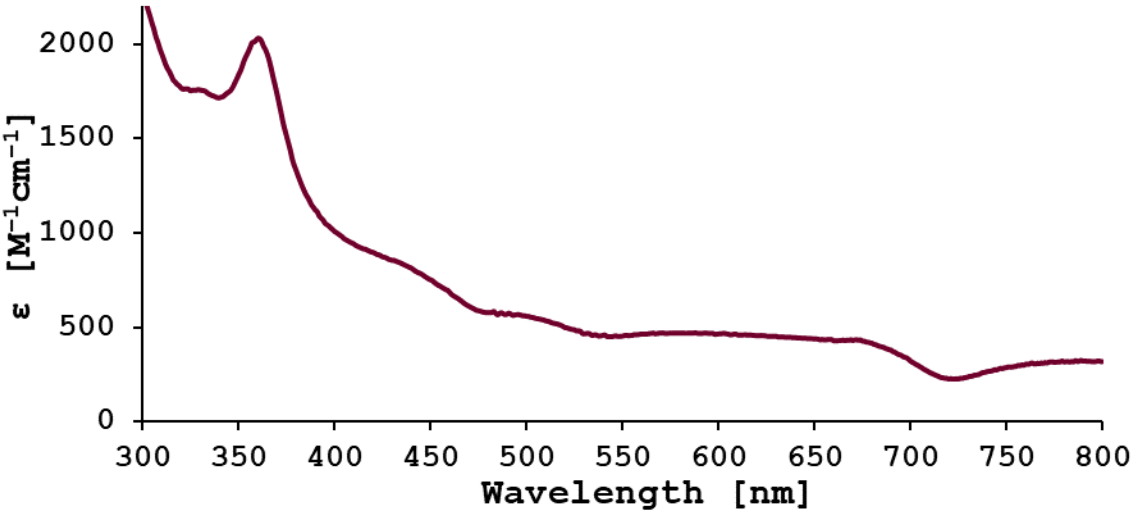

Figure S3.3. UV-Visible spectrum of a 1 mM THF solution of **1-Ce** recorded at room temperature.

References

(1) Kundu, K.; White, J. R. K.; Moehring, S. A.; Yu, J. M.; Ziller, J. W.; Furche, F.; Evans, W. J.; Hill, S. *Nat. Chem.* **2022**, *14*, 392–397.

(2) Moehring, S. A.; Beltrán-Leiva, M. J.; Páez-Hernández, D.; Arratia-Pérez, R.; Ziller, J. W.; Evans, W. J. *Chem. – A Eur. J.* **2018**, *24* (68), 18059–18067.

(3) Moehring, S. A.; Miehlich, M.; Hoerger, C. J.; Meyer, K.; Ziller, J. W.; Evans, W. J. *Inorg. Chem* **2020**, *59*, 3207–3214.

(4) Moore, W. N. G.; Ziller, J. W.; Evans, W. J. *Organometallics* **2021**, *40* (18), 3170–3176.

(5) Ryan, A. J.; Ziller, J. W.; Evans, W. J. *Chem. Sci.* **2020**, *11*, 2006–2014.

(6) Corbey, J. F.; Woen, D. H.; Palumbo, C. T.; Fieser, M. E.; Ziller, J. W.; Furche, F.; Evans, W. J. *Organometallics* **2015**, *34*, 3909–3921.

(7) Gun'ko, Y. K.; Hitchcock, P. B.; Lappert, M. F. *J. Organomet. Chem.* **1995**, *499* (1–2).

(8) Palumbo, C. T.; Darago, L. E.; Windorff, C. J.; Ziller, J. W.; Evans, W. J. *Organometallics* **2018**, *37* (6), 900–905.

(9) Cassani, M. C.; Duncalf, D. J.; Lappert, M. F. *J. Am. Chem. Soc.* **1998**, *120*, 12958–12959.

(10) Gun'ko, Y. K.; Hitchcock, P. B.; Lappert, M. F. *Organometallics* **2000**, *19* (15), 2832–2834.

(11) Kotyk, C. M.; Fieser, M. E.; Palumbo, C. T.; Ziller, J. W.; Darago, L. E.; Long, J. R.; Furche, F.; Evans, W. J. *Chem. Sci.* **2015**, *6*, 7267–7273.

(12) Patel, D.; Tuna, F.; McInnes, E. J. L.; McMaster, J.; Lewis, W.; Blake, A. J.; Liddle, S. T. *Dalt. Trans.* **2013**, *42*, 5224–5227.

(13) Patel, D.; Moro, F.; McMaster, J.; Lewis, W.; Blake, A. J.; Liddle, S. T. *Angew. Chem. Int. Ed.* **2011**, *50*, 10388–10392.

(14) Huang, W.; Khan, S. I.; Diaconescu, P. L. *J. Am. Chem. Soc.* **2011**, *133*, 10410–10413.

(15) Kelly, R. P.; Maron, L.; Scopelliti, R.; Mazzanti, M. *Angew. Chem. Int. Ed.* **2017**, *56*, 15663–15666.

(16) Diaconescu, P. L.; Cummins, C. C. *Inorg. Chem.* **2012**, *51*, 2902–2916.

(17) Diaconescu, P. L.; Cummins, C. C. *J. Am. Chem. Soc.* **2002**.

(18) Mougel, V.; Camp, C.; Pécaut, J.; Copéret, C.; Maron, L.; Kefalidis, C. E.; Mazzanti, M. *Angew. Chem. Int. Ed.* **2012**, *51*, 12280–12284.

(19) Evans, W. J.; Traina, C. A.; Ziller, J. W. *J. Am. Chem. Soc.* **2009**.

(20) Arnold, P. L.; Mansell, S. M.; Maron, L.; McKay, D. *Nat. Chem.* **2012**, *4*, 668–674.

(21) Huang, W.; Diaconescu, P. L. *Dalt. Trans.* **2015**, *44* (35), 15360–15371.

(22) Selikhov, A. N.; Mahrova, T. V.; Cherkasov, A. V.; Fukin, G. K.; Kirillov, E.; Alvarez Lamsfus, C.; Maron, L.; Trifonov, A. A. *Organometallics* **2016**, *35*, 2401–2409.

(23) Huang, W.; Le Roy, J. J.; Khan, S. I.; Ungur, L.; Murugesu, M.; Diaconescu, P. L. *Inorg. Chem.* **2015**, *54* (5), 2374–2382.

(24) Huang, W.; Dulong, F.; Wu, T.; Khan, S. I.; Miller, J. T.; Cantat, T.; Diaconescu, P. L. *Nat. Commun.* **2013**, *4*.

(25) Evans, W. J.; Lorenz, S. E.; Ziller, J. W. *Inorg. Chem.* **2009**, *48* (5), 2001–2009.

(26) Wooles, A. J.; Lewis, W.; Blake, A. J.; Liddle, S. T. *Organometallics* **2013**, *32*, 5058–5070.

(27) Monreal, M. J.; Khan, S. I.; Kiplinger, J. L.; Diaconescu, P. L. *Chem. Commun.* **2011**, *47*, 9119–9121.

(28) Diaconescu, P. L.; Arnold, P. L.; Baker, T. A.; Mindiola, D. J.; Cummins, C. C. *J. Am. Chem. Soc.* **2000**, *122* (25), 6108–6109.

(29) Evans, W. J.; Kozimor, S. A.; Ziller, J. W.; Kaltsoyannis, N. *J. Am. Chem. Soc.* **2004**, *126*

(44), 14533–14547.

(30) Palumbo, C. T.; Darago, L. E.; Dumas, M. T.; Ziller, J. W.; Long, J. R.; Evans, W. J. *Organometallics* **2018**, *37*, 3322–3331.

(31) Woen, D. H.; Chen, G. P.; Ziller, J. W.; Boyle, T. J.; Furche, F.; Evans, W. J. *Angew. Chem. Int. Ed.* **2017**, *56* (8), 2050–2053.

(32) Ryan, A. J.; Darago, L. E.; Balasubramani, S. G.; Chen, G. P.; Ziller, J. W.; Furche, F.; Long, J. R.; Evans, W. J. *Chem. Eur. J.* **2018**, *24*, 7702–7709.

(33) Mills, D. P.; Moro, F.; McMaster, J.; Van Slageren, J.; Lewis, W.; Blake, A. J.; Liddle, S. T. *Nat. Chem.* **2011**, *3*, 454–460.

(34) Rinehart, J. D.; Fang, M.; Evans, W. J.; Long, J. R. *Nat. Chem.* **2011**, *3*, 538–542.

(35) Rinehart, J. D.; Fang, M.; Evans, W. J.; Long, J. R. *J. Am. Chem. Soc.* **2011**, *133* (36), 14236–14239.

(36) Fieser, M. E.; Macdonald, M. R.; Krull, B. T.; Bates, J. E.; Ziller, J. W.; Furche, F.; Evans, W. J. *J. Am. Chem. Soc.* **2015**, *137* (1), 369–382.

(37) Kotyk, C. M.; MacDonald, M. R.; Ziller, J. W.; Evans, W. J. *Organometallics* **2015**, *34* (11), 2287–2295.

(38) Coles, M. P.; Hitchcock, P. B.; Khvostov, A. V.; Lappert, M. F.; Li, Z.; Protchenko, A. V. *Dalt. Trans.* **2010**, *39* (29), 6780–6788.

(39) Hitchcock, P. B.; Huang, Q. G.; Lappert, M. F.; Wei, X. H. *J. Mater. Chem.* **2004**, *14* (21), 3266–3273.

(40) Daniel, S. D.; Lehn, J. S. M.; Korp, J. D.; Hoffman, D. M. *Polyhedron* **2006**, *25* (2), 205–210.

(41) Cassani, M. C.; Gun'ko, Y. K.; Hitchcock, P. B.; Lappert, M. F. *Chem. Commun.* **1996**, *0*,

1987–1988.

(42) Pang, F.; Boggs, J. E.; Pulay, P.; Fogarasi, G. *J. Mol. Struct.* **1980**, *66*, 281–287.

(43) Xiao, Y.; Zhao, X. K.; Wu, T.; Miller, J. T.; Hu, H. S.; Li, J.; Huang, W.; Diaconescu, P. L. *Chem. Sci.* **2021**, *12* (1), 227–238.

(44) Aspinall, H. C.; Bradley, D. C.; Hursthouse, M. B.; Sales, K. D.; Walker, N. P. C.; Hussain, B. *J. Chem. Soc. Dalt. Trans.* **1989**.

(45) Yang, L.; Powell, D. R.; Houser, R. P. *Dalt. Trans.* **2007**, No. 9, 955–964.

(46) Edelmann, F. T. *Synthetic Methods of Organometallic and Inorganic Chemistry, Volume 6: Lanthanides and Actinides*; Herrmann, W. A., Ed.; 1996.

(47) Manzer, L. E. *Inorg. Chem.* **1978**, *17* (6), 1552–1558.

(48) *APEX2*; Version 2014.11-0; Bruker AXS, Inc.: Madison, WI, 2014.

(49) *SAINT*; Version 8.34a; Bruker AXS, Inc.: Madison, WI, 2013.

(50) Sheldrick, G. M. *SADABS*; Version 2014/5; Bruker AXS, Inc.: Madison, WI, 2014.

(51) Sheldrick, G. M. *SHELXTL*; Version 2014/7; Bruker AXS, Inc.: Madison, WI, 2014.

(52) *International Tables for Crystallography*, Vol. C.; Prince, E., Ed.; Dordrecht: Kluwer Academic Publishers., 2006.

(53) Parsons, S.; Flack, H. D.; Wagner, T. *Acta Crystallogr. Sect. B Struct. Sci. Cryst. Eng. Mater.* **2013**, *69* (3), 249–259.

APPENDIX A

Crystallographic tables

† $OAr^* = 2,6\text{-}Ad_2\text{-}4\text{-}{}^t\!Bu\text{-}C_6H_2O^-$, where Ad is 1-adamantyl
‡ $R = SiMe_3$

Table A1. Crystal data and structure refinement for $Lu(OAr^*)_3$.

Identification code	jrw25 (Jessica White)	
Empirical formula	$C_{96}\ H_{137}\ Lu\ O_3$	
Formula weight	1514.02	
Temperature	133(2) K	
Wavelength	0.71073 Å	
Crystal system	Monoclinic	
Space group	$P2_1/n$	
Unit cell dimensions	a = 14.7454(12) Å	α = 90°.
	b = 29.237(2) Å	β = 108.8157(13)°.
	c = 22.0531(18) Å	γ = 90°.
Volume	8999.3(13) $Å^3$	
Z	4	
Density (calculated)	1.117 Mg/m^3	
Absorption coefficient	1.142 mm^{-1}	
F(000)	3232	
Crystal color	colorless	
Crystal size	0.569 x 0.386 x 0.295 mm^3	
Theta range for data collection	1.199 to 28.282°	
Index ranges	$-19 \le h \le 19, -38 \le k \le 38, -29 \le l \le 29$	
Reflections collected	201896	
Independent reflections	22343 [R(int) = 0.0578]	
Completeness to theta = 25.242°	100.0 %	
Absorption correction	Semi-empirical from equivalents	
Max. and min. transmission	0.7461 and 0.6554	
Refinement method	Full-matrix least-squares on F^2	
Data / restraints / parameters	22343 / 18 / 912	
Goodness-of-fit on F^2	1.186	
Final R indices [I>2sigma(I) = 19679 data]	R1 = 0.0468, wR2 = 0.1059	
R indices (all data, 0.75 Å)	R1 = 0.0538, wR2 = 0.1086	
Largest diff. peak and hole	2.229 and -4.477 $e.Å^{-3}$	

Table A2. Crystal data and structure refinement for [K(crypt)][Lu(OAr*)$_3$]·3Et$_2$O.

Identification code	jrw26 (Jessica White)	
Empirical formula	C_{120} H_{189} K Lu N_2 O_{12}	
Formula weight	2065.79	
Temperature	133(2) K	
Wavelength	0.71073 Å	
Crystal system	Triclinic	
Space group	$P\bar{1}$	
Unit cell dimensions	a = 16.3861(17) Å	α = 84.5286(18)°.
	b = 16.7674(17) Å	β = 82.7989(18)°.
	c = 22.820(2) Å	γ = 62.6481(15)°.
Volume	5519.9(10) Å^3	
Z	2	
Density (calculated)	1.243 Mg/m^3	
Absorption coefficient	0.992 mm^{-1}	
F(000)	2218	
Crystal color	purple	
Crystal size	0.274 x 0.267 x 0.198 mm^3	
Theta range for data collection	1.369 to 28.282°	
Index ranges	$-21 \le h \le 21$, $-22 \le k \le 22$, $-30 \le l \le 30$	
Reflections collected	124026	
Independent reflections	27368 [R(int) = 0.0633]	
Completeness to theta = 25.242°	100.0 %	
Absorption correction	Semi-empirical from equivalents	
Max. and min. transmission	0.8017 and 0.7228	
Refinement method	Full-matrix least-squares on F^2	
Data / restraints / parameters	27368 / 0 / 1240	
Goodness-of-fit on F^2	1.055	
Final R indices [I>2sigma(I) = 22821 data]	R1 = 0.0465, wR2 = 0.1110	
R indices (all data, 0.75 Å)	R1 = 0.0631, wR2 = 0.1183	
Largest diff. peak and hole	4.488 and -0.890 e.Å^{-3}	

Table A3. Crystal data and structure refinement for [(18-crown-6)K(μ-Cp^{Me})K(18-crown-6)][$Cp^{Me}{}_3$Gd].

Identification code	jrw9 (Jessica White)	
Empirical formula	C60 H100 Gd K2 O15	
Formula weight	1296.84	
Temperature	133(2) K	
Wavelength	0.71073 Å	
Crystal system	Monoclinic	
Space group	$P2_1/c$	
Unit cell dimensions	a = 9.5943(12) Å	α = 90°.
	b = 26.125(3) Å	β = 90.6408(17)°.
	c = 25.258(3) Å	γ = 90°.
Volume	6330.5(14) $Å^3$	
Z	4	
Density (calculated)	1.361 Mg/m^3	
Absorption coefficient	1.241 mm^{-1}	
F(000)	2728	
Crystal color	purple	
Crystal size	0.484 x 0.243 x 0.042 mm^3	
Theta range for data collection	1.121 to 28.323°	
Index ranges	$-12 \le h \le 12$, $-34 \le k \le 34$, $-32 \le l \le 33$	
Reflections collected	75865	
Independent reflections	15384 [R(int) = 0.0585]	
Completeness to theta = 25.500°	99.9 %	
Absorption correction	Semi-empirical from equivalents	
Max. and min. transmission	0.7457 and 0.6288	
Refinement method	Full-matrix least-squares on F^2	
Data / restraints / parameters	15384 / 0 / 680	
Goodness-of-fit on F^2	1.027	
Final R indices [I>2sigma(I) = 11511 data]	R1 = 0.0421, wR2 = 0.0962	
R indices (all data, 0.75 Å)	R1 = 0.0669, wR2 = 0.1070	
Largest diff. peak and hole	2.443 and -0.921 $e.Å^{-3}$	

Table A4. Crystal data and structure refinement for $[K(crypt)]_2\{[(R_2N)_2Ce]_2(\mu\text{-}\eta^6\text{:}\eta^6\text{-}C_6H_5Me)\}\bullet C_4H_8O$.

Identification code	jrw3 (Jessica White)	
Empirical formula	$C_{67}\ H_{151}\ Ce_2\ K_2\ N_8\ O_{12}\ Si_8 \bullet C_4H_8O$	
Formula weight	1916.21	
Temperature	88(2) K	
Wavelength	0.71073 Å	
Crystal system	Orthorhombic	
Space group	$P2_12_12_1$	
Unit cell dimensions	a = 16.554(3) Å	α = 90°.
	b = 16.572(3) Å	β = 90°.
	c = 36.453(6) Å	γ = 90°.
Volume	10000(3) $Å^3$	
Z	4	
Density (calculated)	1.273 Mg/m^3	
Absorption coefficient	1.131 mm^{-1}	
F(000)	4044	
Crystal color	purple	
Crystal size	0.348 x 0.325 x 0.251 mm^3	
Theta range for data collection	1.229 to 27.103°	
Index ranges	$-21 \le h \le 21$, $-21 \le k \le 21$, $-46 \le l \le 46$	
Reflections collected	112070	
Independent reflections	22067 [R(int) = 0.0611]	
Completeness to theta = 25.500°	100.0 %	
Absorption correction	Semi-empirical from equivalents	
Max. and min. transmission	0.7457 and 0.6096	
Refinement method	Full-matrix least-squares on F^2	
Data / restraints / parameters	22067 / 0 / 941	
Goodness-of-fit on F^2	1.062	
Final R indices [I>2sigma(I) = 19517 data]	R1 = 0.0402, wR2 = 0.0779	
R indices (all data, 0.78 Å)	R1 = 0.0532, wR2 = 0.0835	
Absolute structure parameter	-0.015(4)	
Largest diff. peak and hole	1.111 and -1.015 $e.Å^{-3}$	

Table A5. Crystal data and structure refinement for $[(THF)(R_2N)_2Tb]_2(\mu\text{-}Cl)_2$.

Identification code	jrw21 (Jessica White)	
Empirical formula	$C_{32}H_{88}Cl_2N_4O_2Si_8Tb_2$	
Formula weight	1174.52	
Temperature	88(2) K	
Wavelength	0.71073 Å	
Crystal system	Monoclinic	
Space group	$P2_1/n$	
Unit cell dimensions	a = 14.1272(6) Å	α = 90°.
	b = 12.9851(5) Å	β = 114.6185(5)°.
	c = 16.3862(7) Å	γ = 90°.
Volume	2732.7(2) $Å^3$	
Z	2	
Density (calculated)	1.427 Mg/m^3	
Absorption coefficient	2.869 mm^{-1}	
F(000)	1200	
Crystal color	colorless	
Crystal size	0.333 x 0.304 x 0.208 mm^3	
Theta range for data collection	1.605 to 29.574°	
Index ranges	$-19 \le h \le 19$, $-18 \le k \le 18$, $-22 \le l \le 22$	
Reflections collected	40812	
Independent reflections	7657 [R(int) = 0.0220]	
Completeness to theta = 25.500°	100.0 %	
Absorption correction	Semi-empirical from equivalents	
Max. and min. transmission	0.7462 and 0.6665	
Refinement method	Full-matrix least-squares on F^2	
Data / restraints / parameters	7657 / 0 / 238	
Goodness-of-fit on F^2	1.087	
Final R indices [I>2sigma(I) = 7156 data]	R1 = 0.0156, wR2 = 0.0329	
R indices (all data, 0.72 Å)	R1 = 0.0178, wR2 = 0.0336	
Largest diff. peak and hole	0.469 and -0.365 $e.Å^{-3}$	

Table A6. Crystal data and structure refinement for $[K(crypt)]_3[\{(R_2N)_2Tb\}_2(\mu\text{-}\eta^6\text{:}\eta^6\text{-}C_6H_5Me)][K(NR_2)_2(THF)_2]$.

Identification code	jrw20 (Jessica White)	
Empirical formula	$C_{105}\ H_{240}\ K_4\ N_{12}\ O_{20}\ Si_{12}\ Tb_2$	
Formula weight	2802.40	
Temperature	88(2) K	
Wavelength	0.71073 Å	
Crystal system	Monoclinic	
Space group	$P2_1/c$	
Unit cell dimensions	a = 16.5046(12) Å	α = 90°.
	b = 16.8543(13) Å	β = 91.0314(12)°.
	c = 53.625(4) Å	γ = 90°.
Volume	14915(2) $Å^3$	
Z	4	
Density (calculated)	1.248 Mg/m^3	
Absorption coefficient	1.206 mm^{-1}	
F(000)	5952	
Crystal color	purple	
Crystal size	0.397 x 0.274 x 0.273 mm^3	
Theta range for data collection	1.139 to 25.682°	
Index ranges	$-20 \le h \le 20$, $-20 \le k \le 20$, $-65 \le l \le 65$	
Reflections collected	173061	
Independent reflections	28309 [R(int) = 0.0667]	
Completeness to theta = 25.242°	100.0 %	
Absorption correction	Semi-empirical from equivalents	
Max. and min. transmission	0.7456 and 0.6443	
Refinement method	Full-matrix least-squares on F^2	
Data / restraints / parameters	28309 / 0 / 1434	
Goodness-of-fit on F^2	1.211	
Final R indices [I>2sigma(I) = 24123 data]	R1 = 0.0831, wR2 = 0.1861	
R indices (all data, 0.82 Å)	R1 = 0.0965, wR2 = 0.1924	
Largest diff. peak and hole	3.303 and -4.321 $e.Å^{-3}$	